



AALBORG UNIVERSITY
DENMARK

Aalborg Universitet

Investigating fungal-produced phoenicin as a possible electrolyte candidate for a redox flow battery

Wilhelmsen, Charlotte Overgaard

DOI (link to publication from Publisher):
[10.54337/aau527275062](https://doi.org/10.54337/aau527275062)

Publication date:
2022

Document Version
Publisher's PDF, also known as Version of record

[Link to publication from Aalborg University](#)

Citation for published version (APA):
Wilhelmsen, C. O. (2022). *Investigating fungal-produced phoenicin as a possible electrolyte candidate for a redox flow battery*. Aalborg Universitetsforlag. Ph.d.-serien for Det Ingeniør- og Naturvidenskabelige Fakultet, Aalborg Universitet <https://doi.org/10.54337/aau527275062>

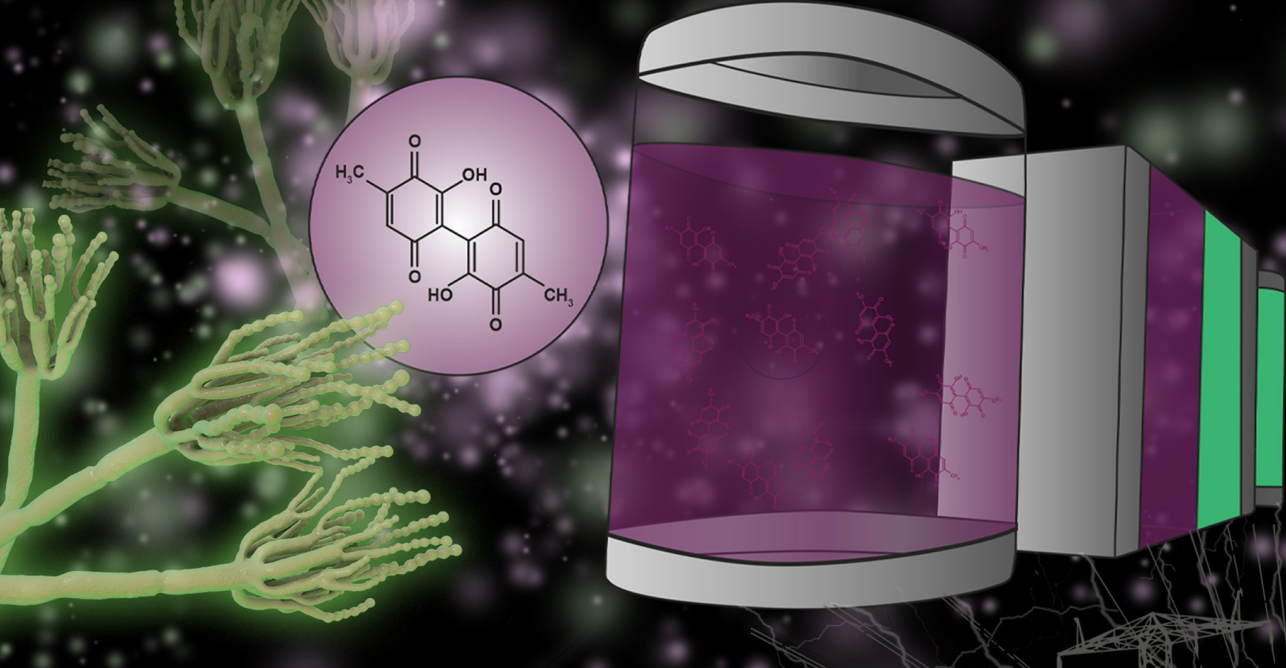
General rights

Copyright and moral rights for the publications made accessible in the public portal are retained by the authors and/or other copyright owners and it is a condition of accessing publications that users recognise and abide by the legal requirements associated with these rights.

- Users may download and print one copy of any publication from the public portal for the purpose of private study or research.
- You may not further distribute the material or use it for any profit-making activity or commercial gain
- You may freely distribute the URL identifying the publication in the public portal -

Take down policy

If you believe that this document breaches copyright please contact us at vbn@aub.aau.dk providing details, and we will remove access to the work immediately and investigate your claim.



INVESTIGATING FUNGAL-PRODUCED PHOENICIN AS A POSSIBLE ELECTROLYTE CANDIDATE FOR A REDOX FLOW BATTERY

BY
CHARLOTTE OVERGAARD WILHELMSSEN

DISSERTATION SUBMITTED 2022



AALBORG UNIVERSITY
DENMARK

INVESTIGATING FUNGAL-PRODUCED PHOENICIN AS A POSSIBLE ELECTRO- LYTE CANDIDATE FOR A REDOX FLOW BATTERY

by

Charlotte Overgaard Wilhelmsen



AALBORG UNIVERSITY
DENMARK

Dissertation submitted 13th December 2022

Dissertation submitted: 13-12-2022

PhD supervisor: Associate Professor Jens Muff,
Aalborg University

PhD co-supervisor: Associate Professor Jens Laurids Sørensen,
Aalborg University

PhD committee: Professor Kim Lambertsen Larsen (chair)
Aalborg University, Denmark

Professor Anders Bentien
Aarhus University, Denmark

Senior Research Fellow Dénes Kónya
Hungarian Academy of Science, Hungary

PhD Series: Faculty of Engineering and Science, Aalborg University

Department: Department of Chemistry and Bioscience

ISSN (online): 978-87-7573-779-6
ISBN (online): 2446-1636

Published by:
Aalborg University Press
Kroghstræde 3
DK – 9220 Aalborg Ø
Phone: +45 99407140
aauf@forlag.aau.dk
forlag.aau.dk

© Copyright: Charlotte Overgaard Wilhelmsen

Printed in Denmark by Stibo Complete, 2023

Preface

The present thesis was submitted in accordance with the requirements for obtaining the Ph.D. degree at the Faculty of Engineering and Science, Aalborg University.

The thesis is based on work carried out in the period from June 2019 to November 2022, at the Department of Chemistry and Bioscience, Aalborg University Esbjerg, at the Center for Energy and Environmental Chemistry, Jena (CEEC Jena) at Friedrich Schiller University in Jena Germany, and the Department of Energy Conversion and Storage at the Technical University of Denmark (DTU). The research project was fully supported by Novo Nordisk Foundation grant no. NNF18OC0034952.

During this Ph.D. project, I have been enrolled at the Department of Chemistry and Bioscience, Faculty of Engineering and Science. To develop further scientific research, I spend three months at the CEEC Jena in collaboration with Professor Dr. Ulrich S. Schubert and Dr. Martin Hager, and one week in the laboratory of Professor Dr. Johan Hjelm at DTU, Lyngby.

This Ph.D. study is based on the following papers:

1. **Wilhelmsen, C.O.**; Kristensen, S.B.; Nolte, O.; Volodin, I.; Christiansen, J.V.; Isbrandt, T.; Sørensen, T.; Petersen, C.; Sondergaard, T.E.; Nielsen, K.L.; Larsen, T.O.; Frisvad, J.C.; Hager, M.; Schubert, U.S.; Muff, J.; Sørensen, J.L. (2022) *Demonstrating the use of a Fungal Synthesized Quinone in a Redox Flow Battery*. Batteries & Supercaps, doi:10.1002/batt.202200365
2. **Wilhelmsen, C.O.**; Kavounis-Pasadakis, A.; Christiansen, J.V.; Isbrandt, T.; Almind, M.R.; Larsen, T.O.; Hjelm, J.; Sørensen, J.L., Muff, J. (2022) *Four-Electron Energy Storage in Biosynthesized Phoenicin Flow Battery Negolyte*. Manuscript submitted to ACS Sustainable Chemistry & Engineering
3. **Wilhelmsen, C.O.**; Muff, J.; Sørensen, J.L. (2022) *Are biologically synthesized electrolytes the future in green energy storage?* Manuscript submitted to Energy Storage

I have been involved in the following publication as a side project in which a model for estimating the lifetime of an aqueous organic redox flow battery was developed. Additionally, the study provides a guide for the power converter design considering large-scale integration.

4. Tang, Z.; Sangwongwanich, A.; Yang, Y., **Wilhelmsen, C.O.**; Kristensen, S.B.; Sørensen, J.L.; Muff, J.; Blaabjerg, F. (2021) *Lifetime Modelling and Analysis of Aqueous Organic Redox-flow Batteries for Renewable Energy Application*. IEEE Energy Conversion Congress and Exposition (ECCE), doi: 10.1109/ECCE47101.2021.9595507

Acknowledgements

First and foremost, I would like to thank my supervisor Associate Professor Jens Muff for the opportunity to perform this research and to be a part of the fungal battery project. His supervision, scientific advice, and positive attitude have been valuable and helpful throughout this journey, which I appreciate. Secondly, I would like to thank Associate Professor Jens Laurids Sørensen for being my co-supervisor, and for supporting and inspiring me with lots of good ideas as well as for his help in the scientific publication process. Thank you both for keeping me motivated.

I want to thank Professor Dr. Schubert for allowing me to be a part of his research group at Friedrich Schiller University in Jena. A thank you to Dr. Martin Hager for welcoming me into their laboratory, and for making my external stay possible which was valuable and crucial for the scientific process of my Ph.D. Furthermore, I want to express my gratitude towards Ivan and Oliver for your guidance and for introducing me to new approaches and methods. Thank you for sharing your knowledge, and for the following Zoom meetings whenever I needed your support and inspiring inputs in the publication process. I wish to thank Professor Johan Hjelm for welcoming me into his laboratory at DTU Lyngby and for supporting me in my research. A special thank you to Alex for keeping me in good company when I visited your lab. Thank you for a fun and very learn full week, with nice experiments, long days, and good talks.

For all their help in the lab, I would like to thank Linda and Dorte. Thank you for always being positive and for our talks about spinning and Tour de France. I want to give a big thank you to Heidi for listening during the hard times of my Ph.D. study. Thank you to all my colleagues at AAU Esbjerg for the good working environment.

I want to thank Sebastian for introducing me to the topic, to experimental procedures, as well as for your knowledge-sharing and good talks. A special thank goes to Mikkel for supporting and helping me from the beginning to the end of my Ph.D. journey, for the good talks in our office, and for always listening and giving me good advice.

I would like to show my deepest gratitude and appreciation to my family and friends for supporting me. I am looking forward to spending more time with you again. A special thank you to my father for always believing in me, for being a great role model, and for your endless support and warm hugs. Finally, a thank you to my boyfriend for your invaluable help and support during the last three years. Thank you.

Charlotte Overgaard Wilhelmsen
November 2022
Esbjerg, Denmark

English summary

Most of the worldwide energy consumption is provided by fossil fuel-based energy sources, which influence climate change due to air pollution, and with the harmful effects of CO₂ emissions, the interest in using energy from renewable energy sources has increased annually. Despite the carbon-free and inexhaustible characteristics of renewables, the intermittent and unpredictable behavior of these sources limits them from completely replacing the use of fossil fuels.

To overcome the intermittency of renewables and to accelerate the green energy transition, different energy storage devices are being extensively researched with one of them being the redox flow battery. This technology offers flexible designs due to the possibility of power and energy being scaled independently. The vanadium flow battery has been the most developed and researched until now; however, redox flow batteries using aqueous organic electrolyte materials, such as quinones, have gained increased attention. The quinones studied in the literature are mostly synthesized from non-renewable feedstocks. Inspired by naturally occurring quinones, this project aimed to investigate the potential of using fungal quinone phoenicin as an electrolyte candidate for a redox flow battery.

In the initial study, I investigated phoenicin as the first fungal quinone to be used in a redox flow battery. The experimental investigations of phoenicin were performed during my external stay at Friedrich Schiller University in Jena. The experiments and methods performed in this study worked as a foundation for future research on using fungal quinones as electrolytes in redox flow batteries. By characterizing the electrochemical properties of phoenicin, produced in 95% purity by *Penicillium atrosanguineum*, it was found that phoenicin could work as a potential negolyte in a redox flow battery, with it being redox-active and hereby being capable of participating in two-electron redox reactions. After testing phoenicin in a volumetrically unbalanced compositionally symmetric flow cell, in which the stability at different redox states was investigated, it was found that phoenicin suffered from chemical degradation when dissolved in a high alkaline supportive electrolyte. Cell-cycling test in a redox flow battery showed that phoenicin could be charged and discharged as the negative electrolyte for 14 days with a capacity loss below 50% in total. Therefore, the findings in this study demonstrated the concept of using a fungal quinone to store energy, and phoenicin hereby worked as a proof of concept for such an approach.

Next up, I evaluated the influence of phoenicin purity by investigating a mix of four phoenicin forms, produced by *Penicillium phoeniceum* in higher yields. The experimental investigations of the phoenicin mix were performed during my visit to the laboratories at the Technical University of Denmark. By using a similar approach as in the previous study, the electrochemical properties were determined to be comparable to the ones obtained from phoenicin in the first study. However, instead of involving a two-electron redox reaction, I discovered that the phoenicin mix involved a four-

electron reaction per phoenicin molecule. The ability to involve four electrons per phoenicin molecule was also seen in the battery test. Being able to obtain 1111 charge and discharge cycles (13 days of cycling) proved that, despite having a mix of phoenicin forms, including phoenicin dimer, it could still be used as the negative electrolyte in a redox flow battery. Further investigations proposed that phoenicin suffered from Michael attack on the unsubstituted carbon positions when dissolved in a highly alkaline supportive electrolyte, and different degradation products such as the addition of hydroxyl groups to the phoenicin molecules as well as different stages of polymerization such as phoenicin dimer, trimer, quadromers, etc. were identified. The findings in this study demonstrated that having a mix of phoenicin forms involved a four-electron reaction per phoenicin molecule, hereby utilizing the full potential of the phoenicin mix by reaching capacities corresponding to two-electron reaction per benzoquinone group (four-electrons per phoenicin molecule).

The research made in this dissertation can be used as a guideline for future research in using fungal quinones as electrolyte material for redox flow batteries. It clearly illustrates the potential of using fungal quinones for renewable energy storage, and I believe that this research subject is worth investigating in the future.

Dansk resume

Største delen af verdens energiforbrug stammer fra fossile brændstoffer som forurener miljøet og dermed bidrager til klimaændringer, og med de skadelige virkninger af CO₂ udledning er interessen i at anvende energi fra vedvarende energikilder steget med årene. På trods af at de vedvarende energikilder er CO₂ neutrale og er en evig kilde til energi, så begrænser deres uforudsigelighed deres potentiale for fuldstændigt at erstatte brugen af fossile brændstoffer.

For at løse udfordringen med vedvarende energikilders uforudsigelighed og dermed accelerere den grønne omstilling, forskes der i potentialet af forskellige teknologier til energilagring, hvoraf en af dem er redox flowbatteri teknologien. Denne teknologi tilbyder fleksible design grundet mulighederne for at skalere power og energi uafhængigt. Vanadium redox flowbatteriet er indtil nu blevet undersøgt mest, men redox flowbatterier der anvender vandopløselige organisk elektrolyt materialer, så som quinoner, har fået mere opmærksomhed. De quinoner der er blevet forsket i indtil nu, er syntetisk produceret fra ikke-bæredygtige kilder. Inspireret af naturligt fremkommende quinoner, er formålet med dette projekt at undersøge potentialet af at anvende svampe quinonen phoenicin som en elektrolyt kandidat til et redox flowbatteri.

Først undersøgte jeg phoenicin som den første svampe quinon til at blive brugt i et redox flowbatteri. De eksperimentelle undersøgelser blev lavet under mit udlandsophold ved Friedrich Schiller University i Jena. Forsøgene og metoderne der blev anvendt i dette studie skulle danne grundlag for fremtidig forskning indenfor brugen af svampe quinoner som elektrolytter i redox flowbatterier. Ved at karakterisere phoenicins elektrokemiske egenskaber fandt jeg ud af at phoenicin, produceret af *Penicillium atrosanguineum* med 95% renhed, var redox aktivt og i stand til at indgå i reversible to-elektron reaktioner og hermed have potentialet for at blive brugt negativ elektrolyt i et redox flowbatteri. Efter at have testet phoenicins stabilitet i forskellige redox stadier i et symmetrisk batteri celle set up, hvor samme koncentrationer men forskellige volumener blev anvendt, viste det sig at phoenicin blev kemisk nedbrudt efter at blive opløst i høj basisk elektrolyt. En redox flowbatteri test viste at phoenicin, som den negative elektrolyt, kunne lades og aflades i 14 dage med et kapacitetstab på under 50% i alt. Disse resultater demonstrerede derfor konceptet ved at bruge en svampe quinon til at lagre energi, og dermed er phoenicin et slags proof-of-concept.

Efterfølgende undersøgte jeg hvilken rolle phoenicins renhed spiller ved at teste et mix af fire phoenicin stadier som var produceret af *Penicillium phoeniceum* i større mængder. Analyserne af phoenicin mixet blev foretaget under mit besøg i laboratorierne på Dansk Teknisk Universitet.

Ved at bruge samme fremgangsmåde som ved det rene phoenicin i det første studie, viste de elektrokemiske egenskaber for phoenicin mixet at være sammenlignelige med det rene phoenicins. Dog viste det sig at phoenicin mixet var i stand til at indgå i fire-

elektron reaktioner per phoenicin molekyle i stedet for to. At phoenicin mixet kunne indgå i fire-elektron reaktioner blev ligeledes vist ved batteri test. I og med at det var muligt at opnå 1111 ladninger og afladninger i løbet af en tidsperiode på 13 dage viste det sig at det stadig var muligt at bruge phoenicin som negativ elektrolyt i et redox flowbatteri på trods af at det var et mix af forskellige phoenicin former og heriblandt phoenicin dimer. Yderligere undersøgelser viste at phoenicin blev nedbrudt ved en Michael-addition når det opløses i høj base, hvori flere nedbrydningsprodukter så som hydroxyleret phoenicin og forskellige polymerisering produkter som phoenicin dimer, trimer, quadromerer osv. blev identificeret. Resultaterne i dette studie viste derfor at et mix af forskellige phoenicin former medførte en fire-elektron reaktion for hvert phoenicin molekyle, hvorved det fulde kapacitetspotentiale for phoenicin opnås svarende til en to-elektron reaktion for hvert benzoquinon gruppe i molekylet (fire-elektron reaktion for hvert phoenicin molekyle).

Indholdet af forskningen i denne thesis kan derfor blive brugt som en guideline/protokol til fremtidig forskning indenfor brugen af svampe quinoner som elektrolytter i redox flowbatterier. Det viser klart at der er et potentiale ved at bruge svampe quinoner til at lagre vedvarende energi og jeg tror på at dette forskningsområde er værd at forske videre på fremtiden.

Table of contents

Preface	III
Acknowledgments	V
English summary	VI
Dansk resume	VIII
Aim	XII
Chapter 1. Introduction	1
1.1. Energy storage.....	2
1.2. Redox flow batteries	5
1.2.1. Aqueous organic redox flow batteries.....	8
1.3. Quinones (and quinone RFBs)	11
1.3.1. Naturally quinones	13
1.3.2. Phoenicin.....	14
1.3.3. Quinone degradation mechanisms.....	17
Chapter 2. Electrolyte characterization	19
2.1. Electrochemical properties	19
2.1.1. Redox potential and reversibility	21
2.1.2. Mass transfer	23
2.2. Solubility.....	26
2.3. Electrolyte stability in a redox flow battery	26
2.3.1. Symmetric cell cycling test	30
Chapter 3. Summary of results and discussions from papers	33
3.1. Demonstrating the use of a Fungal Synthesized Quinone in a Redox Flow Battery.....	32
3.2. Four-Electron Energy Storage in Biosynthesized Phoenicin Flow Battery Negolyte.....	42
3.2.1. Discussion of findings from Paper 1 and Paper 2	46
3.3. Are biologically synthesized electrolytes the future in green energy storage?	48
Chapter 4. Conclusions and perspectives	51
Literature list	55

Appendix A1. Quinone table	77
Papers.....	81

Aim

This dissertation is a part of a multidisciplinary project involving research with the goal of getting one step closer to being able to store renewable energy by using sustainable materials. The idea of using fungal-produced natural electroactive compounds to store energy made rise to a large multidisciplinary project, founded by the Novo Nordisk foundation to develop a fungal battery.

This project relies on an already-known storage technology called the redox flow battery technology, which uses liquid electrolytes to store energy. Many different materials have already been researched as electrolytes, including e.g., inorganic and organic compounds. In this project, we developed a new electrolyte based on a quinone compound produced by fungi and tested this in a redox flow battery.

Even though the electrolyte is one part of the puzzle in getting closer to an environmentally friendly and cheap storage device, the electrolyte properties and production itself came with lots of tasks. To develop a fungal battery, the multidisciplinary project included several work packages to cover all aspects of electrolytes based on fungal compounds.

Previous, initial research, also made by our group, made the foundation for the fungal battery project, Figure 1 (denoted 0 in the figure). This included especially an extensive simulation study, in which all known fungal quinones and their representative redox potentials were identified and collected in a database. From this database, the most promising quinone, concerning the simulated redox potential, the availability due to production, etc. was selected for further investigation in the fungal battery project work packages, which are illustrated in Figure 1.

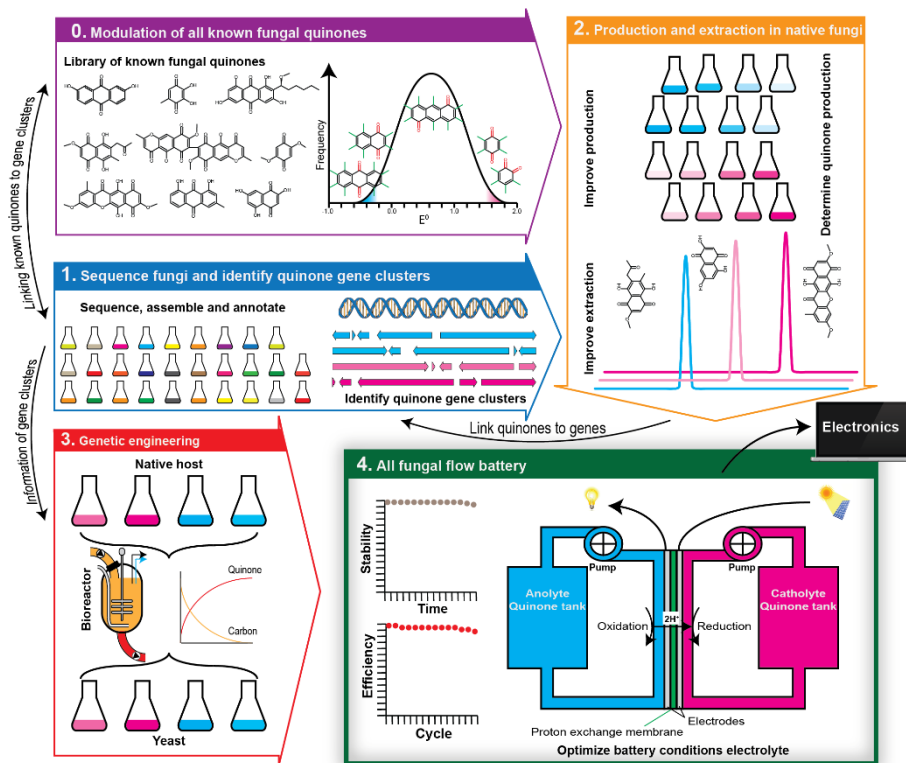


Figure 1. Overview of the fungal battery project showing the initial research performed in another project (0) as well as work packages 1-4, which cover all aspects of the fungal battery project.

The work packages in the fungal battery project, seen in the figure, can be described as the following:

1. Genome sequencing of fungal strains to identify the gene clusters responsible for the production of the fungal quinones of interest.
2. Development of production and extraction procedures for producing the fungal quinone of interest. This also includes further optimization to produce and deliver the selected fungal quinone to be tested in a redox flow battery.
3. Genetic engineering to enhance the production of quinone production.
4. Electrochemical characterization of the selected quinone and test in a lab-scale redox flow battery.

With the research in these work packages, the intention was to develop a sustainable and cheap production of a stable and good-performing electrolyte to store renewable energy.

Among these work packages, my Ph.D. project aims to cover work package number 4, dealing with electrochemical characterization and battery testing of the delivered fungal quinone. This means, that my project largely depended on the fungal quinone production and delivering from the other work packages. Because of the novelty and initial stage of the fungal battery project, quinone production was more time-consuming than first estimated. This means that more effort was put into producing a larger amount of one single fungal quinone. The fungal quinone that was produced and delivered for my Ph.D. project, was phoenicin. One reason for choosing phoenicin was due to it being produced in a rather pure amount from the fungal culture. Since most fungal strains can produce various amounts of compounds, we believed that phoenicin was a good first fungal-produced quinone candidate to test in my project.

Since all of the work packages of the fungal battery project passed off in parallel, the extent of research in my Ph.D. project was limited to the amount of phoenicin compound I received. This means that my research was planned and performed due to the limited amount of phoenicin, whereas amounts of battery tests and characterization studies were kept to a minimum to cover and identify as much information about this interesting compound as possible.

This Ph.D. project aimed to investigate the potential of using the naturally occurring and biosynthesized quinone phoenicin as the active material in an electrolyte for a redox flow battery, which can be divided into the following research questions:

- How does phoenicin electrochemically behave and is it suitable to be tested as an electrolyte in a redox flow battery?
- How many electrons is possible to store per molecule in phoenicin?
- How can the stability of phoenicin be determined?
- Is it possible to use phoenicin as an electrolyte in a redox flow battery? If so, how does this biosynthesized quinone perform compared to other quinones found in the literature?
- How do the purity and composition of phoenicin influence the potential of phoenicin as an electrolyte candidate for a redox flow battery?

Phoenicin worked as a proof of concept of using a fungal quinone in a redox flow battery, and the aim of this study can be summarized into the following objectives:

- Electrochemical investigations of the fungal quinone phoenicin to characterize the reversibility, redox potential, diffusion coefficient, and electron transfer rate constant.
- Stability study of phoenicin as an electrolyte in a redox flow battery with respect to the capacity, chemical- and electrochemical stability, and efficiencies.
- Evaluation of the purity of phoenicin necessary for use as an electrolyte in a redox flow battery.

Chapter 1. Introduction

With the continuously growing population as well as economic growth in developing countries and technological developments, global energy consumption and demand increase annually [1], [2], and combined with the harmful effects of the CO₂ emissions on the environment, the interest in renewable energy has increased worldwide [3], [4]. The global energy demand is expected to grow by 25% in 2040 and double by 2050 [1]. Most supply of today's energy consumption is provided by generators connected to the grid. These are fueled by fossil fuels in most cases, which causes air pollution and damage to the environment. The resources to fossil fuels are limited and the reserve levels are by the end of 2020 predicted to last 48.8 years for natural gas, 53.5 years for oil, and 139 years for coal [5], as well as these, are geographically dependent. Despite that, more than 80% of the worldwide energy consumption is still provided by these, as seen in Figure 2 [1].

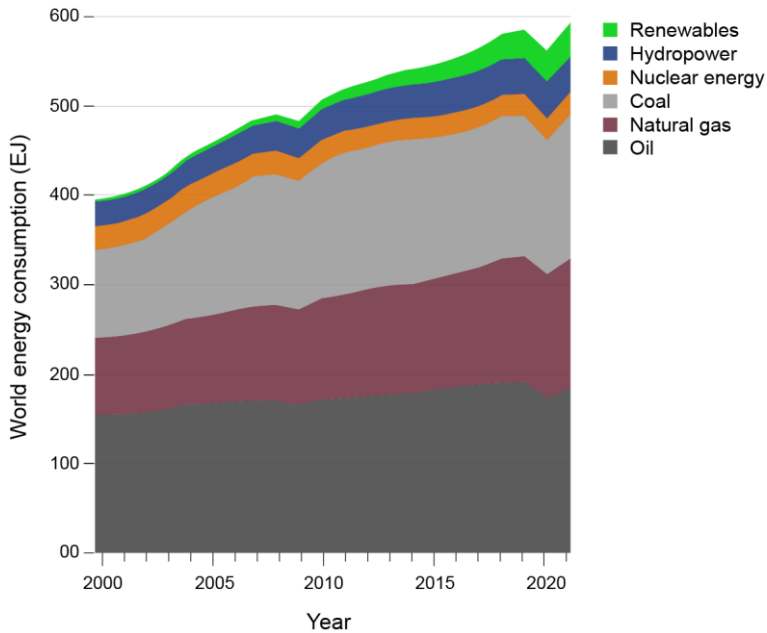


Figure 2. Total world energy consumption divided by fuel in exajoules. The evolution for each fuel source can be seen from 2000 to 2021 [6].

The major parts of the total energy consumption are electricity, transport as well as heating, and with increased use of electric vehicles and portable electronic devices, digitalization and electrification, the electricity demand is expected to increase further [5], [7]. To reduce carbon emissions and to meet the increasing worldwide energy

demand, the world aims for producing clean and green electricity by using renewable energy sources [8]. As seen in Figure 2, energy from renewables is already being employed at an annually increasing rate [2]. In 2019, 5.0% of the total annual energy consumption was provided by energy from renewables [9]. This contribution increased to 5.7% in 2020[10] and further to 6.7% in 2021 [6]. In Denmark, the amount of energy from renewables increases too, and in 2021, the total annual energy consumption provided by renewables reached 40.6% [11]. However, to further reduce the consumption of energy generated from fossil fuels and hereby climate changes due to pollution, the transition towards using more energy from renewables must be accelerated [12]. For this to succeed, a complete paradigm shift is required when it comes to energy production and consumption. The current global energy trade involves risks and insecurity as these are highly affected by global pandemics and geopolitical conflicts. In 2019, around 25% of oil, 40% of natural gas, and 50% of coal used in the EU were imported from Russia, and considering the current world energy crisis, becoming independent from foreign energy suppliers has never been more important [5], [13].

Unlike fossil fuels, renewable energy sources such as solar and wind are inexhaustible, have carbon-free characteristics, and are available for free. However, the availability of these sources varies in amounts at different time periods resulting in low reliability [8], [14]. To overcome the intermittent and unpredictable behavior of renewables, cheap and scalable storage technologies need to be developed to ensure a stable and sustainable energy supply for the future, that relies on renewable energy sources [4], [15], [16]. Additionally, the technology must also offer long-duration energy storage by being flexible and capable of storing energy in durations of hours, days, weeks, and seasons [17], [18].

1.1. Energy storage

The intermittency of renewable solar energy and wind power leads to periods with both high and low energy production during the day, which can vary up to 80% within time scales of minutes to hours [19]. This supports the need for storage technologies even more since the energy demand and consumption do not match this variability of available energy from renewables. The availability of surplus energy at the peak production does not always match the demand, resulting in surplus energy in the peak production periods as well as a lack of energy when the energy demand exceeds the energy production, as seen in Figure 3 [20], [21].

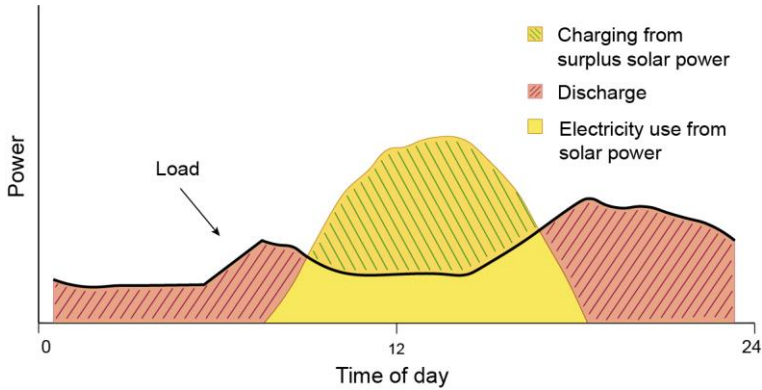


Figure 3. Energy storage management in a single day, using solar power. The scenario shows the average electricity load and solar production for a typical day in March or September in Denmark [22]. The variation in energy load demand can be seen during the day as well as how the load can be supplied by the solar energy available during the sunny hours. The use of an energy storage device illustrates how this can be charged from the surplus solar power (marked as charging), which can be released at peak load times or when the energy production from renewables is low (marked as discharge).

The electricity demand also varies during the day and so does the cost. At peak load time, the electricity demand is high and exceeds the energy production from renewables, and the grid infrastructure needs to be designed to tolerate this peak load time [23]–[25]. Energy storage systems should solve this by storing excess electricity from the grid and returning it whenever the demand exceeds the energy production from renewables, thereby making it possible to easily meet the demand without using costly power generation plants fueled by fossil fuels [23], [26]–[28]. For the storage system to balance the demand and renewable power generation, a fast response time to sudden fluctuations is needed.

The traditional lithium-ion batteries used in e.g., electronics and transportation industries due to their high energy density, lightweight, low self-discharge, and high efficiencies., etc., cannot work as a feasible long-duration grid-scale energy storage technology as they do not feature the possibility to cost-effectively store enough renewable energy required to facilitate the long discharge durations needed for regulating the intermittency of renewable energy sources [23], [29]. Besides this, factors such as their high cost[30], scarcity[31], and fire hazards from their organic solvents also limit their use as a grid-scale storage solution [2], [3], [32]. To increase the discharge duration of lithium-ion batteries, the cost would also increase since more cell packs are required [18]. Other known storage technologies such as electrical energy storage (e.g. capacitors) and mechanical energy storage (e.g. flywheels) are also limited to being used for short-duration grid services because of high self-discharge ratios and they are both cost prohibitive as examples [2], [3], [16], [33], [34].

A technology framework of high interest is the Power-to-X (P2X), which is a technology that transforms renewable electric power (P) into something else (X). In

Denmark, it defines the process of converting electricity from renewables into hydrogen. This is done by an electrolyzer through the electrolysis process (split of water into hydrogen and oxygen) using electricity from renewable energy [1]. Through this process, surplus energy from renewables can be stored as hydrogen for future electricity uses. By sending the hydrogen through a fuel cell, hydrogen is recombined with oxygen to produce water and electricity with low pollutant emissions [1]. It is expected that this technology will play a key role in future energy systems. Hydrogen can be stored in large capacities for a long time and is environmentally friendly. However, this comes with high costs and concerns about safety in case of leakage [17].

Because of global differences worldwide due to local resources available, the transition to renewables might be solved differently from place to place, and it is believed that the solution might be a combination of different approaches [26], [33]. The different storage technologies all come with advantages and disadvantages, and none of them can meet all the requirements at once, when cost, performance, availability, scalability, environment, etc., are considered [19].

The redox flow battery (RFB) is another viable, cost-effective, and safe technology that has been recognized for large-scale stationary energy storage, and offers energy and power to be scaled independently, as well as short response times (depending on the electrolyte kinetics) [3], [29], [35]–[37]. The RFB technology could be used to match the energy supply from renewables to the demand since the technology, in contrast to lithium-ion batteries, offers the ability of long-duration discharge e.g., due to the ability to decouple energy and power as well as lower self-discharge ratios, which is a result of having the electrolytes stored in separate reservoirs [29], [34], [38]–[40]. Flexibility in the energy and power ratio is an advantage as the energy density refers to the energy possible to store per unit volume or mass whereas the power density refers to the energy transfer rate possible per unit volume or mass, thereby making it possible to design the RFB device for the specific needs [16].

1.2. Redox flow batteries

The redox flow battery technology uses rechargeable electrochemical devices to store energy, which is converted between stored chemical energy and electrical energy [3], [41]. The energy is stored in a pair of soluble redox-active species with disparate electrochemical potentials, which is dissolved in a supportive electrolyte i.e., a salt in the main solvent such as water. The liquid electrolytes are kept in external tanks, which makes it possible to scale energy storage capacity (e.g. electrolyte reservoir volume and concentration of the redox-active compounds) and power (battery size) independently [3], [12], [41], [42]. These properties offer flexible designs to cover specific needs and make this technology suitable for grid-scale stationary energy storage [19]. A schematic representation of an RFB can be seen in Figure 4. It consists of an electrochemical cell and two separate reservoirs (which contain the electrolytes), circulating peristaltic pumps to ensure electrolyte flow, current collectors, electrodes, and a membrane.

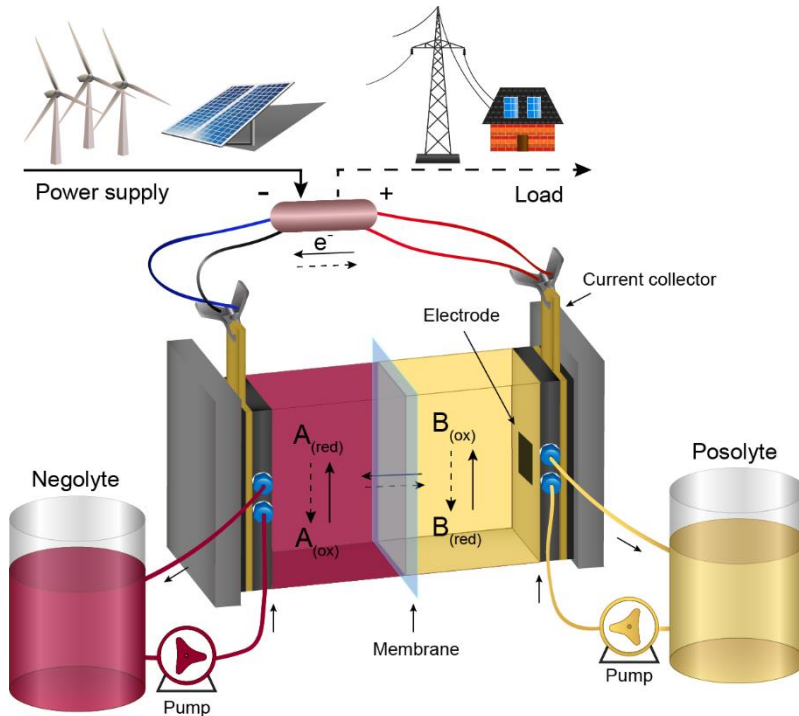
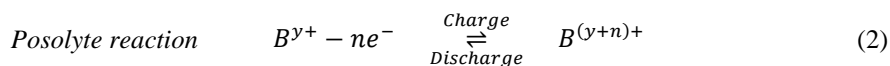
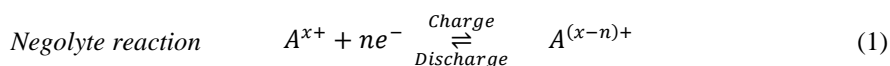


Figure 4. Schematic of a redox flow battery cell, containing an electrochemical cell and two separate reservoirs for the electrolytes. The two half-cells are separated by a membrane and the current collectors are connected to the power source/load. Solid arrows indicate the charging process, while dashed arrows indicate the discharging process. The small arrows indicate the flow direction.

The electrolytes are pumped into their representative half-cells during operation, where an electrochemical reaction takes place at the electrode area, which often consists of porous carbon electrode material [43]. The two half-cells are separated by an ion-selective membrane that prevents the mixing of the electrolytes while allowing transport for charge-carrying ions to ensure charge balancing during operation [3], [19]. The membrane needs to be mechanical and chemically stable towards the cycling conditions and the electrolyte solvent [40]. For the electrodes, a high surface area and good conductivity concerning the mass and electron transport are preferred. These properties as well as the reaction kinetics of the reactive species in the electrolytes on the electrodes influences the performance when it comes to energy and power densities, cycling stability, and energy efficiency [40].

The electrolyte with the lower redox potential function as the negative electrolyte and is called the negolyte (or anolyte), while the electrolyte with the higher redox potential is the positive electrolyte and is called the posolyte (or catholyte). During charging, electrons are transferred from the posolyte (being oxidized) towards the negolyte (being reduced) as seen below, and the opposite reaction occurs during discharging [44]–[46].



With the negolyte having a lower redox potential than the posolyte, the charging process proceeds as an unspontaneous reaction, driven by the energy from the power supply, whereas during discharge, energy can be released spontaneously. The cell voltage is determined by the difference between the redox potential of the active materials used in the posolyte and negolyte. A big difference between the redox potentials is preferable so a high cell voltage is reached, which results in higher current densities [47].

Stationary batteries must be able to operate for years to become a successful solution for renewable energy storage, and the stability and performance of the electrolytes must be well-established [48]. Besides disparate electrochemical potentials, properties such as solubility, kinetics, cycling stability, etc. should be considered when selecting the redox-active compounds for the electrolytes [49]. Due to the long discharge durations, the cost of the system in kWh depends more likely on the cost of the electrolytes rather than the cost of the electrochemical cell [3]. Therefore, electrolyte optimization is largely investigated to lower the cost as well as reach better performance and stability.

Many chemistries have already been investigated and studied as the active material for RFB electrolytes. To date, the vanadium flow battery (VFB) is the most researched and commercialized RFB system[40] since it can be operated at high concentrations, offers long cycle life, high-power density, fast charge and discharge, quick response times[2], [50] as well as limited electrolyte crossover due to the use of closely related vanadium complexes as electrolytes. These consist of the $\text{VO}_2^+/\text{VO}^{2+}$ couple ($\text{V}^{5+}/\text{V}^{4+}$ oxidation state) as the posolyte and the $\text{V}^{3+}/\text{V}^{2+}$ couple ($\text{V}^{3+}/\text{V}^{2+}$ oxidation state) as the negolyte both dissolved in a sulfuric acid electrolyte [12], [41], [51], [52]. VFBs allow a lifespan of 15,000-20,000 charge/discharge cycles[53] and the literature even suggests that 270,000 charge-discharge cycles have been demonstrated [54], [55].

Challenges to commercialized implementation of the VFBs are associated with the fact that vanadium is costly and associated with mining, and there are environmental drawbacks due to the impact of the highly corrosive electrolyte [29], [56], [57]. To deal with the high cost of vanadium, electrolyte recycling has been considered since no vanadium is lost during the operation [53], [58]. Even though the cross-over is limited, some extent of cross-over is still occurring due to the small size of the vanadium ions by diffusion and migration resulting in a change in electrolyte concentration or volume and self-discharge reactions [59]–[62]. Having both redox pairs of the same chemical element allows for the reconstruction of the original state of the electrolytes by rebalancing/remixing the electrolyte [56], [59], [61]. Yet, some plants are built around the world with storage capacities ranging from 0.1 – 6 MWh and are used e.g., for peak shaving and as backup systems, etc.[2].

Another challenge seen with the RFB technology is the restrictions due to the environmental temperature. If the RFB should be operated in all areas of the world, the electrolytes must be stable in all operating temperature conditions. Looking at the VFB, the temperature needs to be above 10°C due to the instability seen for V^{2+} , V^{3+} , and V^{4+} at lower temperatures [63], [64]. At temperatures below 10°C and above 40°C, the vanadium ions precipitate; however, this stability also depends on the concentration of the vanadium ions and the sulfonate solution [65]. For large-scale implementation, this temperature dependency would require temperature control, which comes with energy loss and further increases the overall operation cost [66].

In most cases and practical systems, the VFB electrolytes often consist of concentrations of 1.6 – 1.8 M vanadium, which yields volumetric capacities of 42.9 – 48.2 Ah L⁻¹ [62], [67]. Nevertheless, studies have achieved higher volumetric capacity by reaching solubilities up to 2.5 M with a mixed electrolyte of vanadium sulfate and chloride[66] and 3.0 M by adding precipitation inhibitors [67].

Growing research and interest in aqueous organic redox flow batteries (AORFBs), which builds on water-soluble organic molecules to be used as electrolytes, have been seen over the past decade [40], [49]. Using organic active materials could offer the possibilities of lower cost and environmentally friendly scalable electrolytes since

many of them are abundant and bio-sourced, which are advantages over the vanadium system [40], [41], [68], [69].

1.2.1. Aqueous organic redox flow batteries

The use of water-soluble organic redox couples to constitute the positive and negative electrolyte solutions in RFBs has been investigated since the 2010s [70]–[72]. Among some of the organic compounds researched are quinones, viologen, TEMPO (2,2,6,6-tetramethylpiperidine-1-oxyl), and ferrocenes [70]. An overview of some organic compounds researched in the literature, their redox potential, and their volumetric capacities are provided in Figure 5. The organic compounds show comparable volumetric capacities with that of the vanadium species and are even higher in some cases. The volumetric capacity possible to obtain is directly linked to the solubility of the compound in the used solvent [39]. For example, this is the reason for the high volumetric capacity that can be obtained for quinone compound 5, seen in Figure 5 (DHBQ), which shows very high solubility in 1 M KOH [73].

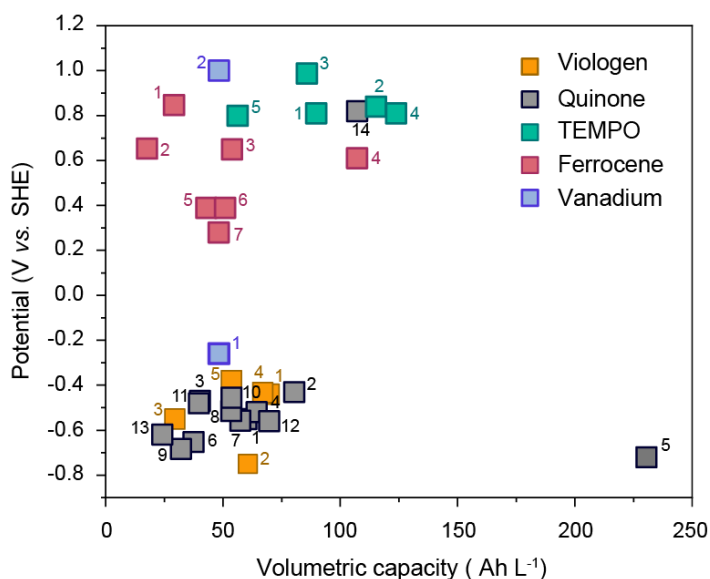


Figure 5. Overview of the redox potential and volumetric capacity (based on solubility) of some organic compounds tested in RFBs to compare with that of a VFB. **Viologen:** ¹ [(NPr)₂TTz]Cl₄[74], ² [PyrPv]Cl₄[75], ³ R-Vi[76], ⁴ MV[77], ⁵ BTMAP-Vi[78], [79]. **Quinone:** ¹ Bislawsonel[68], ² PEGAQ[80], ³ 2,6-DPPEAQ[32], ⁴ 2,3-HCNQ[49], ⁵ DHBQ[73], [81], ⁶ 2,3-DHAQ[82], ⁷ 1,8-BDPAQCl₂[83], ⁸ 2,6-DBEAQ[29], ⁹ 2,6-DHAQ[84], ¹⁰ DBAQ[85], ¹¹ DPivOHAQ[85], ¹² DCDHAQ[86], ¹³ 2,6-N-TSAQ[50], ¹⁴ DHDMSBS[87]. **TEMPO:** ¹ Pyr-TEMPO[75], ² TMAAcNH-TEMPO[88], ³ TMA-TEMPO[77], ⁴ TMAP-TEMPO[79], ⁵ 4-HO-TEMPO[89]. **Ferrocene:** ¹ Na₄[Fe^{II}(Dcbpy)₂(CN)₂][90], ² Fc3 and ³ Fc4[91], ⁴ FeNCI[92], ⁵ (NH₄)₄[Fe(CN)₆][93], ⁶ BTMAP-Fc[78], ⁷ Fc(SPr)₂[94]. **Vanadium:** ¹ V³⁺/V²⁺ and ² V⁴⁺/V⁵⁺[62], [67], [95], [96].

Ferrocenes are organometallic compounds that are studied as posolyte materials for RFB electrolytes due to their stable and reversible redox reactions [91], [94]. They are based on low-cost materials well-suitable for large-scale production [92]. Despite this, many of them are only soluble in organic solvents and decomposition of ferrocene compounds has been observed when tested in RFB systems, especially degradation has been seen for the oxidized form of ferrocene [4], [78], [91], [92], [97]. To improve ferrocene solubility in water, different modifications have been proposed e.g., ammonium-functionalization of ferrocene derivatives [92].

Viologens are established redox components offering a rapid and reversible transition between stable oxidation states, and low reduction potentials [76]. They are researched as potential negolytes, and with their good solubility in neutral pH conditions, they offer high theoretical volumetric capacities, as well as low environmental impact [98], [99]. However, they suffer from temporal capacity fade due to radical dimerization [98].

TEMPO and its derivatives are stable and offer good chemical reversibility, fast kinetics, good solubility in neutral pH, and low cost [40], [77], [100]. They are promising candidates to be used as posolyte materials as they show positive redox potential. Despite this, they suffer from decomposition and self-discharge so improvements in the stability of the redox states are needed to ensure longer cycle life and higher efficiency when used in an RFB [100], [101].

Besides the solubility of the redox-active compounds, the number of electrons involved in the redox reaction influences the capacity possible to achieve in the RFB. This has raised interest in organic compounds offering multielectron transfer reactions.[102] Such compounds are quinones, which undergo two-electron reactions over various potentials[103], [104], and with most of them having open sites on the carbon ring, many different structural modifications are possible [105]. Most quinones have been researched as the negolyte material due to negative redox potentials, but some quinones have also been seen tested as posolyte material [70], [103]. As seen in Figure 5, some quinones offer high volumetric capacity due to high solubility as well as multielectron reactions. However, with the current state-of-the-art ion exchange membranes, high quinone solubility is likely not practical because hydroquinones are small molecules ($100 - 200 \text{ g mol}^{-1}$) that can permeate these membranes [70]. Furthermore, most quinones suffer from degradation processes influencing the stability and battery lifetime.

In general, drawbacks of the organic species used in RFBs are low energy density, low practical volumetric capacity, and low chemical stability as the organic molecules are susceptible to degradation reactions such as Michael addition, disproportionation, dimerization, etc.[29], [39]. Another cause for the low energy density seen for AORFB is the low operating voltage which is restricted by the stability window of the aqueous electrolyte and limited by the oxygen evolution in high-potential and by the

hydrogen evolution in low-potential operations [106], [107]. But taking safety, the environment, and availability into account, water is the most optimal choice as a solvent for the electrolytes in the RFB. Other advantages of using water as a solvent are good ion solubility and conductivity [36].

On the other side, organic redox-active molecules are of high interest as they offer many possibilities and variations in electrochemical and physical properties, which can be tailored using chemical synthesis and/or molecular engineering [42], [49]. This includes among others the possibility of chemical modifications and functionalization resulting in improved performance in the terms of voltage and energy density [29]. For example, the voltage can be regulated by adding electron-donating groups, such as hydroxyl groups (lower the redox potential of the molecule), or electron-withdrawing groups, such as sulfonic acid groups (elevate the redox potential) [15], [49]. The addition of such groups also tends to increase the solubility in aqueous solutions, which has been seen in much research already [36], [47], [108]. These possibilities allow for shaping the cell potential by modifying the redox-active species, as well as obtaining higher energy density by increasing solubility. In practice, a high cell potential is preferable since the opposite would provide lower stack power density and efficiency of the battery performance resulting in increased costs [70].

Even though the capacity can be increased by simply making larger electrolyte reservoirs, the available space, as well as cost, must be considered. Another way of increasing the volumetric capacity is by looking at the number of electrons stored per unit volume as well as increasing the solubility [80], [109]. Therefore, especially quinones are of high interest and have been one of the main candidates researched for RFB electrolytes [108].

1.3. Quinones (and quinone RFBs)

Benzoquinones, naphthoquinones, and anthraquinones have been explored widely as active materials in RFB electrolytes, and the structure of the three common quinone types can be seen in Figure 6 [47].

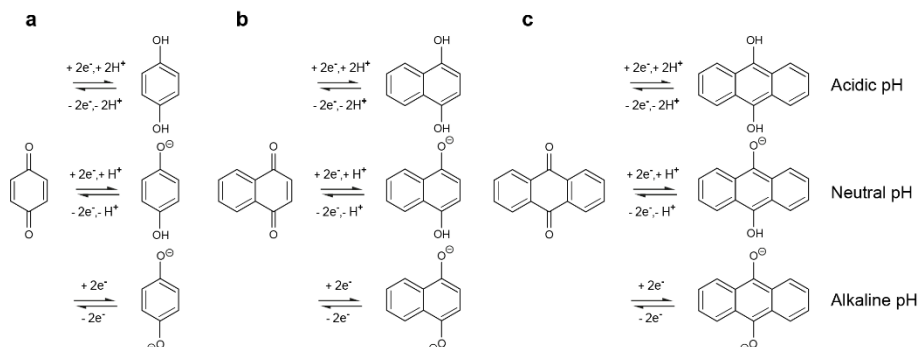


Figure 6. Structures of the common quinone types and their corresponding reduction reaction in different pH. The two carbonyl groups are placed in *para*-positions in the structures shown. a) 1,4-Benzoquinone [110]–[113], b) 1,4-naphthoquinone [68], [108], [114]–[117], c) anthraquinone [43], [50], [118]–[122].

Quinones consist of aromatic ring structures (benzene rings) linked with carbonyl groups. They are divided according to the number of benzene rings in the backbone structure [123], [124]. Having the simplest structure, benzoquinones consist of one aromatic ring with two carbonyl groups placed in either *ortho*- or *para*-position, while naphthoquinones are bis-cyclic aromatic and anthraquinones are multi-cyclic aromatic hydrocarbons [4], [125].

In an aqueous solution, quinones undergo reversible two-electron reactions due to them having two carbonyl groups present in their structures [4], [126]. The redox properties of the quinones largely depend on the operating conditions such as the supportive electrolyte and pH. As seen in Figure 6, the pH impacts which protonated form of the reduced and oxidized species that participate in the redox reaction [36]. At low pH, the reduction reaction proceeds as a single-step two-electron two-proton process. At high pH, the reduction reaction is a two-electron process and does not involve protons. In a neutral pH solution, the reduction reaction is somewhere in between and proceeds as a one-proton two-electron reaction or proceeds as seen in a high alkaline solution [127], [128]. Furthermore, the reduction potential varies with pH and becomes more negative with increasing pH. Since a low reduction potential of the negolyte is preferred to achieve high cell voltage of the RFB, alkaline supportive electrolytes are often used [129].

Quinones are well-researched in this field, and some performance characteristics seen from RFB full-cell cycling experiments in the literature with different quinones as

electrolyte material can be seen in Table A1. As seen in the table, especially anthraquinone derivatives have been investigated over the years, and they show good solubility in both acidic solutions through sulfonation and in alkaline solutions through hydroxylation. Because of the low redox potentials observed for many of them, they are good candidates for negolyte materials [47], [130]. The anthraquinones also show better cycling stability compared to benzoquinones, which can be reasoned by greater chemical stability due to the additional two rings. The temporary stability and theoretical capacity of the quinones summarized in Table A1 are illustrated in Figure 7.

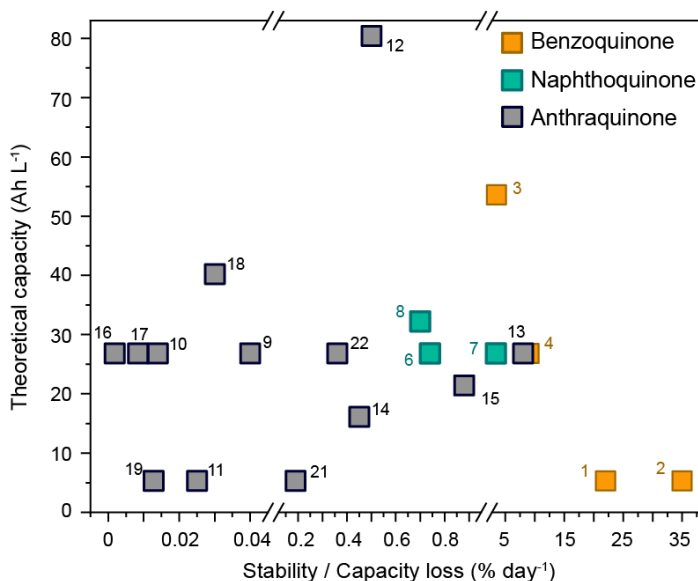


Figure 7. Summary of quinone stability vs. theoretical capacity obtained from the RFB cycling conditions shown in Table A1. ¹DMBQ[131], ²DMOBQ[131], ³DHDMBS[87], ⁴DHBQ[73], ⁶Bislawson[68], ⁷2,3-HCNQ[49], ⁸NQSO[129], ⁹2,6-DBEAQ[29], ¹⁰2,6-DPPEAQ[32], ¹¹2,6-N-TSAQ[50], ¹²PEGAQ[80], ¹³2,6-DHAQ[84], ¹⁴2,3-DHAQ[82], ¹⁵1,8-BDPAQCL₂[83], ¹⁶DPivOHAQ[85], ¹⁷DBAQ[85], ¹⁸DCDHAQ[86], ¹⁹AQDP[132], ²¹DAEAQ[133], ²²1,3,5,7-THAQ[134].

By using different synthetic approaches, the stability of anthraquinones has been improved remarkably and research in the anthraquinones such as 2,6-DBEAQ, 2,6-DPPEAQ, and DBAQ have shown good long-term stability with a capacity fade rate in the range of $8 \times 10^{-3} - 4 \times 10^{-2} \% \text{ day}^{-1}$ (also seen in Figure 7 and Table A1), and the fade rate has even been reported as low as $1.8 \times 10^{-3} \% \text{ day}^{-1}$ when DPivOHAQ was cycled against ferrocyanide [85]. Despite the good long-term stability reported for these anthraquinones, the high synthetic cost still hinders their use in large-scale applications [50].

Lowering the cost of the electrolyte material is of huge importance for the scalability of this technology. Most of the quinones tested as electrolytes in RFBs are synthetically produced from non-renewable feedstocks and the cost of these organic

compounds mainly relates to the complexity and scale of the synthesis [70], [135]. Crude oil is rich in anthracene, which can be oxidized on large scale to anthraquinone. Raw components from coal tar are also used on large scale to synthesize naphtho- and anthraquinones [125]. But relying on the production of electrolytes from fossil-derived hydrocarbon sources does not suit as a sustainable solution due to the large volume of electrolytes needed for energy storage [136]. If RFBs with quinone electrolytes should be considered as the future storage technology for renewable energy sources, the quinones should be highly available and of low cost. Therefore, sustainable and cheap production with the low environmental impact of the quinones is highly preferred [20], [137]. Nevertheless, quinones, with their reversible redox activity, are also widely distributed in nature and can be found in plants, bacteria, and fungi [123], [138], [139].

1.3.1. Naturally quinones

The research on quinones derived from renewable feedstocks is limited in the literature. Until now, only a few examples have been demonstrated for use as active materials for RBS electrolytes. A potential renewable bio-source of precursors for quinone production is lignin (one of the main components in wood waste) [40], [140]. From lignin, 4-hydroxy-3-methoxybenzaldehyde (vanillin) can be extracted, which can further be oxidized to 2-methoxy-1,4-hydroquinone (MHQ) [136]. In 2020, Schlemmer et al. synthesized MHQ from vanillin, which can be purchased from Sigma Aldrich. In alkaline conditions, they further oxidized MHQ to produce 2-methoxy-1,4-quinone (MQ). The solubility of MHQ was measured to be 140 g L^{-1} in 0.5 M phosphoric acid, giving a volumetric capacity of 5.36 Ah L^{-1} , which is below the values seen for quinones in Figure 5. Cycling of MHQ in phosphoric acid against para-benzoquinone (pBQ), a coulombic efficiency of 97 – 99% was reported with an average capacity loss of $0.35\% \text{ cycle}^{-1}$. Taking the synthesis procedure into account, they calculated the material cost to be approx. 7.5 EUR kg^{-1} of MHQ [136].

Another case is 2-hydroxy-1,4-naphthoquinone (2-HNQ), known as “lawsone”, which is found in nature by being extracted from the leaves of henna trees as well as from the flowers of water hyacinths, resulting in a low-cost red-orange dye. Lawsone offers the possibility of a reversible two-electron redox reaction from quinone form to phenol form. This reaction offers a potential of -0.49 V vs. SHE and a solubility of 0.47 M in 1 M KOH giving a volumetric capacity of 25.19 Ah L^{-1} for a two-electron reaction [49]. Poor cycling stability has been observed for lawsone when cycled against ferrocyanide in KOH [141]. The reason for this low stability has been hypothesized to be caused by a Michael attack on the open aromatic C-H position. To deal with this issue, Tong et al. linked two lawsone units together via their open positions hereby creating a naphthoquinone dimer (2,2'-bis(3-hydroxy-1,4-naphthoquinone) called “bislawsone” and doubling the number of electrons possible to transfer per molecule. This was done by a one-step radical dimerization of lawsone with the use of inexpensive chemicals and solvents [68]. The reduction potential was decreased to

-0.55 V vs. SHE in 1 M KOH and a higher solubility of 0.56 M was seen. With a four-electron transfer, this solubility would yield a volumetric capacity of 60 Ah L⁻¹ in 1 M KOH solution, and the cycling performance of bislawsone in an RFB can be seen in Table A1.

In another study, lawsone has been mixed with NQ-S by a nucleophilic attack in high pH KOH solution to produce NQ-SO. This increased the solubility to 1.26 M in 1 M KOH (lawsone 0.42 M in 1 M KOH [108]). Besides the results seen in Table A1, the authors also tested a full-cell RFB setup using a higher concentration of 1.2 M NQ-SO against ferrocyanide. However, increasing NQ-SO concentration resulted in decreased cycle stability. The authors ascribed this to the suppression of NQ-SO dimerization when using lower concentrations [108].

In the fungal battery project, we believe that replacing quinones synthesized from non-renewable feedstocks with naturally occurring quinones produced by e.g., fungi offers higher availability and a more sustainable electrolyte production for large-scale applications since they can grow in industrially scaled bioreactors on cheap substrates [125], [142].

In research before the fungal battery project, Kristensen et al. made a simulation study in which the reduction potential and solubility in an aqueous solution for naturally occurring quinones were made. This screening identified the properties of 990 naturally occurring quinones and worked as the foundation for exploring potential candidates to be used as electrolyte material in an RFB. It also demonstrated the large potential and possibilities of using natural sources to produce quinones. Among the 990 identified naturally occurring quinones, 358 are produced by fungi [135]. Filamentous fungi produce secondary metabolites including quinones, and the production can be up-scaled and produced for industrial needs with relatively cheap substrates and waste products [125], [143]–[146].

Based on a systematic screening of the fungal quinones found in the simulation study [135] as well as considering the availability and the possibilities within the production of phoenicin, this compound was selected as the first candidate for a fungal quinone to be tested in a redox flow battery as the active material in the negative electrolyte.

1.3.2. Phoenicin

Phoenicin is an interesting compound with a dimeric benzoquinone structure, which is similar to oosporein and to that of a benzoquinone dimer [147], [148]. This structure, Figure 8a, possesses the potential of a four-electron transfer per phoenicin unit, which makes phoenicin a really interesting quinone to test as an RFB electrolyte candidate [149]. As reported for the structurally similar 2,2'-bis-*p*-benzoquinone (BBQ), the structure also predicts a four-electron reaction per molecule [150].

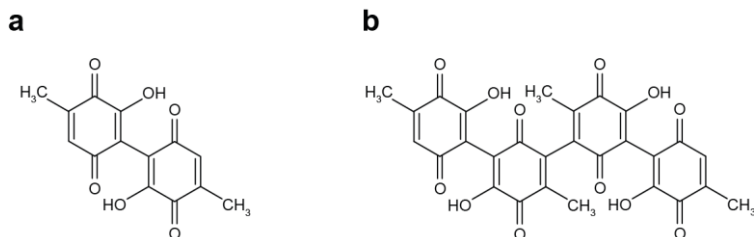


Figure 8. Structures of a) phoenicin and b) phoenicin dimer.

Phoenicin is a deep red pigment produced by several *Penicillium* species such as *P. atrosanguineum*, *P. manginii* [151], and *P. phoeniceum* [152]. There are many possibilities to improve phoenicin production, e.g. growth conditions optimization and genetic engineering [125].

The phoenicin used in the following studies, Paper 1 and Paper 2 (discussed in Chapter 3), was produced by two *Penicillium* species; *P. atrosanguineum*, and *P. phoeniceum* in two separate batches (produced and provided by work package 2, the Department of Biotechnology and Biomedicine at the Technical University of Denmark, DTU). The production, as well as composition and purity of phoenicin, varies with the wildtype *Penicillium* species as well as the growing conditions, and during fungal cultivation, phoenicin is produced and released from the mycelium into the growth medium [143], [153].

Initially, the phoenicin used in the first study (Paper 1 [154]) of this dissertation was produced by *P. atrosanguineum*. Incubation of phoenicin spores in Czapek-yeast-broth (CY) growth media for 14 days at 25°C in darkness resulted in a dark red supernatant. The supernatant was filtered, acidified (pH 2), and extracted with a three-step liquid:liquid partitioning. These steps involved extraction with ethyl acetate, redissolved in ethyl acetate and partitioning with sodium hydrogen carbonate water, and a final step of extraction using ethyl acetate. For acidification, trifluoroacetic acid was used. After evaporation of the organic phase and freeze-drying, without any further modifications, the resulting extract contained a concentration of 1.24 g L⁻¹ liquid media of which 95% was phoenicin, having a structure seen in Figure 8a [154].

The biosynthetic pathway of phoenicin in *P. atrosanguineum* has been identified, and since it is believed that fungal quinones share common biosynthetic pathway traits, this discovery can be used to enhance fungal quinone production by generic engineering and to modify and design the quinone structure to improve performance, stability, etc. [154]. It was predicted that the gene cluster for phoenicin involves a polyketide synthase (PhS1), a transcription factor (PhS3), a hydroxylase (PhS4), and a laccase (PhS5) as seen in Figure 9a. To further validate this, a clustered regularly interspaced short palindromic repeats (CRISPR)/Cas9 approach was used to disrupt the PhS1, which stopped the phoenicin production, as seen in Figure 9b.

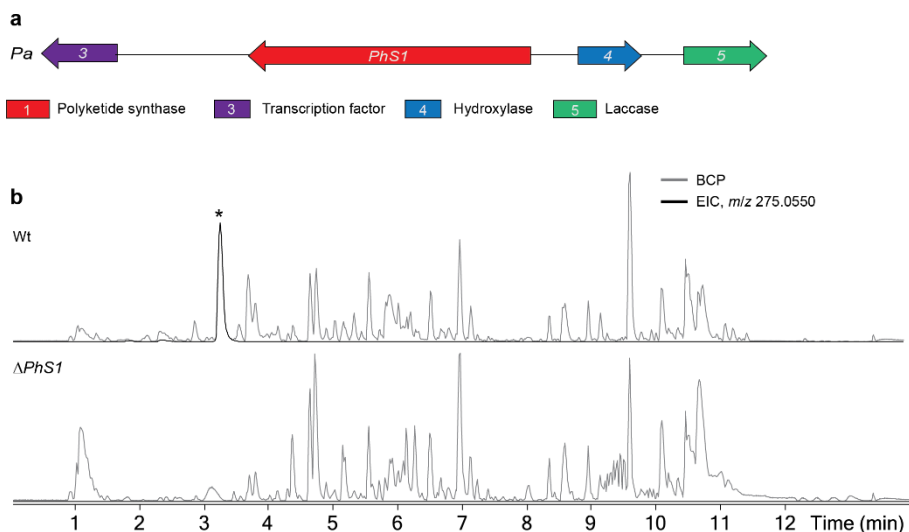


Figure 9. The predicted gene cluster for phoenicin. a) Gene clusters involved in phoenicin biosynthesis in *P. atrosanguineum*. b) Base peak chromatograms and the ion chromatogram for phoenicin in *P. atrosanguineum* wildtype (Wt) and a PhS1 disrupted transformant (Δ PhS1) [154].

The production of phoenicin from different species has recently been studied using different growth media [143]. When cultivating *P. atrosanguineum* for 11 days using CY-based media with 90 g L^{-1} sucrose, which corresponded to a carbon-to-nitrogen ratio of 38.6. Using this media, a phoenicin production of around 1.3 g L^{-1} was obtained. However, when cultivating *P. phoeniceum* under the same experimental conditions, a mean phoenicin production of 4.2 g L^{-1} was obtained. This was improved even further by lowering the incubation time to seven days, giving a mean phoenicin production of 4.9 g L^{-1} [143].

This optimization of phoenicin production made phoenicin more feasible and even more interesting to investigate. Therefore, *P. phoeniceum* was used to produce the phoenicin used in the second study (Paper 2) of this dissertation, from the above-described optimized method. In this case, ethyl acetate was used for the extraction supernatant and hydrochloric acid was used for acidification. However, the phoenicin produced from this optimized method consists of several forms of phoenicin, including phoenicin dimer, Figure 8b. With this structure of two linked phoenicin units, it can be speculated if even more electrons can be involved with the phoenicin dimer. With the discovery of the phoenicin dimer, this phoenicin batch was investigated as an RFB negolyte material to discover if the presence of the phoenicin dimer affects the stability, the possible capacity to be stored per molecule, and the performance of the battery.

1.3.3. Quinone degradation mechanisms

Long-term capacity loss during operation would require frequent replacement of the electrolytes to keep the total available battery capacity sufficient, resulting in higher costs [4]. Quinones are susceptible to structural decomposition, and conversion into redox-inactive molecules, leading to irreversible capacity loss over time [155]; therefore, several mechanisms have been identified and proposed as a cause for capacity loss seen in quinone RFBs. Much effort has been put into improving the stability of quinones when used as electrolyte active material in RFBs, especially since the annual replacement cost of the electrolytes is inversely proportional to the electrolyte lifetime [3]. As described earlier, quinones participate in reversible electron transfer reactions due to their carbonyl groups. However, the electron transfer reactions can also be irreversible in cases where the reaction product undergoes side reactions forming redox-inactive compounds [156].

Many of the quinone structures consist of aromatic rings with one or more unsubstituted carbon atoms. In benzo- and naphthoquinone structures, the unsubstituted carbon atoms next to the carbonyl groups are prone to Michael addition when reacting with the aqueous solvent, which is seen as one typical cause for the capacity loss [87], [157], [158]. Figure 10a shows a case of Michael addition of water to benzoquinone.

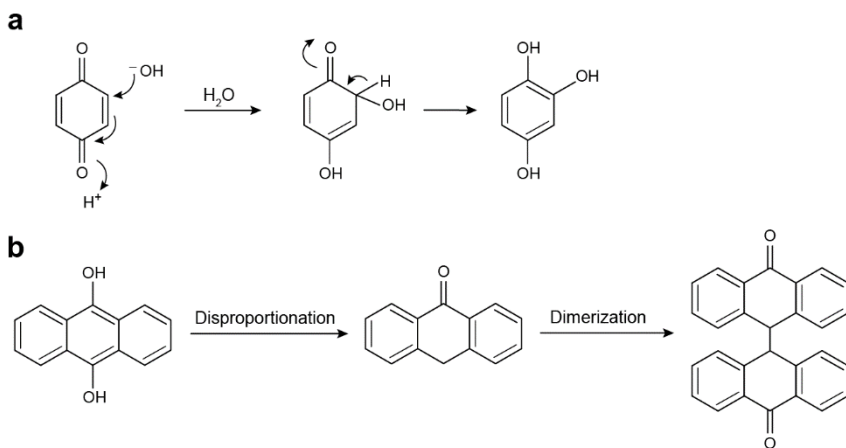


Figure 10. Typical degradation mechanisms found for quinones. a) Michael addition. Nucleophilic attack of water to an unsubstituted carbon atom on benzoquinone [4], [156], [157]. b) Anthrone formation of the reduced state of anthraquinone followed by dimerization due to oxidation [3], [50], [119], [159].

In some cases, the degradation product of Michael addition can still be redox active. However, to further utilize the fully substituted compounds, an excess of active material in the other electrolyte would be necessary. Moreover, the Michael addition during cycling operation also results in lowering the redox potential, which affects the cell voltage [160].

The Michael addition reaction can be limited by molecular optimization of the quinone by adding either electron-donating groups or electron-withdrawing groups onto the open aromatic C-H position, hereby blocking the unsubstituted carbon [68], [70]. The blocking strategy was used in a study made by Yang et al., where they tested the DHBQ against ferrocyanide in a full-cell battery [73]. As seen in Table A1, the battery suffered from high-capacity loss, which they attributed to degradation caused by Michael addition due to DHBQ having two unsubstituted positions in the structure. They reduced the capacity loss from 0.24% to 0.02% cycle⁻¹ by lowering the electrolyte pH from 14 to 12 and hereby lowering the concentration of hydroxide ions. They also successfully improved the stability of the cell by blocking the two unsubstituted positions by polymerization of DHBQ. Battery cell cycling of polymerized DHBQ against ferrocyanide at pH 14 resulted in an even lower capacity loss of 3.8×10^{-2} % cycle⁻¹ [73].

Another degradation mechanism studied in the literature is the anthrone formation and dimerization, which is often seen for anthraquinones, Figure 10b [4], [159], [161], [162]. Such a case was seen for 2,6-DHAQ. To study the decomposition of 2,6-DHAQ, Goulet et al. identified the degradation product to be 2,6-dihydroxyanthrone (DHA) as a result of cell cycling. Further oxidation of DHA resulted in irreversible anthrone dimerization [159]. Even though the dimers can be redox active in some cases, this still negatively affects the cycling performance by lowering the operating cell voltage (due to changes in redox potential) and a lower capacity due to twice the molecular weight meanwhile maintaining the same numbers of possible electrons to react. To limit the irreversible anthrone dimerization, they reduced the state of charge (SOC which describes the ratio of the stored charge to the maximum possible capacity [163]) from accessing 99.9% to only accessing around 88% of the theoretical capacity when charging. By doing so, they decreased the amount of degradation product formed, resulting in increased stability, and the capacity fade rate was reduced from 5.6% day⁻¹ to 0.14% day⁻¹ [159].

Studies show that the extent of dimerization depends on the electrolyte concentration used in the RFB cell cycling and high self-dimerization of AQDS at high concentrations was reported for bisulphonated quinones [164], [165]. As a result of this, dimerization prevents the full oxidation of the molecule, which means there will be unstable redox-active species in highly concentrated electrolytes [166].

Another reason for the capacity loss is the reaction with atmospheric oxygen. Quinones in the reduced state (hydroquinone) are known for their sensitivity toward molecular oxygen [167]. Oxidation of the reduced state by molecular oxygen would lead to self-discharge if oxygen is present. The reaction with ambient air is not considered a hindrance to the practical implementation of RFBs since the protection of the electrolyte against ambient oxygen has been successfully realized in commercial-scale VFB by purging an inert gas, such as argon, in the electrolyte reservoir headspace [32].

Chapter 2. Electrolyte characterization

The role of the electrolyte is to work sufficiently in a redox flow battery concerning charge-discharge cycles, hereby storing and releasing energy. Therefore, for a new compound to be considered as a potential electrolyte material in an RFB, several investigations and characterizations must be performed. This is typically done in a specific order, which among others includes electrochemical characterization and flow battery cell cycling. This chapter describes how electrolytes are characterized with respect to electrochemical properties and performance in a redox flow battery cell.

Before testing the compound as an electrolyte in a redox flow battery cell, electrochemical characterizations are made by using a specialized electrochemical cell setup. To save time and effort, this is done before battery cell testing, as battery tests use a more complex setup as well as more compound material.

2.1. Electrochemical properties

Being able to participate in redox reactions is one critical requirement for working as an active compound in an RFB. The redox activity is related to the redox potential of the molecule, which denotes the ability to either accept or donate electrons. The more positive redox potential, the more likely the molecule is to be reduced (acceptance of electrons), and the more negative redox potential, the more likely the molecule is to be oxidized (donation of electrons). The diffusion coefficient, D , and the electron transfer rate constant, k^0 , are both fundamental properties of a redox-active compound and are essential parameters governing the performance of an RFB. The charge and mass transfer affect the energy efficiency (ratio of energy output between discharge and charge) and power density (power output per membrane area) of the RFB [19], [35], [168]. With this in mind, knowing how the reactant is transported to the electrode surface, and how the product leaves it is of high importance [169], and information about mass transport can be extracted from the study of electron-transfer processes.

If we take a deeper look into one of the RFB half-cells, the mass transport and electrode reactions are illustrated as an example in Figure 11. When power is supplied to the battery, electrons are transferred from the active materials in the posolyte (by oxidation) through the positive electrode towards the negative electrode resulting in negolyte reduction. For this to happen, the active materials in the electrolytes must be transported, via diffusion, to the electrode to either donate or accept electrons. The diffusion of the active material from the bulk solution towards the active electrode area is determined by D , which is preferred to be as high as possible to ensure fast

transfer of the molecules. The charge transfer occurs at the electrode surface; therefore, the faster the diffusion, the more molecules are transported to the electrode, resulting in more charge being transferred [47]. When the molecules have been transported to the electrode surface, it is time for the redox reaction to take place. The k^0 determines the rate of the redox reaction, which is a measure of how fast the molecule is either oxidized or reduced. A fast cell reaction comes with a high k^0 allowing high current densities. Therefore, these parameters are important to investigate when searching for new electrolytes for RFBs.

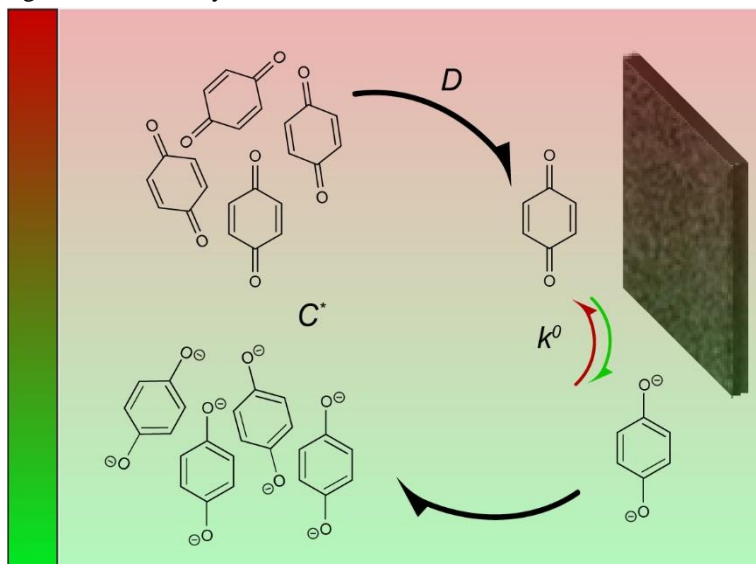


Figure 11. Negative half-cell example of an electrode reaction during charge and discharge of the electrolyte in a high alkaline environment. The bar indicates the charge level with green being fully charged and red being fully discharged. The quinone is reduced during charging (accepts two electrons), while it is oxidized during discharging (loses two electrons).

The electrochemical properties are characterized by the measurements of voltage and currents through the electrolyte. In the case of RFBs, measurements are typically done through testing in a flow battery or electrochemical cells using methods such as cyclic voltammetry (CV) or rotating disc electrodes (RDE). These are dynamic techniques (recording of time-dependent occurrences) in which a potentiostat is used to control the potential and the current is measured as a function of the potential [170]. Common for the voltammetric techniques is the need for electrodes to be in direct contact with the electrolyte solution of interest to study the charge transport/transfer in the electrolyte [170]. Three electrodes serve this purpose and include a working (WE), a reference (RE), and a counter electrode (CE) immersed in the electrolyte. The electrochemical reaction takes place at the WE, of which electrical potential is controlled with reference to the RE to ensure that the real potential is the same as the applied cell

voltage [163], [171]. This is possible due to the RE having a fixed potential as no current passes through this electrode [170]. When applying a potential to the electrodes, the corresponding currents are measured, and this potential-current relationship is determined by the electrochemical reaction that is investigated [172], [173]. During the electrochemical reaction at the WE, a number of electrons are transferred, which are counter-balanced at the CE, and the voltammetric signals hereby provide information about the electron transfer steps of a reaction [174]. To be able to determine the magnitude of the flowing current, the surface area of the WE need to be smaller than the surface area of the CE so that the flowing current is limited by the WE [170].

Cyclic voltammetry is a widely used technique for the characterization of electrochemically active systems and can be used to study everything from simple redox processes to multielectron-transfer processes [171]. The technique is good to use as an initial electrochemical investigation of the redox potential, reversibility, kinetics, and diffusion coefficients of the electrolyte/redox active material [37], [42].

2.1.1. Redox potential and reversibility

Figure 12 shows a typical cyclic voltammogram (DHBQ dissolved in high pH KOH). As the arrow indicates, the CV was obtained by scanning negatively from 0.0 V toward the negative limit of -1.2 V and reversed to the upper limit of 0.0 V, at a scan rate of 100 mV s⁻¹.

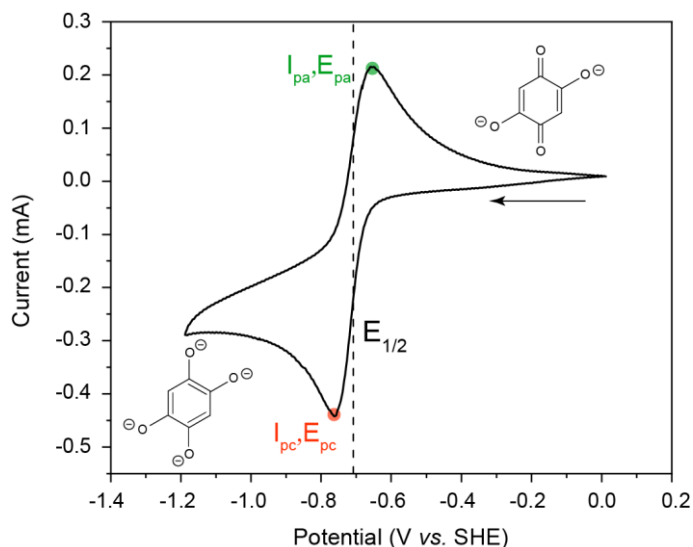


Figure 12. Cyclic voltammogram of 1 mM DHBQ in 1 M KOH (own data). The green dot illustrates the anodic peak for oxidation and the structure of the oxidized form of DHBQ is shown. The red dot illustrates the cathodic peak for reduction, and the structure of DHBQ in its reduced form is shown.

Looking at the negative scan, a cathodic peak (I_{pc}) appeared at a peak potential (E_{pc}) of -0.76 V vs. SHE. At this point, the potential is sufficient for the reduction of DHBQ to take place, resulting in an electrical current, and the DHBQ molecules around the electrode surface are present in the reduced form (structure to the left) [175]. When changing the scan direction, an anodic peak (I_{pa}) appeared at a peak potential (E_{pa}) of -0.65 V vs. SHE. Here, the oxidation of DHBQ near the electrode surface takes place, resulting in the oxidized form of DHBQ seen to the right in Figure 12 [176]. Along with a continuous increase in the potential, a current drop can be observed after the anodic peak current, which indicates the oxidation process becomes limited by the diffusion of species to the electrode surface. This also accounts for the reduction process [175].

The cyclic voltammogram can be used to extract information about the reversibility of the system. In the case of a reversible process, several criteria must be fulfilled. First of all, the term denotes a reaction that can proceed in either of the two directions, e.g., both oxidation and reduction, through equilibrium states [169]. The surface concentrations of the oxidized and reduced species are related to the electrode potential (E) following the Nernst equation, Eq. 3 [175].

$$E = E^{0'} + \frac{RT}{nF} \ln \frac{C_{Ox}}{C_{Red}} \quad (3)$$

Where $E^{0'}$ is the formal potential (experimental determined), R is the universal gas constant, T is the temperature, n is the number of electrons, F is the Faraday's constant (which is the charge of one mol of electrons[170]), and C_{Ox} and C_{Red} are the concentrations of the oxidized and reduced species at the electrode surface. Relating this to the CV, the concentrations of the oxidized and reduced species at the electrode surface change over time during the potential scan as the redox species go through electron transfer reactions to reach the Nernst-defined equilibrium, which is visible through the current response in the CV [175]. This means, that when $C_{Ox} = C_{Red}$, then the measured potential of the system is the $E^{0'}$ resulting in $E = E^{0'}$ [177].

The average of the cathodic and anodic peak potentials denotes the half-wave potential ($E_{1/2}$)[178], [179], which can be found using Eq. 4 [180].

$$E_{1/2} = \frac{E_{pa} + E_{pc}}{2} \quad (4)$$

When the process is reversible, $E_{1/2}$ can be assumed to be equal to $E^{0'}$. Since $E^{0'}$ only accounts for reversible cases, $E_{1/2}$ will be used in this thesis as it also extends to quasi-reversible cases [181]. For a reversible process with fast kinetics, the separation of the peak potentials is about 59 mV for a one-electron reaction. A peak separation that is larger than $0.059/n$ V, could indicate poor reversibility. The ratio between the two

peak currents is equal so that $I_{pa}/I_{pc} = 1$, and the closer the ratio is to 1, the better reversibility [182].

In most cases, electron-transfer processes are preceded and followed by a chemical reaction [171]. Coupling chemical reactions to electron transfer reactions can lead to changes in the peak potentials and/or the peak currents, and the effect of chemical reactions is often expressed in terms of changes within the ratio of these, e.g., sharper peaks in the CV means faster oxidation or reduction on the electrode surface, as well as a smaller separation between peak potentials, indicates faster redox processes, and vice versa [50]. The irreversible process is when the reaction only proceeds in one direction and when the kinetics is very sluggish resulting in a slow reaction. In the case of a quasi-reversible behavior, the process is something between reversible and irreversible, having intermediate kinetics [169], which can be identified when the peak split increases with an increase in scan rate [181], [183].

2.1.2. Mass transfer

Faradaic currents are generated as a result of the reduction or oxidation of molecules when they reach the electrode surface and are proportional to the charge passing through the electrode. For the molecules to reach the electrode surface, the following three different mechanisms are possible: diffusion (as a result of concentration gradient), migration (as a result of an electric field/electrical potential gradient), and convection (as a result of stirring or hydrodynamic transport) [170], [177]. As a result of the reduction or oxidation reaction, a concentration gradient between the area near the electrode and the bulk solution emerges, and diffusion-controlled mass transport occurs; hence, diffusion should always be considered [169], [171], [184]. Since an RFB is operated under forced convection, the diffusion of the active species from the electrolyte interface to the active surface on the electrode has a strong influence on the performance of the battery [42], [164].

To determine the diffusion coefficient, the influence on the mass transport by migration can be reduced or neglected by using a supportive electrolyte of a much larger concentration compared to the one for the redox active species. The influence on mass transport by convection can be avoided by using a stationary system with no stirring or vibrations [177].

The scan rate controls the time scale of the experiment [171]. By increasing the scan rate, the experimental time scale decreases, thereby also decreasing the time available for the chemical reaction. By studying the scan rate dependency of the CV, D of the active species can be estimated by using Randles-Sevcik analysis and hereby be directly extracted from the measured voltammograms [41], [42], [174]. For a reversible

process, the peak currents are given by the Randles-Sevcik equation, Eq. 5 [41], [158], [185].

$$i_p = 2.69 \times 10^5 n^{3/2} A D^{1/2} C^* \nu^{1/2} \quad (5)$$

Where i_p is the peak current (amperes), n is the number of electrons involved in the half-reaction for the redox couple, F is the Faradays constant, C^* is the bulk concentration of active materials (mol L^{-1}), ν is the scan rate (V s^{-1}), A is the electrode area (cm^2), and D is the diffusion coefficient ($\text{cm}^2 \text{s}^{-1}$).

A linear relationship between the square root of the scan rate and the measured peak currents indicates good chemical reversibility of the investigated redox process as well as a diffusion-controlled process [41], [51], [180], [182], [186]. In the case of good linearity, D can be obtained from the slope of this linear relationship.

A supplement to the CV technique is the RDE-based technique, in which a rotating planar WE is used to creating a centrifugal force to the electrolyte near the electrode surface so that it is continuously replaced by bulk solution. For that reason, the mass transport rate is precisely controlled by the rotation rate of the rotating electrode, steady-state currents are quickly obtained, and a more quantitative analysis of the kinetics can be obtained by using a rotating electrode compared to a stationary electrode [175], [187]. As bulk solution moves toward the electrode surface, a thin layer called the diffusion layer develops at the electrode surface, and the thickness of this depends on the rotation rate of the RDE. Only diffusion takes place in this layer, and the effect of convection can be neglected.

Figure 13 shows an example of data that can be obtained from an RDE experiment. Here, linear sweep voltammetry (LSV) was used starting from -0.4 V where no reactions occur, to -1.42 V vs. SHE using various rotation rates. To reach steady-state conditions (no change in currents with time), the scan rate for the RDE measurements must be low enough to allow the equilibrium to establish at the electrode surface [187]. In the figure, it can be seen that at potentials between -1.1 to -1.42 V vs. SHE , the current depends on the rotation rate (and weekly depends on changes in potential). This region is defined as the mass transport limited region. At potentials more positive than -0.75 V vs. SHE , it is seen that the current does not depend on the rotation rate; therefore, this region is defined as the kinetic limited region. At voltages between -1.1 to -0.75 V vs. SHE , the current is assumed to be under mixed control of both [188].

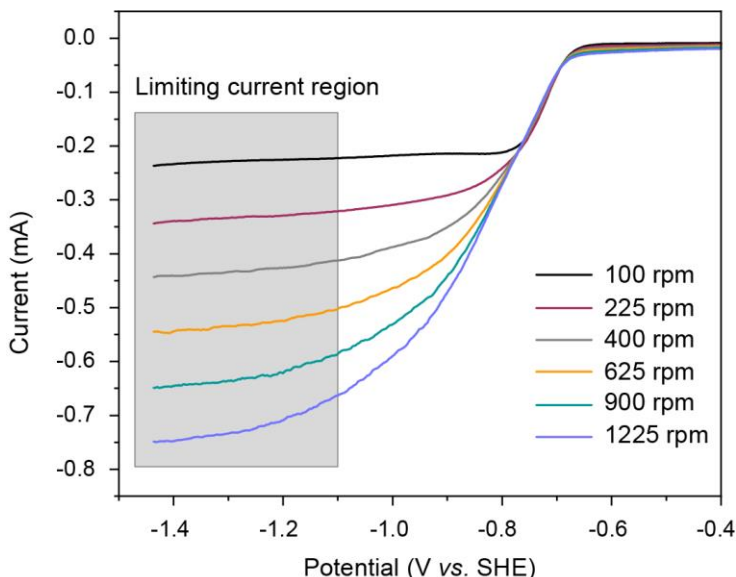


Figure 13. Example of LSV scans from an RDE experiment of 1 mM DHBQ in 1 M KOH with a scan rate of 5 mV s^{-1} . It is seen how the current response varies with the rotation rate. (Own data)

The current plateau in the resulting RDE voltammogram exhibits characteristics of the limiting current (i_{lim}), which is the current flowing at the point where the electrode reaction is mass transfer limited [49]. This means that the reaction is proceeding at its maximum rate possible, so the reactants are consumed immediately when it is brought to the electrode surface [177]. When the electrode reaction is completely controlled by mass transport, the D can be determined by the Levich equation (Eq. 6), which describes the relationship between the i_{lim} to the square root of the rotation rate of the electrode ($\omega^{1/2}$) [70], [188].

$$i_{lim} = 0.62nFAC^*D^{2/3}\nu^{-1/6}\omega^{1/2} \quad (6)$$

Where ω is the rotation rate (rad s^{-1}), ν is the kinematic viscosity ($\text{m}^2 \text{ s}^{-1}$). If the relationship between the i_{lim} and the $\omega^{1/2}$ is linear, the reaction is mass transfer limited and hereby diffusion controlled. By fitting i_{lim} versus $\omega^{1/2}$ (Levich plot), and the resulting fit is a linear line, the slope can be used to extract D , using Eq. 7 [186], [188].

$$\text{slope of levich plot} = 0.620nFAC^*D^{2/3}\nu^{-1/6} \quad (7)$$

To determine the rate constant of an electron transfer in the reaction, a Tafel analysis can be used, which relies on the data obtained from the RDE experiment. k^0 can be extracted from the current-potential characteristics described by the Butler-Volmer equation, Eq. 8 [177].

$$i = nFAk^0 [C_{Ox}(0, t)e^{-\alpha f(E-E^{0'})} - C_{Red}(0, t)e^{(1-\alpha)f(E-E^{0'})}] \quad (8)$$

Where i is the current, C_{Ox} is the concentration of oxidized species, C_{Red} is the concentration of reduced species, α is the transfer coefficient, f is F/RT , and $E-E^{0'}$ is the overpotential.

α is a measure of how the transition state of the reaction occurs and is a measure of the symmetry of the energy barrier [177]. A system with a large k^0 is preferable as this means that a faster equilibrium will be attained, whereas a smaller k^0 means sluggish kinetics.

2.2. Solubility

Besides k^0 , the solubility also influences the current density of the system. Solubility is a measure of the maximum possible concentration of the active material per unit volume of the supportive electrolyte. The higher amount of active material that can be dissolved in the solution, the more molecules can be transported to the electrode for the charge transfer reaction, thereby increasing the current density of the system. The solubility of the active material is usually temperature-dependent and often increases with increasing temperature [189]. However, in some cases, elevated temperatures result in the decomposition and precipitations of solid material. Besides this, the concentration needed for the purpose should be considered as the solubility of the active material affects the system costs. In cases with no need for high peak currents, a trade-off could be made to lower the concentration and hereby, the system cost [47].

A common method to measure solubility is ultraviolet-visible (UV-vis) spectroscopy, in which the concentration-dependent absorbance relationship of a solution is used to determine the maximum concentration possible of the active material to be obtained in a supportive electrolyte [47].

2.3. Electrolyte stability in a redox flow battery

After the redox properties of the compound have been determined, it can be tested in a redox flow battery, as either the negolyte material or the posolyte material (depending on the identified redox potential). Some key factors governing the operation of an organic RFB are charge transfer and mass transport processes, operating cell voltage, efficiencies, long-term cycling/stability, etc. [72], [164].

The stability and efficiency can be characterized by flow battery cell cycling experiments. An example of a lab-scale single-cell flow battery test setup can be seen in Figure 14.

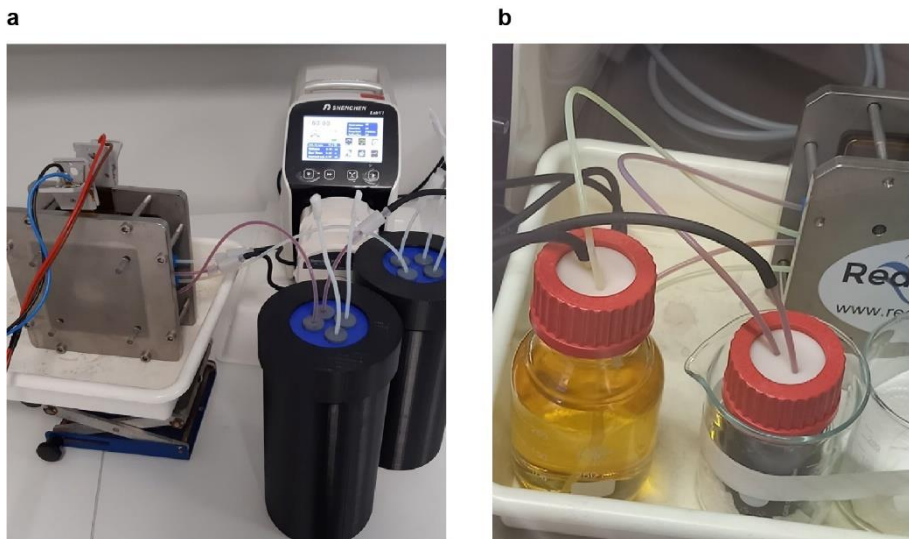


Figure 14. Laboratory set up of flow cell battery test. a) Setup outside glovebox. To reduce the reaction with atmospheric oxygen, the electrolyte reservoirs were submerged in water in sealed compartments (black containers). A peristaltic pump, standing behind, is used to control the electrolyte flow through the battery cell (left). b) The battery setup inside a glovebox to ensure no interactions with atmospheric oxygen, showing the polysolite (yellow) and negolyte (red) cycling through the battery cell (right side). (Own experiment)

To avoid unwanted interactions with atmospheric oxygen leading to uncontrolled oxidation of the redox active material, cycling experiments are most often performed in a glovebox, making it possible to standardize the cycling conditions no matter the chemistry of the redox active material [155]. The efficiency, as well as the lifetime and stability of the active material to work as the electrolyte in an RFB, can be extracted when the cell is continuously charged and discharged either at constant current conditions while recording the corresponding voltage (galvanostatic cycling) or by applying constant voltage conditions while recording the corresponding current (potentiostatic cycling). The latter often provides faster charging and discharging. Figure 15a illustrates a typical galvanostatic cycling profile.

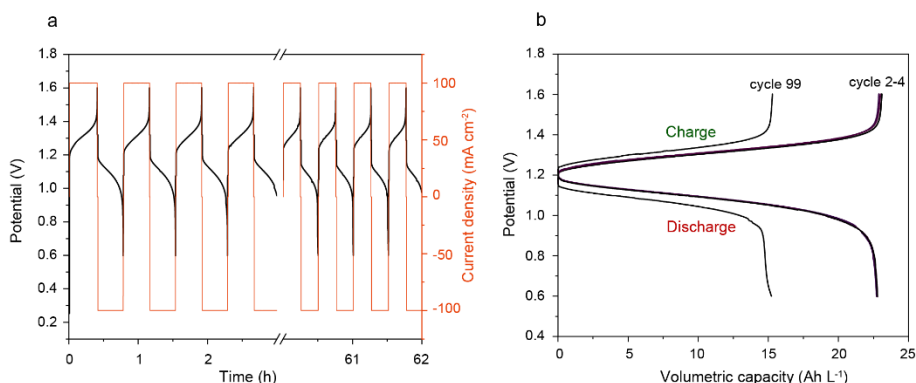


Figure 15. Galvanostatic full cell cycling example of DHBQ as negolyte against ferrocyanide as posolyte. a) A series of charge-discharge curves demonstrating the first four cycles and the last four cycles. The left y-axis represents the measured voltage (black) during charge and discharge. The right y-axis represents the applied constant current (red), which is positive when charging and negative when discharging. b) Voltage vs. volumetric capacity plot of cycles 2-4 and cycle 99 for both charging and discharging. (Own data)

With galvanostatic cell cycling, the capacity can be shown as a function of the voltage, which also illustrates the loss seen during long-term cell cycling (Figure 15b). In galvanostatic cell cycling, the capacity obtained can be directly related to the polarization resistance of the battery cell including the resistance from the electrolyte and membrane as well as from changes in the electrolyte mass transport and kinetics [45], [155]. Using only galvanostatic cell cycling does not allow for the determination of electrolyte cycling stability on its own, since the capacity fade also reflects the changes in the internal resistance of the cell, which would affect and limit the available capacity to be accessed along with the experiment [32]. Sometimes a combination of galvanostatic and potentiostatic cell cycling is used, also called constant-current-constant-voltage cycling. In this case, a constant current is applied until the potential limit has been reached, whereafter the voltage is kept constant until the current drops to a pre-defined limit [190]. This is used to ensure that the full SOC range is obtained and allows for the battery to be cycled to the extremes, which is the fully charged and fully discharged state. Therefore, this combination of cycling is usually used to determine the full capacity of the battery.

When testing a new compound as the electrolyte in an RFB, it should be made the capacity limiting side so that the cycling results can mostly be ascribed to this compound. This requires that an excess amount of the other electrolyte is used. The volumetric theoretical capacity (Q_{theo}) defines the maximum amount of charge possible to store due to the given electrolyte concentration and volume. This value is often given in Ah L^{-1} from Eq. 9.

$$Q_{theo} = \frac{m \times n \times F}{M \times V} \quad (9)$$

Where m is the mass of the active compound (g), M is the molar mass (g mol^{-1}) and V is the volume (L). The RFB performance is also measured based on capacity utilization, e.g., how close the practical capacity measured is to that of the theoretical [45]. Multiplying the volumetric capacity and the voltage (U) gives the energy density (E) of the system in Wh L^{-1} , Eq. 10.

$$E = Q \times U \quad (10)$$

Another interesting measure to obtain from the cell cycling tests is the open circuit voltage (OCV), which is a measure of the maximum voltage that can be generated by the RFB [191]. Theoretically, the OCV is determined by the difference in redox potentials between the negolyte and posolyte and hereby depends on the active materials used for the electrolytes. That is why a big difference in redox potentials is preferable as this results in a bigger OCV. The electrical quality of the battery is indicated by the coulombic efficiency (CE) and voltage efficiency (VE). The CE is measured by the ratio between the total charge released during discharge compared to the total charge stored during charge, Eq. 11 [45].

$$CE = \frac{Q_{\text{discharge}}}{Q_{\text{charge}}} \quad (11)$$

Factors influencing the CE are electrolyte crossover and unwanted side reactions. A high CE is preferable as it indicates good chemical reversibility and low membrane crossover [192]. The VE is a measure of the ratio between the average discharge voltage compared to the average charging voltage during a cycle, Eq. 12.

$$VE = \frac{V_{\text{discharge}}}{V_{\text{charge}}} \quad (12)$$

The VE is found by cycling with constant current density (galvanostatic cell cycling) and this efficiency relates to the different sources of overvoltage, i.e., kinetics, ohmic, and mass transport losses, which all affect the VE negatively [20]. Combining the two efficiencies result in energy efficiency (EE), which measures the extent of the energy supplied during charge that can be extracted during discharge, Eq. 13 [46], [193].

$$EE = CE \times VE \quad (13)$$

As mentioned earlier, electrolyte precipitation, reactant crossover through the membrane, unwanted reactant side reactions, and degradation reactions of the redox-active material into redox-inactive compounds are all examples that cause the capacity to decline resulting in a decreased performance with continuous cycling [48], [155]. The crossover of redox species through the membrane contaminates the electrolyte and often results in permanent losses in both the CE and the battery capacity [38]. The issue with electrolyte crossover can be mitigated by the use of the same redox-active material on both sides of the RFB[38], or by testing different membranes for the

specific full-cell system [29]. Nevertheless, to develop a sustainable and eco-friendly RFB, research suggests that the solution should be found using asymmetric chemistries by using different bio-sourced organic redox-active compounds as electrolytes because of the higher open cell potential this comes with [40].

However, one drawback of the full-cell cycling method is the lack of sufficient information on the electrolyte stability in the individual half-cell. The flow cell cycling method generates information about the full cell performance and stability as a unity, whereas the method cannot be used to describe a single electrolyte and its stability. For this, another method called symmetric cell cycling can be used [163].

2.3.1. Symmetric cell cycling test

In the symmetric cell setup, the electrolyte of interest is used in both half-cells, and by cycling in a flow battery, the stability of this single electrolyte can be determined under flow cell conditions avoiding any interference from other species [42]. By turning the focus on one single electrolyte, the symmetric cell cycling setup is a step towards being able to differentiate between causes for capacity loss and it allows individual electrolytes to be studied separately, which makes it well-suited to the durability determination of the electrolyte [48], [155]. One advantage of this method is that the impact of electrolyte crossover as a cause for capacity loss can be neglected [29], [163]. When applying different cycling techniques, one can distinguish if the capacity loss is caused by chemical or electrochemical decomposition [155].

In the symmetric cell setup, electrolyte solutions of identical reactant concentrations are used in two separate electrolyte reservoirs. To address a capacity limiting side (CLS), volume differences in the electrolyte reservoirs are utilized so that the capacity loss seen in the test can be attributed to this, Figure 16. Having identical reactants and concentrations in both reservoirs allows the cycling of both the oxidized and reduced state of the active species to determine stability in either of the states [37]. Initially, the CLS and the non-capacity limiting side (NCLS) contain the electrolyte pre-mixed at 50% SOC making it possible to access the entire SOC range of the CLS [42].

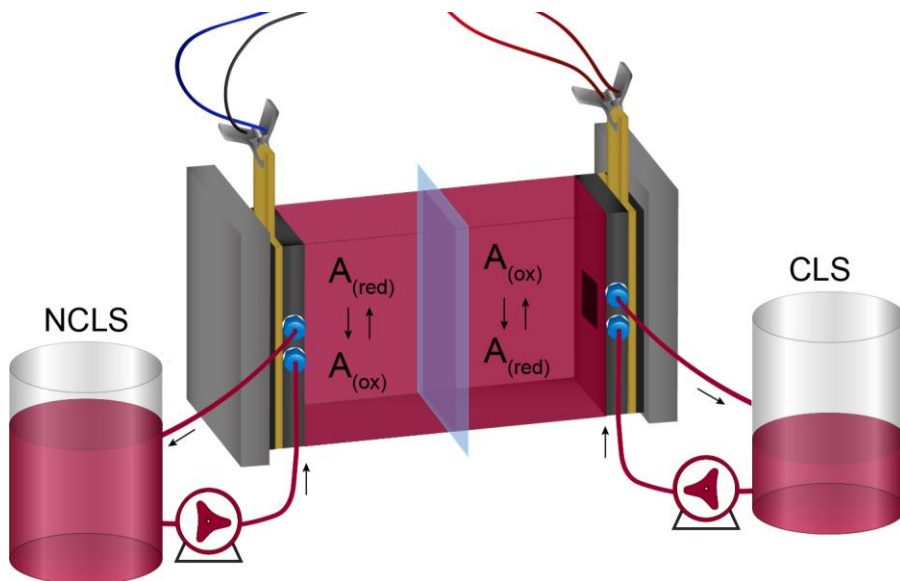


Figure 16. Schematic representation of a setup used for symmetric cell cycling experiments. Different reservoir volumes represent the CLS and the NCLS. The same electrolyte is used in both half-cells. The arrows at the tubes represent the flow direction.

The difference in volumes allows the CLS to be taken to different SOC_s, and by implementing cycling pauses at different SOC of the CLS, the chemical stability of the CLS in its oxidized and reduced state can be identified, and so can the stability and interactions of the CLS with the supporting electrolyte [29], [49], [155]. Therefore, this technique can be used to identify if the capacity fade is caused by purely chemical forms of degradations depending on SOC_s, cycling rate, electrochemical decomposition, or a combination [155].

Chapter 3. Summary of results and discussions from papers

In this section, a summary of the results and discussions from the two research papers that make up this dissertation will be presented.

- Paper 1. Demonstrating the Use of a Fungal Synthesized Quinone in a Redox Flow Battery. (Published in Batteries & Supercaps)
- Paper 2. Four-Electron Energy Storage in Biosynthesized Phoenicin Flow Battery Negolyte. (Submitted to ACS Sustainable Chemistry & Engineering)
- Paper 3. Are biologically synthesized electrolytes the future in green energy storage? (Submitted to Energy Storage)

3.1. Demonstrating the Use of a Fungal Synthesized Quinone in a Redox Flow Battery

The purpose of this paper was to investigate and demonstrate the concept of using a fungal-produced bio-quinone to store energy, Figure 17, hereby making a proof of concept and bringing the research within electrolytes for RFBs a step closer to sustainable production. Phoenicin was the first fungal-produced quinone to be tested as an RFB electrolyte active material. The phoenicin used in this paper was produced by *P. atrosanguineum* with an extract containing 95% pure phoenicin. The results discussed in the following will be centered around the function of phoenicin as the active material in the negative electrolyte in an RFB.

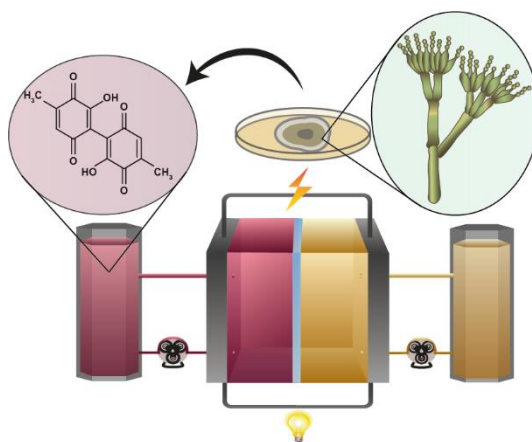


Figure 17. The concept of a fungal battery illustrates the use of the fungal-produced phoenicin in an RFB to store energy [154].

Initial voltammetric investigations by CV analysis showed that phoenicin has a half-wave potential of -0.37 V vs. SHE when dissolved in a 1 M KOH solution. Coupling phoenicin with ferrocyanide in a battery would give a theoretical operating voltage of 0.86 V (Figure 18a). The reversibility of phoenicin was studied through Randles-Sevcik analysis. First, we measured the peak current from various scan rates, as seen in Figure 18b, which visually demonstrates an increasing peak current with an increase in the scan rate. Phoenicin shows the behavior of a quasi-reversible redox reaction due to the change in peak splits with increasing scan rate [178], [180], [194], which is also supported by the ratio between the anodic and cathodic peak current is smaller than 1 (0.56 for a scan rate of 10 mV s^{-1}), indicating that the reduction of phoenicin is faster than the oxidation [195]. At scan rates between $5 - 500$ mV s^{-1} , this ratio was independent of the scan rate; though, at the very low scan rates of 1 and 2 mV s^{-1} , this ratio decreased with decreasing scan rate, resulting in greater irreversibility, which can be explained by the fact that a lower scan rate would allow more time for degradation mechanisms to take place [175], [181].

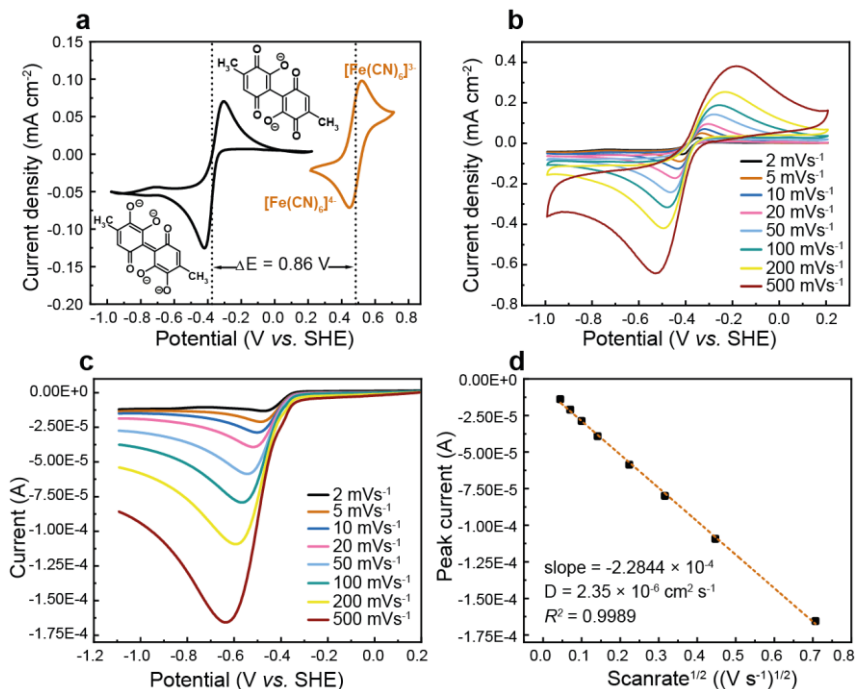


Figure 18. Cyclic voltammetry and Randles-Sevcik analysis of phoenicin. **a)** Voltammograms of phoenicin and ferrocyanide both in 1 M KOH. **b)** CV of phoenicin in 1 M KOH at various scan rates. **c)** LSV of phoenicin in 1 M KOH of cathodic currents at various scan rates. **d)** Plot of cathodic peak current vs. square root of scan rate, obtained from the Randles-Sevcik analysis [154].

In our voltammetric investigations, we assume that the start concentration of the phoenicin solution is in its fully oxidized form; therefore, the Randles-Sevcik analysis of the peak current vs. scan rate dependency was only performed for the cathodic reaction, Figure 18c. This dependency yielded a linear line, Figure 18d, and with an R^2 value close to that of 1, we assume that the reduction reaction is mostly diffusion-controlled [180].

When further investigating the kinetic parameters by RDE experiments, I experienced some difficulties. In the first experiment, an absence of linear dependency between the limiting current and the square root of the rotation rate (Levich plot) occurred, which indicated some irregularities as decreasing currents over time were observed. Due to the linearity seen from the Randles-Sevcik analysis (Figure 18d), it should be possible to measure kinetic parameters by RDE. Therefore, different reasons for the absence of linearity in the Levich plot were investigated, such as the passivation of the working electrode. A UV-vis spectrum of the test solution was taken before and after the RDE experiment, Figure 19a. Besides this, an LSV scan was taken at the beginning and the end of the RDE experiment using a rotation rate of 2500 rpm, Figure 19b. By comparing the difference in currents measured before and after the

experiment with the difference in the concentration measured before and after the experiment, it was demonstrated that the working electrode did not suffer from passivation by phenicin during the experiment.

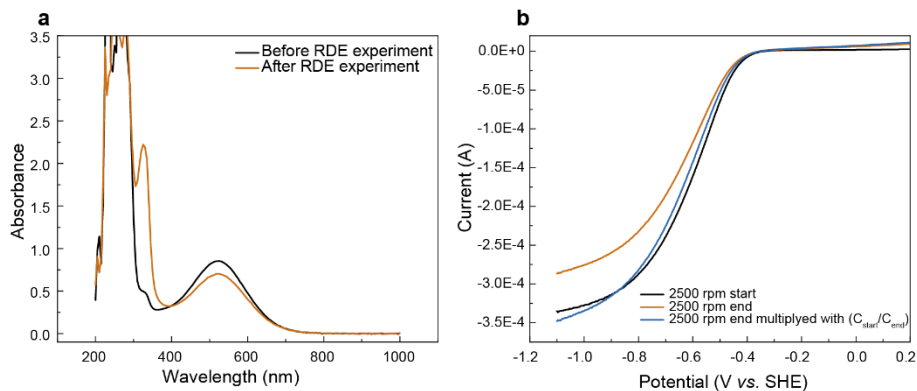


Figure 19. Supporting investigations for the RDE experiment. a) UV-vis spectra of the phenicin solution before and after the RDE experiment. b) LSV scans taken with a rotation rate of 2500 rpm at the beginning and the end of the RDE experiment. The blue line represents the currents at the end of the experiment multiplied by $(C_{\text{start}}/C_{\text{end}})$ [154].

Along with the sample used in the RDE experiment, a UV-vis spectrum was also taken of a sample that was kept from the initial solution (not used in the RDE experiment). The decay over time was nearly the same, whereas we demonstrated that the decay of the phenicin concentration seen in Figure 3a did not happen because of interaction with the cell electrodes. We, therefore, ascribe the decrease in currents, Figure 19b, to phenicin degradation in the bulk solution. To deal with this, the average concentration of the measurements taken before and after the RDE experiment was used to calculate the diffusion coefficient of phenicin. Since the degradation of phenicin seems to depend on time, four separate RDE experiments were made. The scans for each rotation rate from the four separate experiments were averaged and can be seen in Figure 20.

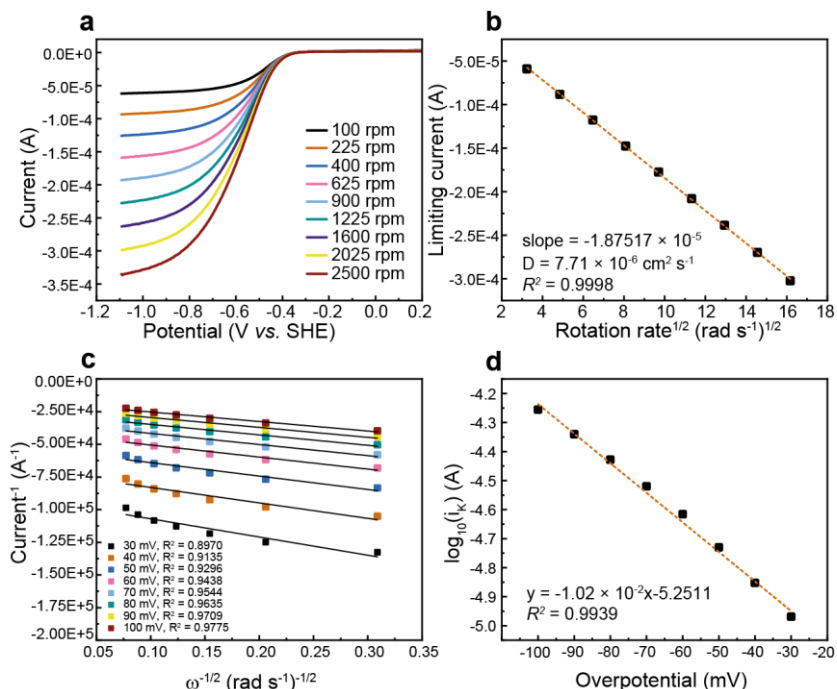


Figure 20. RDE experiment of phenocin. a) LSV scans of phenocin in 1 M KOH at different rotation rates. The scans were made from high to low rotation rates. The plot shows the average of four separate experiments. b) Levich-plot of limiting current vs. square root of rotation rates. c) Koutecky-Levich plot of overpotentials from -30 to -100 mV. d) Tafel plot [154].

After optimizing the experimental procedure as described above, fitting the dependency of the limiting current vs. the square root of rotation rate now results in a linear line with a high R^2 value close to 1, Figure 20b. This means, that the limiting negative current increases with increasing rotation rates, and the high R^2 value obtained in the Levich-plot (Figure 20b) supports the assumption of a diffusion-controlled reduction reaction [51]. Using the slope from the Levich-plot and the average concentration measured by UV-vis, a diffusion coefficient of $7.71 \times 10^{-6} \text{ cm}^2 \text{ s}^{-1}$ was determined, which is comparable to the diffusion coefficients seen for other quinones tested as RFB electrolytes, indicating suitability for testing phenocin as the negolyte in an RFB [41].

In some cases, the Tafel equation is used to determine k^0 . To use the Tafel equation, some experimental conditions must be fulfilled. The Tafel equation is valid for overpotentials above 118 mV and systems with the equilibrium of oxidized and reduced species [177]. Since the kinetically limited current region in this experiment is not much higher than -100 mV overpotential (Figure 4c), meanwhile taking the assumption of having only oxidized species in the phenocin bulk solution, the Tafel equation

does not suit this case. Therefore, the Butler-Volmer equation, Eq. 8, as described in Chapter 2.1.2, was used to determine the k^0 .

According to RDE assumptions of constant mass transfer, the near electrode concentration ($C(0,t)$) is equal to the bulk concentration (C^*), and by also assuming only oxidized species in the bulk solution in our experiment, the reduced related part of the equation can be neglected as the concentration of reduced phoenicin in the bulk is zero, rearranging the equation to Eq. 14.

$$i = nFAk^0[C_{Ox}^*(0,t)e^{-\alpha f(E-E^0)}] \quad (14)$$

Which can be converted to the logarithmic form, Eq. 15.

$$\log_{10}(i) = -2.3\alpha \frac{F(E-E^0)}{RT} + \log_{10}(nFAk^0C_{Ox}^*) \quad (15)$$

With a good linear fit in the Tafel plot, Figure 20d (R^2 is 0.99), the intercept and the slope were used to find the value for k^0 to be $1.56 \times 10^{-4} \text{ cm s}^{-1}$ and the value for α to be 0.6, respectively, by Eq. 16 and 17 for a two-electron reaction.

$$\text{intercept} = \log_{10}(nFAk^0C_{Ox}^*) \quad (16)$$

$$\text{slope} = -\alpha F/2.3RT \quad (17)$$

Making a symmetric cell cycling test is not necessary when studying the performance of phoenicin as an RFB electrolyte. However, due to the novelty of this compound, this method was prioritized to obtain more information about the stability of phoenicin as an electrolyte and how it behaves under oxidation and reduction.

The experiment was performed in the glovebox to ensure no reactions with atmospheric oxygen. The experiment had a run time of around 12 days in total, and when cycling, small overpotentials of $\pm 300 \text{ mV}$ with a current cutoff of 2.5 mA were used. We implemented pauses of 24 hours duration at SOC of 0, 5, 10, 50, 100, 95, and 90% for the CLS in this order during the experiment. The CLS was charged to specific SOC, and then left isolated for 24 hours with the electrolytes being kept in their representative reservoir to avoid electrolyte interactions with the cell materials i.e., membrane, electrodes, etc. Det capacity measured before and after the pause was used to determine the electrolyte stability of the different SOC states of the phoenicin.

As seen in Figure 21, phoenicin showed the best stability when being kept in its reduced form (high SOC), with a capacity loss of $4\% \text{ day}^{-1}$. This is a much lower rate than seen when phoenicin was kept at low SOC (0% SOC) in its oxidized form for 24 hours, where a loss of $18.0\% \text{ day}^{-1}$.

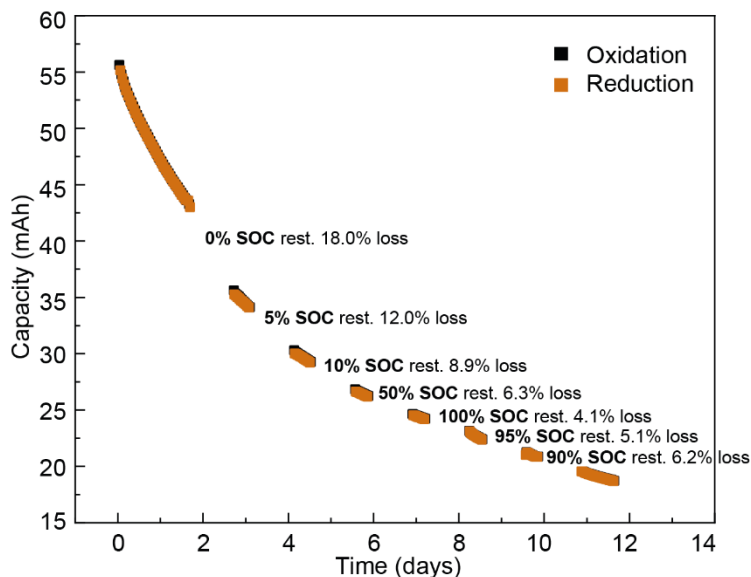


Figure 21. Symmetric cell cycling experiment of phoenicin showing the capacity loss over time both during cycling and the pauses at different fixed SOC's [154].

The capacity loss measured during all the pauses was attributed to chemical degradation since a loss was observed when phoenicin was kept at all SOC's and no current was applied to the system. The capacity loss observed in the pauses was larger compared to the loss measured during the cell cycling in between. From this observation, we assumed that phoenicin suffers from chemical degradation, which is time-dominated as well as related to the SOC in terms of the concentration of the oxidized and reduced forms of phoenicin, meanwhile being less related to the cycling rate [155].

The electrolytes were not investigated further after the experiment but based on the literature [73], [196], [197], we proposed the mechanism seen in Figure 22. Due to the unsubstituted carbon atoms in the phoenicin molecule, we believed that Michael addition of hydroxyl ions was likely to occur.

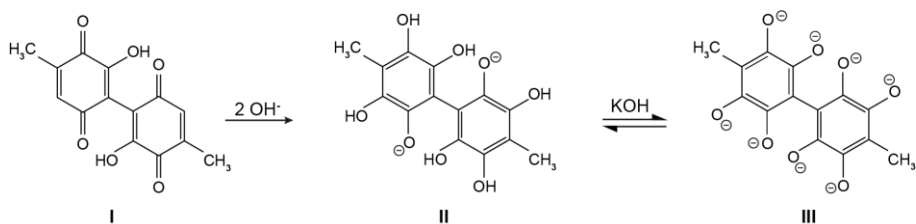


Figure 22. Proposed degradation mechanism of phoenicin. A Michael nucleophilic addition of OH^- on the unsubstituted carbon atoms in the phoenicin molecule (I), resulting in aromatization (II). Since the reaction is taking place in KOH, deprotonations are proposed as a cause of the high pH (III) [154].

To test the potential of phoenicin as a negolyte in an RFB, phoenicin was paired against ferrocyanide as the posolyte. To avoid a reaction with atmospheric oxygen, the full-cell cycling experiment was performed inside a nitrogen-filled glove bag. An ATR-IR device was connected to the phoenicin electrolyte to monitor the composition by recording a spectrum every 90 seconds of the experiment. The battery was cycled in the potentiostatic regime with holds at 1.6 V when charging and 0.6 V when discharging for almost 15 days (119 cycles) and assumed that phoenicin was cycled in its full SOC range.

With the initial capacity of 235.1 mAh in the experiment matching the theoretical one of 214.4 mAh for a two-electron reaction, these results suggest that phoenicin involves a two-electron reaction per molecule.

The full-cell cycling test showed an average capacity loss of $2.85\% \text{ day}^{-1}$ ($0.35\% \text{ cycle}^{-1}$) during the full runtime of the experiment, Figure 23a.

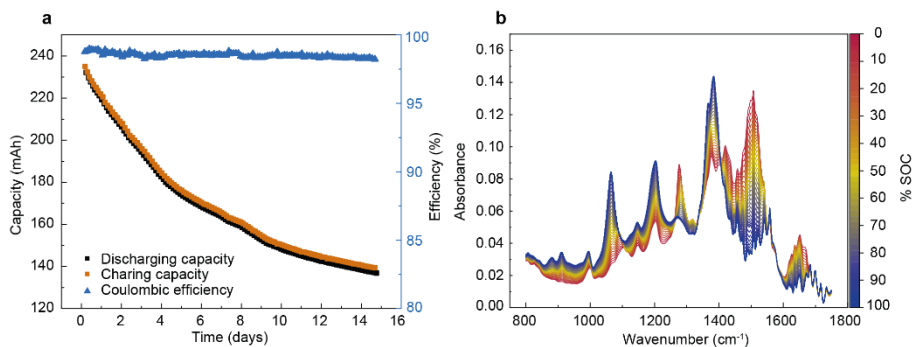


Figure 23. Full cell battery cycling results. a) Capacity and efficiency evolution of the full experiment. b) Stack plot showing the changes in the ATR-IR spectra of phoenicin with respect to the SOC of one charging half-cycle [154].

The battery test also showed good coulombic efficiency, averaging around 98.5% over the entire runtime as well as an energy efficiency of 36.9%. The coulombic efficiency of 98.5% indicates losses due to e.g. cross over of phoenicin or phoenicin degradation [168]. No visible crossover was observed after the test, but due to the findings from the symmetric cell cycling test, it can be expected that the degradation of phoenicin could be a reasonable reason for the coulombic efficiency not being 100%.

A degradation of phoenicin during cell cycling was supported by the ATR-IR spectra recorded during the full experiment. The stack plot in Figure 23b shows a clear difference in spectra when the SOC of phoenicin was varied during charge and discharge. Moreover, by comparing the spectra recorded from the first charge and discharge cycle to the last charge and discharge cycle, some changes in the electrolyte composition

of both the reduced and oxidized state of phoenicin were observed, Figure 24, which we attributed to phoenicin degradation.

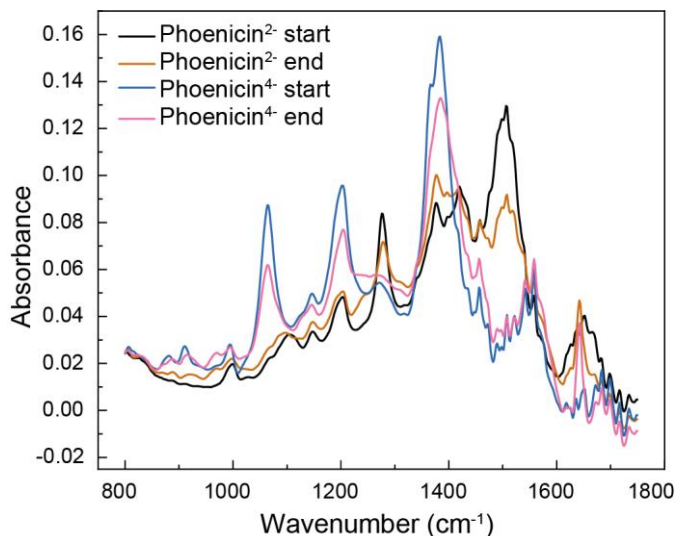


Figure 24. ATR-IR spectra recorded for the phoenicin negolyte showing the first charge and discharge cycle as well as the last charge and discharge cycle of the full cell cycling experiment. Phoenicin²⁻ is the oxidized form (discharged) while phoenicin⁴⁻ is the reduced form (charged) [154].

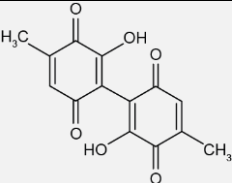
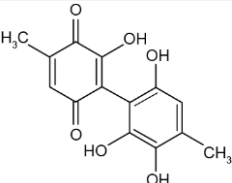
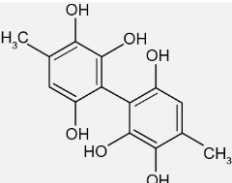
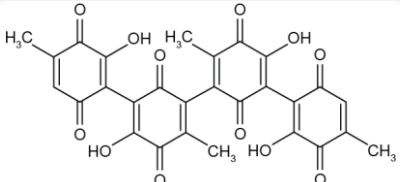
The investigations made in this paper illustrate the potential of phoenicin to be used as a negative electrolyte in an RFB. The electrochemical investigations demonstrated the quasi-reversible behavior as well as a diffusion-controlled reduction reaction of phoenicin. With the half-wave potential of -0.37 V vs. SHE, phoenicin could work as a potential negolyte material when paired with compounds having higher half-wave potentials. The electrochemical investigations as well as the battery experiments made in this paper suggest that the phoenicin batch used (produced by *P. atrosanguineum* with 95% purity) involves a two-electron reaction per phoenicin molecule. These findings conclude the first and second research questions.

The stability of phoenicin was demonstrated using symmetric cell cycling, which showed that phoenicin was more stable in its reduced state, as well as using full-cell cycling, in which a capacity loss of 2.85% day⁻¹ was observed, hereby concluding research question three. Both cycling tests suggested that phoenicin suffers from chemical degradation. The results demonstrated that it is possible to use the fungi-produced quinone phoenicin to work as the negolyte in an RFB since it was both charged and discharged over several days, answering research question number four.

3.2. Four-Electron Energy Storage in Biosynthesized Phoenicin Flow Battery Negolyte

As a follow-up study to the findings in Paper 1, this paper aims to investigate the influence of the purity and composition of phoenicin on the electrochemical behavior as well as the stability and performance in a redox flow battery (research question five). The phoenicin used in Paper 2 was produced by *P. phoeniceum* and four forms of phoenicin were identified in the extract, Table 1. Phoenicin still made up most of the extract with 82.7%, with a phoenicin dimer extent of 7%.

Table 1. Structures and amounts in % of the four phoenicin forms identified in the extract used in this study [198].

Phoenicin form	Structure	Molar mass (g mol ⁻¹)	% of total extract
Phoenicin C ₁₄ H ₁₀ O ₆		274.23	82.7%
Phoenicin quinol C ₁₄ H ₁₂ O ₆		276.21	9.3%
Phoenicin diquinol C ₁₄ H ₁₄ O ₆		278.23	1.0%
Phoenicin dimer C ₂₈ H ₁₈ O ₁₂		546.38	7.0%

In Paper 1, the data obtained from the cycling experiments as well as from the investigations of the diffusion coefficient and electron transfer rate suggested a two-electron reaction per phoenicin unit. The phoenicin tested in Paper 2 differed from the

composition of the batch tested in Paper 1, so the first aspect considered in Paper 2 was the number of electrons possible to be transferred per molecule.

Phoenicin was paired against ferrocyanide in a full-cell battery and cycled galvanostatically between 1.6 V and 0.5 V for 13 days (1111 cycles). The initial capacity was measured to be 15.79 mAh, which is almost twice the theoretical capacity of 8.21 mAh for a two-electron reaction per phoenicin unit and matches the theoretical capacity of a four-electron reaction better, as seen in Figure 25a. From this, it was assumed that a four-electron reaction per phoenicin unit was more likely to occur, meaning that the carbonyl groups present in the molecule structure were fully utilized.

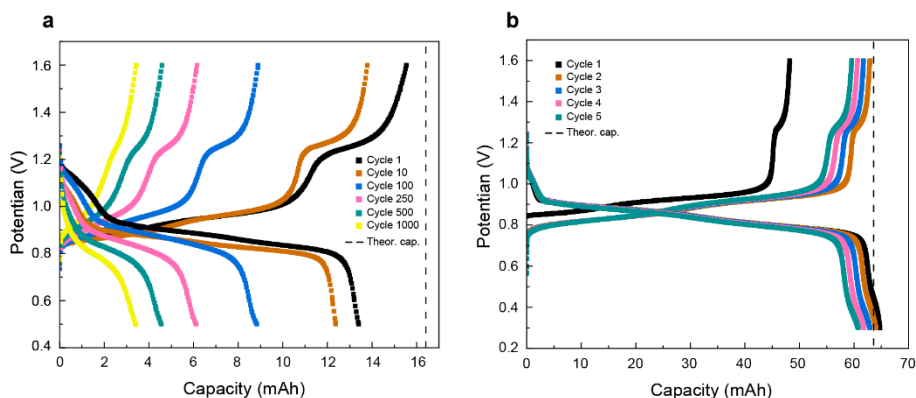


Figure 25. Cell potential vs. capacity curves obtained from cell cycling tests of phoenicin against ferrocyanide. a) Phoenicin concentration of 1.48×10^{-2} M. b) Phoenicin concentration 6.36×10^{-2} M. Theoretical capacity corresponds to a four-electron reaction per phoenicin molecule in both cases [198].

This observation was further supported by an additional battery test, using a higher phoenicin concentration, in which the initial experimental capacity matched that of a four-electron reaction per phoenicin molecule, as seen in Figure 25b.

This was also backed up by electrochemical investigations by CV and RDE studies. The half-wave potential of phoenicin used in this study was determined to be -0.28 V vs. SHE and from the proportional relationship between the peak current and the square root of the scan rate as well as from the increasing peak splits with increasing scan rate, phoenicin shows the behavior of a quasi-reversible and mostly diffusion-controlled redox reaction. From the RDE experiment, a D of 4.93×10^{-6} $\text{cm}^2 \text{s}^{-1}$ for four electrons per phoenicin molecule (two electrons per benzoquinone group). To validate this, we performed Diffusion-ordered spectroscopy (DOSY) of a sample with low concentration ($<9 \times 10^{-2}$ M), resulting in a D of 6×10^{-6} $\text{cm}^2 \text{s}^{-1}$. From the RDE experiment, a k^0 of 6.86×10^{-4} cm s^{-1} was determined assuming a four-electron reaction per phoenicin molecule.

The full-cell cycling test showed an average capacity loss of $6.2\% \text{ day}^{-1}$ ($0.071\% \text{ cycle}^{-1}$) during the full runtime of the experiment, Figure 26a, and a coulombic efficiency of 99.27%, Figure 26b.

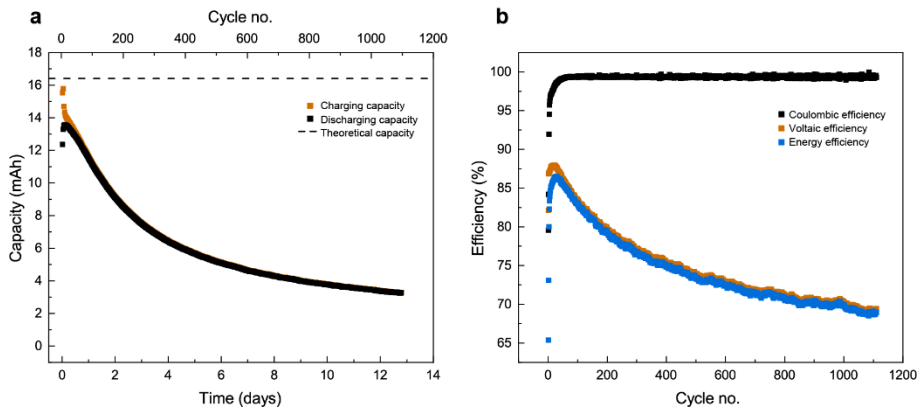


Figure 26. Stability and efficiencies from the cell cycling test of phenocin against ferrocyanide, with a phenocin concentration of $1.48 \times 10^{-2} \text{ M}$. a) Capacity loss over time. b) Efficiencies [198].

We did not observe any leaking from the experiment. Some extent of the capacity loss was ascribed to electrolyte crossover through the membrane, since indications of phenocin were detected, by $^1\text{H-NMR}$, in the polysulfate after the battery test.

By investigating the stability of phenocin in an alkaline solution (KOH), a series of $^1\text{H-NMR}$ spectra, Figure 27, showed that the ratio of protons from the benzene rings (around $\delta > 6 \text{ ppm}$) to the protons from the methyl groups (around $\delta \sim 2 \text{ ppm}$) decrease with time, indicating structural changes in phenocin. We ascribed the disappearance of the benzylic H peak with time to the removal of the benzylic H through Michael addition.

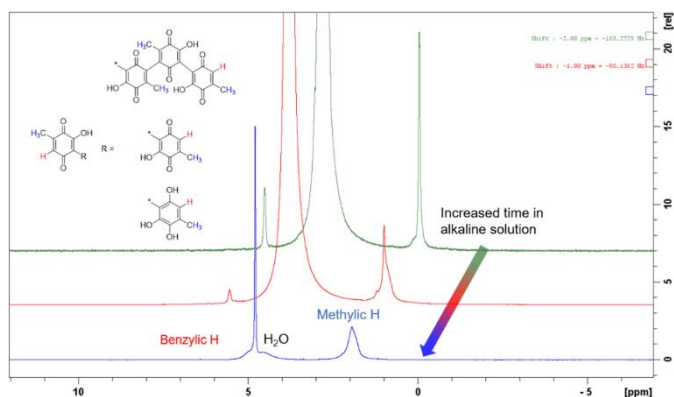


Figure 27. $^1\text{H-NMR}$ spectra of phenocin in 1 M KOH with increased time in the alkaline solution, indicating phenocin degradation [198].

Liquid chromatography-mass spectrometry (LC-MS) analysis of phoenicin in KOH after one week showed masses corresponding to phoenicin with additional hydroxyl groups as well as different stages of polymerization. The detected degradation products were identified as a mixture of, phoenicin with two additional hydroxyl groups (oosporein), phoenicin dimer, phoenicin trimer, etc.

The investigations made in this paper demonstrated that despite having a mix of phoenicin forms in the extract, it can still be used as a negative electrolyte in an RFB. The battery experiments, supported by the electrochemical investigations, suggest that the phoenicin batch used (produced by *P. phoeniceum* with 7% phoenicin dimer) involves a four-electron reaction per phoenicin molecule. Therefore, in this study, we were able to utilize the full potential of the phoenicin mix by reaching capacities corresponding to two-electron reactions per benzoquinone group, hereby answering research question number five.

3.2.1. Discussion of findings from Paper 1 and Paper 2

Based on the findings in Papers 1 and 2, we demonstrated that phenicin, biosynthetically produced by *P. atrosanguineum* and *P. phoeniceum*, can be used as a negolyte in an RFB. Table 2 summarizes the electrochemical properties found in the papers as well as the stability in a full-cell battery paired against ferrocyanide.

Table 2. Summary of results obtained from Papers 1 and 2.

Study	$E_{1/2}$ (V vs. SHE)	D ($\text{cm}^2 \text{s}^{-1}$)	k^0 (cm s^{-1})	Electrons (per phenicin molecule)	Cap. loss (per cycle / per day)	CE (%)
Paper 1 phenicin	-0.37	7.71×10^{-6}	1.56×10^{-4}	2	0.35% / 2.85%	98.5
Paper 2 Phenicin mix	-0.28	4.93×10^{-6}	6.86×10^{-4}	4	0.07% / 6.20%	99.3

The phenicin used in the studies differed by the producers as well as the composition, with Paper 2 investigating the phenicin mix (including the phenicin dimer). As seen in the table, the phenicin composition does matter as the results obtained in the papers varied. We discovered that phenicin is prone to Michael addition when dissolved in KOH. This was demonstrated in Paper 2, in which the attack on the unsubstituted carbon positions in the phenicin mix was measured by $^1\text{H-NMR}$ analysis.

The reduction potential of phenicin in Paper 1 was lower compared to that of the phenicin mix. Due to phenicin suffering from Michael attack when dissolved in KOH, this difference can be explained by phenicin having more unsubstituted carbon positions per phenicin molecule compared to phenicin dimer, resulting in a lower reduction potential due to the OH^- attacks.

From the RDE experiments, a D of $4.93 \times 10^{-6} \text{ cm}^2 \text{ s}^{-1}$ for four electrons per phenicin molecule (two electrons per benzoquinone group) was determined in Paper 2, which was further validated by DOSY analysis to be $6 \times 10^{-6} \text{ cm}^2 \text{ s}^{-1}$. This is similar to the diffusion coefficient determined in Paper 1, and the D being slightly lower in Paper 2 can be a result of the phenicin dimer being a larger molecule that moves more slowly. However, looking at the k^0 , the phenicin mix performs better, which can also be seen from the coulombic efficiency from the battery test being higher compared to the one obtained in Paper 1.

Phoenicin from Paper 1 and phoenicin mix from Paper 2 both suffered from capacity loss during cell cycling in a full-cell battery test against ferrocyanide. Comparing the capacity loss observed per cycle, the phoenicin mix performed better. However, when looking at the temporal metric of capacity loss observed per day, the phoenicin in Paper 1 performed better. From a cycling point of view, having a mix of phoenicin forms would be preferable, as this metric is used to suggest the expected lifetime of a system cycled daily to provide grid-scale storage. However, if the capacity loss observed is related to the chemical degradation of active species, it is more appropriate to use the capacity loss per day when comparing stability. Since we ascribed most of the capacity loss to the chemical degradation of phoenicin in KOH, the pure phoenicin used in Paper 1 was found to be the most stable.

Finally, when looking at the number of electrons possible to store in phoenicin, we saw that the studies made in Paper 2 suggested a four-electron reaction for each phoenicin molecule, which was double the amount seen in Paper 1. We assume that the mix of phoenicin forms, and especially the phoenicin dimer was being utilized to its full potential by reaching the full capacity. We explained this behavior again to the phoenicin dimer being more resistant to Michael addition due to the fewer unsubstituted positions per molecule.

Since this study was made as a proof of concept on using fungal-produced quinones to store energy, and because no structural modifications were made to phoenicin, I believe that this is a good starting point to demonstrate the potential of this research project. The investigations made in Papers 1 and 2 work as a foundation for future research on fungal quinones to be used as electrolyte materials in RFBs.

3.3. Are biologically synthesized electrolytes the future in green energy storage?

With the proof-of-concept of using the biologically synthesized phoenicin as the electrolyte in an RFB, the challenges and prospects of using fungi to produce electrolytes were further discussed in Paper 3. This paper relates to the results obtained in Paper 1 and discusses how phoenicin compares to chemically synthesized quinones that have been investigated thoroughly. The kinetic parameters measured for phoenicin are comparable to those obtained by other quinones, Table 3.

Table 3. Summary of the diffusion coefficient and electron transfer rate constant of different quinones used for RFBs. All values are determined from RDE experiments using a glassy carbon working electrode.

Quinone	Supportive electrolyte	D ($\text{cm}^2 \text{s}^{-1}$)	k^0 (cm s^{-1})	Electrons (per molecule)	Ref.
BQDS	1 M H_2SO_4	5.1×10^{-6}	-	2	[164]
Bislawsonone	1 M KOH	4.54×10^{-6}	-	4	[68]
AQ-1,6-3E-OH	1 M KCl	2.94×10^{-6}	6.14×10^{-3}	2	[80]
2,3-HCNQ	1 M KOH	3.44×10^{-6}	2.07×10^{-3}	2	[49]
Lawsonone	1 M NaCl	6.10×10^{-6}	8.13×10^{-4}	2	[142]
2,6-N-TSAQ	1 M NaOH	5.8×10^{-7}	2.53×10^{-4}	2	[50]
2,3-DHAQ	1 M KOH	3.4×10^{-6}	1.56×10^{-2}	2	[82]
1,8-BDPAQCl ₂	0.5 M KCl	2.99×10^{-6}	6.95×10^{-2}	2	[83]
DPivOHAQ	1 M KCl	2.4×10^{-6}	2.5×10^{-3}	2	[85]
DBAQ	1 M KCl	2.5×10^{-6}	2.9×10^{-5}	2	[85]
DCDHAQ	1 M KOH	1.7×10^{-6}	7.4×10^{-4}	2	[86]
AQDP	1 M KOH	9.5×10^{-7}	3.4×10^{-3}	2	[132]
DHBQ	1 M KOH	3.66×10^{-6}	2.12×10^{-3}	2	[73]
DMBQ	1 M KOH	3.42×10^{-6}	7.70×10^{-5}	2	[131]

Additionally, compared to the chemically synthesized quinones tested as electrolytes in RFBs (Table A1), the capacity loss seen for phoenicin can be placed in the lower end of the published quinones. However, with more than 300 quinones of fungal origin [125], [144], [199], fungi are a promising source of quinone production.

As seen for the phoenicin production, this has already been optimized from 1.24 g L⁻¹, using *P. atrosanguineum*, to yields of 5 g L⁻¹ using *P. phoeniceum* [143]. Similar cases have been found by the quinone bikaverin, which has been produced in yields of 6.83 g L⁻¹ by *Fusarium fujikuroi*. Combining this with the possibilities of overexpressing the quinone biosynthetic gene clusters [200]–[203], we believe that even higher yields can be obtained.

Besides the potential of reaching higher yields with low production costs, another advantage of fungal quinones is the possibility of fungal quinone optimization. As seen already for the chemically synthesized quinones, structural modifications and different synthetic approaches have successfully been used to increase the stability of the quinones, e.g., as seen for DPivOHAQ having a low capacity fade rate of 1.8×10⁻³% day⁻¹, Table A1 [85]. The addition of functional groups has also successfully been studied to increase solubility in aqueous solutions [36], [47], [108]. Based on the simulation study of naturally occurring quinones mentioned earlier in this dissertation, it was discovered that the redox potential is affected by the side chains, which has also been demonstrated in the literature [15], [49]. Having this in mind, further optimization of fungal quinones can be made by adding selected side chains to fungal quinones by using metabolic engineering.

Also, with the possibility of further production optimization and lowering the cost of quinone production, a trade-off of quinone stability could be feasible if the production cost is low enough. With more research within this, we believe that fungal quinones are promising alternatives to quinones derived from non-renewable feedstocks to work as electrolytes in RFBs.

Chapter 4. Conclusions and perspectives

With the worldwide increasing energy production and demand, the need for cost-effective energy storage devices to store energy from renewables is critical in the green energy transition. The redox flow battery based on aqueous organic electrolytes is one promising solution to be used to accelerate the transition towards using more renewable energy, thereby reducing the consumption of energy generated from fossil fuels. However, most electrolyte materials used have mainly been vanadium and aqueous organic electrolyte materials synthesized from non-renewable feedstocks. This dissertation aimed to investigate the potential of using the naturally occurring and biosynthesized quinone phoenicin as an electrolyte for an RFB, intending to get one step closer to sustainable electrolyte production.

In the initial study, phoenicin was investigated as the first fungal quinone to be used in a redox flow battery. Phoenicin used in Paper 1 was produced by the filamentous fungus *Penicillium atrosanguineum* in an extract concentration of 1.24 g L^{-1} of 95% pure phoenicin. From cyclic voltammetry analysis, phoenicin showed a half-wave potential of -0.37 V vs. SHE , and the electrochemical investigations demonstrated the quasi-reversible behavior as well as a diffusion-controlled reduction reaction of phoenicin. Based on rotating disc electrode experiments as well as the assumption of a two-electron reaction per phoenicin molecule, a diffusion coefficient of $7.71 \times 10^{-6} \text{ cm}^2 \text{ s}^{-1}$ was determined, which is comparable to the diffusion coefficients seen for other quinones tested as RFB electrolytes, indicating suitability for testing phoenicin as the negolyte in an RFB when paired with compounds having more positive half-wave potentials. An electron transfer rate of $1.56 \times 10^{-4} \text{ cm s}^{-1}$ was determined, which corresponds to a quasi-reversible behavior of the redox reaction of phoenicin, hereby supporting the finding from the cyclic voltammetry analysis.

Based on the symmetric cell cycling test of phoenicin, it was found that phoenicin suffered from chemical degradation which is both time-dominated as well as related to the state of charge, with phoenicin being more stable when kept in its reduced state. When phoenicin was paired against ferrocyanide in a full-cell battery test, an initial capacity of 11.75 Ah L^{-1} in the experiment matched the theoretical one for a two-electron reaction per phoenicin molecule, which agrees with the electrochemical findings. The cycling experiment showed a capacity fade rate of $2.85\% \text{ day}^{-1}$ ($0.35\% \text{ cycle}^{-1}$) over 14 days (119 cycles) and a coulombic efficiency of 98.5%. This capacity loss was ascribed to the chemical degradation of phoenicin, which was supported by the ATR-IR spectra recorded of phoenicin negolyte during cell cycling. We proposed this degradation to be caused by Michael addition to the unsubstituted positions in the phoenicin molecule. The findings in this study demonstrated the concept of using a fungal quinone to store energy, and phoenicin hereby worked as a proof of concept for such an approach.

The influence of the purity of phoenicin was further evaluated in Paper 2, in which the filamentous fungus *Penicillium phoeniceum* produced a mix of four phoenicin forms in an extract concentration of 5 g L^{-1} , of which 82.7% was phoenicin and 7% was phoenicin dimer. The phoenicin mix showed a half-wave potential of -0.28 V vs. SHE , a diffusion coefficient of $4.93 \times 10^{-6} \text{ cm}^2 \text{ s}^{-1}$ ($6 \times 10^{-6} \text{ cm}^2 \text{ s}^{-1}$ from DOSY analysis), and an electron transfer rate of $6.86 \times 10^{-4} \text{ cm s}^{-1}$, based on a four-electron reaction per phoenicin molecule in the mix. These findings also demonstrated the behavior of a quasi-reversible and mostly diffusion-controlled redox reaction. In a battery test against ferrocyanide as the polysolite, an initial capacity of 1.58 Ah L^{-1} was obtained matching the theoretical one for a four-electron reaction per phoenicin molecule, which agrees with the electrochemical findings. The cycling experiment showed a capacity fade rate of $6.2\% \text{ day}^{-1}$ ($0.071\% \text{ cycle}^{-1}$) over 13 days (1111 cycles) and a coulombic efficiency of 99.3%. Based on the $^1\text{H-NMR}$ analysis showing the attack on the unsubstituted carbon positions in the phoenicin mix, it was discovered that phoenicin is prone to Michael addition when dissolved in KOH. Furthermore, degradation products such as the addition of hydroxyl groups to the phoenicin molecules as well as different stages of polymerization such as phoenicin dimer, trimer, quadromers, etc. were identified. The findings in this study demonstrated that having a mix of phoenicin forms involved a four-electron reaction per phoenicin molecule, hereby utilizing the full potential of the phoenicin mix by reaching capacities corresponding to two-electron reaction per benzoquinone group (four-electrons per phoenicin molecule).

The research made in this dissertation illustrates the potential of phoenicin to be used as a negative electrolyte in an RFB. With more than 300 quinones described across the fungal spectrum, fungi are a promising source for quinone production. Combining this with the possibilities of using genetic engineering approaches to enhance quinone production as well as modifying quinone structures to enhance properties such as stability and solubility, fungal quinones could be promising alternatives to quinones derived from non-renewable feedstocks to work as electrolytes in RFBs.

Phoenicin served as the proof-of-concept of the first fungal quinone to be used as electrolyte material in an RFB. Based on the findings in this project, I believe that phoenicin should be further investigated. This is especially reasoned by the discovery of phoenicin being able to involve a four-electron reaction per phoenicin molecule, as shown in Paper 2. This was an interesting result since more electrons per molecule would decrease the amount of material needed concerning concentration and volume, thereby lowering the cost. Experimental conditions such as supportive electrolyte, pH, membrane material, as well as cyclin conditions are also factors to consider in future investigations.

Several other fungal quinones could also be investigated in future studies in the search of finding the most optimal and sustainable electrolytes to store future renewable energy. The use of genetic engineering to modify the quinone structures should also be

researched, and the influence of modifications in fungal quinone structures should be further tested as potential electrolytes in RFBs by using the same approaches as used for phoenicin.

For the fungal battery to become a potential solution, more research should be made on phoenicin as well as other fungal quinones. For it to succeed, the fungal quinone production should be optimized even more, as well as by using environmentally friendly and cheap solvents and extraction procedures. It is preferable to use genetic engineering for yield optimization and structural modification rather than making further modifications to the compound after being produced. This would both save time and as well as decreasing synthetic costs. Furthermore, the possibilities of producing a fungal quinone with good electrochemical properties as well as high stability and solubility in pH-neutral supporting electrolytes should also be investigated. Considering large-scale applications, pH-neutral electrolytes are preferred due to the risk of leakage and spills and also for them being non-corrosive in nature from a waste point of view.

Literature list

- [1] I. Sorrenti, T. B. H. Rasmussen, S. You, and Q. Wu, “The role of power-to-X in hybrid renewable energy systems: A comprehensive review,” *Renew. Sustain. Energy Rev.*, vol. 165, p. 112380, Sep. 2022, doi: 10.1016/j.rser.2022.112380.
- [2] J. Mitali, S. Dhinakaran, and A. A. Mohamad, “Energy storage systems: a review,” *Energy Storage Sav.*, vol. 1, pp. 166–216, Sep. 2022, doi: 10.1016/j.enss.2022.07.002.
- [3] D. G. Kwabi, Y. Ji, and M. J. Aziz, “Electrolyte Lifetime in Aqueous Organic Redox Flow Batteries: A Critical Review,” *Chem. Rev.*, vol. 120, pp. 6467–6489, Jul. 2020, doi: 10.1021/acs.chemrev.9b00599.
- [4] Y. Liu *et al.*, “Degradation of electrochemical active compounds in aqueous organic redox flow batteries,” *Curr. Opin. Electrochem.*, vol. 32, p. 100895, Apr. 2022, doi: 10.1016/j.coelec.2021.100895.
- [5] M. J. B. Kabeyi and O. A. Olanrewaju, “Sustainable Energy Transition for Renewable and Low Carbon Grid Electricity Generation and Supply,” *Front. Energy Res.*, vol. 9, p. 743114, Mar. 2022, doi: 10.3389/ferng.2021.743114.
- [6] BP, “Statistical Review of World Energy,” 2022.
- [7] A. Gouda, A. Masson, M. Hoseinizadeh, F. Soavi, and C. Santato, “Biosourced quinones for high-performance environmentally benign electrochemical capacitors via interface engineering,” *Commun. Chem.*, vol. 5, p. 98, Aug. 2022, doi: 10.1038/s42004-022-00719-y.
- [8] M. Kiehadroudzeh, A. Merabet, and H. Hosseinzadeh-Bandbafha, “Review of Latest Advances and Prospects of Energy Storage Systems: Considering Economic, Reliability, Sizing, and Environmental Impacts Approach,” *Clean Technol.*, vol. 4, pp. 477–501, Jun. 2022, doi: 10.3390/cleantechnol4020029.
- [9] BP, “Statistical Review of World Energy,” 2020.
- [10] BP, “Statistical Review of World Energy,” 2021.
- [11] Danmarks Statistik, “Stor stigning i energiforbrug i 2021,” 2022. [Online]. Available: <https://www.dst.dk/da/Statistik/nyheder-analyser-publ/nyt/NytHtml?cid=38429>

- [12] R. A. Potash, J. R. McKone, S. Conte, and H. D. Abruña, “On the Benefits of a Symmetric Redox Flow Battery,” *J. Electrochem. Soc.*, vol. 163, pp. A338–A344, Dec. 2016, doi: 10.1149/2.0971602jes.
- [13] B. Zakeri *et al.*, “Pandemic, War, and Global Energy Transitions,” *Energies*, vol. 15, p. 6114, Aug. 2022, doi: 10.3390/en15176114.
- [14] A. Riaz, M. R. Sarker, M. H. M. Saad, and R. Mohamed, “Review on Comparison of Different Energy Storage Technologies Used in Micro-Energy Harvesting, WSNs, Low-Cost Microelectronic Devices: Challenges and Recommendations,” *Sensors*, vol. 21, p. 5041, Jul. 2021, doi: 10.3390/s21155041.
- [15] J. S. Steen *et al.*, “Blatter Radicals as Bipolar Materials for Symmetrical Redox-Flow Batteries,” *J. Am. Chem. Soc.*, vol. 144, pp. 5051–5058, Mar. 2022, doi: 10.1021/jacs.1c13543.
- [16] S. Koohi-Fayegh and M. A. Rosen, “A review of energy storage types, applications and recent developments,” *J. Energy Storage*, vol. 27, p. 101047, Feb. 2020, doi: 10.1016/j.est.2019.101047.
- [17] J. W. McNamara, V. DeAngelis, R. H. Byrne, A. Benson, B. R. Chalamala, and R. Masiello, “Long-duration energy storage in a decarbonized future: Policy gaps, needs, and opportunities,” *MRS Energy Sustain.*, pp. 1–29, Aug. 2022, doi: 10.1557/s43581-022-00037-9.
- [18] Z. Li and Y.-C. Lu, “Advanced aqueous redox flow batteries design: Ready for long-duration energy storage applications?,” *MRS Energy Sustain.*, pp. 1–12, Apr. 2022, doi: 10.1557/s43581-022-00027-x.
- [19] T. M. Gür, “Review of electrical energy storage technologies, materials and systems: challenges and prospects for large-scale grid storage,” *Energy Environ. Sci.*, vol. 11, pp. 2696–2767, 2018, doi: 10.1039/C8EE01419A.
- [20] J. Winsberg, T. Hagemann, T. Janoschka, M. D. Hager, and U. S. Schubert, “Redox-Flow Batteries: From Metals to Organic Redox-Active Materials,” *Angew. Chemie Int. Ed.*, vol. 56, pp. 686–711, Jan. 2017, doi: 10.1002/anie.201604925.
- [21] X. Wei *et al.*, “Materials and Systems for Organic Redox Flow Batteries: Status and Challenges,” *ACS Energy Lett.*, vol. 2, pp. 2187–2204, Sep. 2017, doi: 10.1021/acsenerylett.7b00650.
- [22] Vivaenergi, “Hvordan arbejder et hybrid solcelleanlæg i løbet af dagen?”

<https://www.vivaenergi.dk/doegnrytme> (accessed Nov. 13, 2022).

- [23] N. Khan, S. Dilshad, R. Khalid, A. R. Kalair, and N. Abas, “Review of energy storage and transportation of energy,” *Energy Storage*, vol. 1, p. e49, Jun. 2019, doi: 10.1002/est2.49.
- [24] D. Kucevic, L. Semmelmann, N. Collath, A. Jossen, and H. Hesse, “Peak Shaving with Battery Energy Storage Systems in Distribution Grids: A Novel Approach to Reduce Local and Global Peak Loads,” *Electricity*, vol. 2, pp. 573–589, Nov. 2021, doi: 10.3390/electricity2040033.
- [25] G. Nikiforidis, M. C. M. van de Sanden, and M. N. Tsampas, “High and intermediate temperature sodium–sulfur batteries for energy storage: development, challenges and perspectives,” *RSC Adv.*, vol. 9, pp. 5649–5673, 2019, doi: 10.1039/C8RA08658C.
- [26] B. Cárdenas, L. Swinfen-Styles, J. Rouse, and S. D. Garvey, “Short-, Medium-, and Long-Duration Energy Storage in a 100% Renewable Electricity Grid: A UK Case Study,” *Energies*, vol. 14, p. 8524, Dec. 2021, doi: 10.3390/en14248524.
- [27] J. Liu, C. Hu, A. Kimber, and Z. Wang, “Uses, Cost-Benefit Analysis, and Markets of Energy Storage Systems for Electric Grid Applications,” *J. Energy Storage*, vol. 32, p. 101731, Dec. 2020, doi: 10.1016/j.est.2020.101731.
- [28] M. M. Rana, M. Atef, M. R. Sarkar, M. Uddin, and G. Shafiullah, “A Review on Peak Load Shaving in Microgrid—Potential Benefits, Challenges, and Future Trend,” *Energies*, vol. 15, p. 2278, Mar. 2022, doi: 10.3390/en15062278.
- [29] D. G. Kwabi *et al.*, “Alkaline Quinone Flow Battery with Long Lifetime at pH 12,” *Joule*, vol. 2, pp. 1894–1906, Sep. 2018, doi: 10.1016/j.joule.2018.07.005.
- [30] BP, “Statistical Review of World Energy.” <https://www.bp.com/en/global/corporate/energy-economics/statistical-review-of-world-energy.html> (accessed Nov. 13, 2022).
- [31] M. Miroshnikov *et al.*, “Bioderived Molecular Electrodes for Next-Generation Energy-Storage Materials,” *ChemSusChem*, vol. 13, pp. 2186–2204, May 2020, doi: 10.1002/cssc.201903589.
- [32] Y. Ji *et al.*, “A Phosphonate-Functionalized Quinone Redox Flow Battery at Near-Neutral pH with Record Capacity Retention Rate,” *Adv. Energy Mater.*,

vol. 9, p. 1900039, Mar. 2019, doi: 10.1002/aenm.201900039.

- [33] A. Castillo and D. F. Gayme, “Grid-scale energy storage applications in renewable energy integration: A survey,” *Energy Convers. Manag.*, vol. 87, pp. 885–894, 2014, doi: 10.1016/j.enconman.2014.07.063.
- [34] A. Alhamali, M. E. Farrag, G. Bevan, and D. M. Hepburn, “Review of Energy Storage Systems in electric grid and their potential in distribution networks,” *2016 18th Int. Middle-East Power Syst. Conf. MEPCON 2016 - Proc.*, pp. 546–551, 2017, doi: 10.1109/MEPCON.2016.7836945.
- [35] J. Luo *et al.*, “Unraveling pH dependent cycling stability of ferricyanide/ferrocyanide in redox flow batteries,” *Nano Energy*, vol. 42, pp. 215–221, Dec. 2017, doi: 10.1016/j.nanoen.2017.10.057.
- [36] T. Gaudin and J.-M. Aubry, “Prediction of Pourbaix diagrams of quinones for redox flow battery by COSMO-RS,” *J. Energy Storage*, vol. 49, p. 104152, May 2022, doi: 10.1016/j.est.2022.104152.
- [37] J. D. Milshtein, J. L. Barton, R. M. Darling, and F. R. Brushett, “4-acetamido-2,2,6,6-tetramethylpiperidine-1-oxyl as a model organic redox active compound for nonaqueous flow batteries,” *J. Power Sources*, vol. 327, pp. 151–159, Sep. 2016, doi: 10.1016/j.jpowsour.2016.06.125.
- [38] K. Gong *et al.*, “All-Soluble All-Iron Aqueous Redox-Flow Battery,” *ACS Energy Lett.*, vol. 1, pp. 89–93, Jul. 2016, doi: 10.1021/acsendergylett.6b00049.
- [39] G. Sikukuu Nambafu, “Organic molecules as bifunctional electroactive materials for symmetric redox flow batteries: A mini review,” *Electrochem. commun.*, vol. 127, p. 107052, Jun. 2021, doi: 10.1016/j.elecom.2021.107052.
- [40] M. O. Bamgbopa, A. Fetyan, M. Vagin, and A. A. Adelodun, “Towards eco-friendly redox flow batteries with all bio-sourced cell components,” *J. Energy Storage*, vol. 50, no. February, p. 104352, 2022, doi: 10.1016/j.est.2022.104352.
- [41] G. D. Charlton, S. M. Barbon, J. B. Gilroy, and C. A. Dyker, “A bipolar verdazyl radical for a symmetric all-organic redox flow-type battery,” *J. Energy Chem.*, vol. 34, pp. 52–56, 2019, doi: 10.1016/j.jechem.2018.09.020.
- [42] J. D. Milshtein *et al.*, “High current density, long duration cycling of soluble organic active species for non-aqueous redox flow batteries,” *Energy Environ. Sci.*, vol. 9, no. 11, pp. 3531–3543, 2016, doi: 10.1039/c6ee02027e.

- [43] F. Chu, M. Su, G. Xiao, Z. Tan, and G. Yang, "Analysis of Electrode Configuration Effects on Mass Transfer and Organic Redox Flow Battery Performance," *Ind. Eng. Chem. Res.*, vol. 61, pp. 2915–2925, Feb. 2022, doi: 10.1021/acs.iecr.1c04689.
- [44] A. Z. Weber, M. M. Mench, J. P. Meyers, P. N. Ross, J. T. Gostick, and Q. Liu, "Redox flow batteries: a review," *J. Appl. Electrochem.*, vol. 41, pp. 1137–1164, Oct. 2011, doi: 10.1007/s10800-011-0348-2.
- [45] Y. A. Gandomi *et al.*, "Critical Review—Experimental Diagnostics and Material Characterization Techniques Used on Redox Flow Batteries," *J. Electrochem. Soc.*, vol. 165, pp. A970–A1010, Apr. 2018, doi: 10.1149/2.0601805jes.
- [46] J. Noack, N. Roznyatovskaya, T. Herr, and P. Fischer, "The Chemistry of Redox-Flow Batteries," *Angew. Chemie Int. Ed.*, vol. 54, pp. 9776–9809, Aug. 2015, doi: 10.1002/anie.201410823.
- [47] J. D. Hofmann and D. Schröder, "Which Parameter is Governing for Aqueous Redox Flow Batteries with Organic Active Material?," *Chemie Ing. Tech.*, vol. 91, pp. 786–794, Jun. 2019, doi: 10.1002/cite.201800162.
- [48] R. M. Darling and M. L. Perry, "Half-Cell, Steady-State Flow-Battery Experiments," *ECS Trans.*, vol. 53, pp. 31–38, May 2013, doi: 10.1149/05307.0031ecst.
- [49] C. Wang *et al.*, "High-Performance Alkaline Organic Redox Flow Batteries Based on 2 - Hydroxy-3-carboxy- 1,4-naphthoquinone," *ACS Energy Lett.*, vol. 3, pp. 2404–2409, 2018, doi: 10.1021/acsenerylett.8b01296.
- [50] M. Wu *et al.*, "Highly Stable, Low Redox Potential Quinone for Aqueous Flow Batteries**," *Batter. Supercaps*, p. e202200009, Jun. 2022, doi: 10.1002/batt.202200009.
- [51] S. Liu *et al.*, "A symmetric aqueous redox flow battery based on viologen derivative," *Chinese Chem. Lett.*, vol. 31, pp. 1690–1693, Jun. 2020, doi: 10.1016/j.ccllet.2019.11.033.
- [52] K. Schofield and P. Musilek, "State of Charge and Capacity Tracking in Vanadium Redox Flow Battery Systems," *Clean Technol.*, vol. 4, pp. 607–618, Jun. 2022, doi: 10.3390/cleantechnol4030037.
- [53] E. Sánchez-Díez *et al.*, "Redox flow batteries: Status and perspective towards sustainable stationary energy storage," *J. Power Sources*, vol. 481, p. 228804,

Jan. 2021, doi: 10.1016/j.jpowsour.2020.228804.

- [54] C. Minke, U. Kunz, and T. Turek, “Techno-economic assessment of novel vanadium redox flow batteries with large-area cells,” *J. Power Sources*, vol. 361, pp. 105–114, Sep. 2017, doi: 10.1016/j.jpowsour.2017.06.066.
- [55] A. Parasuraman, T. M. Lim, C. Menictas, and M. Skyllas-Kazacos, “Review of material research and development for vanadium redox flow battery applications,” *Electrochim. Acta*, vol. 101, pp. 27–40, Jul. 2013, doi: 10.1016/j.electacta.2012.09.067.
- [56] J. Winsberg, C. Stolze, S. Muench, F. Liedl, M. D. Hager, and U. S. Schubert, “TEMPO/Phenazine Combi-Molecule: A Redox-Active Material for Symmetric Aqueous Redox-Flow Batteries,” *ACS Energy Lett.*, vol. 1, pp. 976–980, Nov. 2016, doi: 10.1021/acsenerylett.6b00413.
- [57] M. Cazot, G. Maranzana, J. Dillet, F. Beille, T. Godet-Bar, and S. Didierjean, “Symmetric-cell characterization of the redox flow battery system: Application to the detection of degradations,” *Electrochim. Acta*, vol. 321, p. 134705, 2019, doi: 10.1016/j.electacta.2019.134705.
- [58] S. Weber, J. F. Peters, M. Baumann, and M. Weil, “Life Cycle Assessment of a Vanadium Redox Flow Battery,” *Environ. Sci. Technol.*, vol. 52, pp. 10864–10873, Sep. 2018, doi: 10.1021/acs.est.8b02073.
- [59] W. Lee, G. Park, D. Schröder, and Y. Kwon, “Performance enhancement of alkaline organic redox flow battery using catalyst including titanium oxide and Ketjenblack,” *Korean J. Chem. Eng.*, vol. 39, pp. 1624–1631, Jun. 2022, doi: 10.1007/s11814-021-1040-9.
- [60] K. Schafner, M. Becker, and T. Turek, “Capacity balancing for vanadium redox flow batteries through continuous and dynamic electrolyte overflow,” *J. Appl. Electrochem.*, vol. 51, pp. 1217–1228, Aug. 2021, doi: 10.1007/s10800-021-01572-y.
- [61] T. Lagarteira, P. Pacheco, C. Almeida, A. Bentien, R. Monteiro, and A. Mendes, “In-Situ Measurement of Vanadium Crossover for the Vanadium Redox Flow Battery,” *J. Electrochem. Soc.*, vol. 166, pp. A4067–A4072, Dec. 2019, doi: 10.1149/2.0331916jes.
- [62] E. H. Kirk, F. Fenini, S. N. Oreiro, and A. Bentien, “Temperature-Induced Precipitation of V₂O₅ in Vanadium Flow Batteries—Revisited,” *Batteries*, vol. 7, p. 87, Dec. 2021, doi: 10.3390/batteries7040087.

- [63] T. Ma *et al.*, “Porphyrin-Based Symmetric Redox-Flow Batteries towards Cold-Climate Energy Storage,” *Angew. Chemie Int. Ed.*, vol. 57, pp. 3158–3162, Mar. 2018, doi: 10.1002/anie.201713423.
- [64] J. Liu *et al.*, “Materials Science and Materials Chemistry for Large Scale Electrochemical Energy Storage: From Transportation to Electrical Grid,” *Adv. Funct. Mater.*, vol. 23, pp. 929–946, Feb. 2013, doi: 10.1002/adfm.201200690.
- [65] C. Choi *et al.*, “A review of vanadium electrolytes for vanadium redox flow batteries,” *Renew. Sustain. Energy Rev.*, vol. 69, pp. 263–274, Mar. 2017, doi: 10.1016/j.rser.2016.11.188.
- [66] L. Li *et al.*, “A Stable Vanadium Redox-Flow Battery with High Energy Density for Large-Scale Energy Storage,” *Adv. Energy Mater.*, vol. 1, pp. 394–400, May 2011, doi: 10.1002/aenm.201100008.
- [67] S. Roe, C. Menictas, and M. Skyllas-Kazacos, “A High Energy Density Vanadium Redox Flow Battery with 3 M Vanadium Electrolyte,” *J. Electrochem. Soc.*, vol. 163, no. 1, pp. A5023–A5028, 2016, doi: 10.1149/2.0041601jes.
- [68] L. Tong *et al.*, “Molecular Engineering of an Alkaline Naphthoquinone Flow Battery,” *ACS Energy Lett.*, vol. 4, no. 8, pp. 1880–1887, 2019, doi: 10.1021/acsenergylett.9b01321.
- [69] T. Hagemann *et al.*, “(2,2,6,6-Tetramethylpiperidin-1-yl)oxyl-Containing Zwitterionic Polymer as Catholyte Species for High-Capacity Aqueous Polymer Redox Flow Batteries,” *Chem. Mater.*, vol. 31, pp. 7987–7999, Oct. 2019, doi: 10.1021/acs.chemmater.9b02201.
- [70] E. Drazevic, C. Szabo, D. Konya, T. Lund, K. Wedege, and A. Bienten, “Investigation of Tetramorpholinohydroquinone as a Potential Catholyte in a Flow Battery,” *ACS Appl. Energy Mater.*, vol. 2, pp. 4745–4754, Jul. 2019, doi: 10.1021/acsaem.9b00351.
- [71] A. Murali *et al.*, “Understanding and Mitigating Capacity Fade in Aqueous Organic Redox Flow Batteries,” *J. Electrochem. Soc.*, vol. 165, pp. A1193–A1203, Apr. 2018, doi: 10.1149/2.0161807jes.
- [72] B. Yang, L. Hooper-Burkhardt, F. Wang, G. K. Surya Prakash, and S. R. Narayanan, “An Inexpensive Aqueous Flow Battery for Large-Scale Electrical Energy Storage Based on Water-Soluble Organic Redox Couples,” *J. Electrochem. Soc.*, vol. 161, pp. A1371–A1380, Jun. 2014, doi:

10.1149/2.1001409jes.

- [73] Z. Yang *et al.*, “Alkaline Benzoquinone Aqueous Flow Battery for Large-Scale Storage of Electrical Energy,” *Adv. Energy Mater.*, vol. 8, p. 1702056, 2018, doi: 10.1002/aenm.201702056.
- [74] J. Luo, B. Hu, C. Debruler, and T. L. Liu, “A π -Conjugation Extended Viologen as a Two-Electron Storage Anolyte for Total Organic Aqueous Redox Flow Batteries,” *Angew. Chemie Int. Ed.*, vol. 57, pp. 231–235, Jan. 2018, doi: 10.1002/anie.201710517.
- [75] M. Pan *et al.*, “Reversible Redox Chemistry in Pyrrolidinium-Based TEMPO Radical and Extended Viologen for High-Voltage and Long-Life Aqueous Redox Flow Batteries,” *Adv. Energy Mater.*, vol. 12, p. 2103478, Apr. 2022, doi: 10.1002/aenm.202103478.
- [76] H. Li, H. Fan, B. Hu, L. Hu, G. Chang, and J. Song, “Spatial Structure Regulation: A Rod-Shaped Viologen Enables Long Lifetime in Aqueous Redox Flow Batteries,” *Angew. Chemie Int. Ed.*, vol. 60, pp. 26971–26977, Dec. 2021, doi: 10.1002/anie.202110010.
- [77] T. Janoschka, N. Martin, M. D. Hager, and U. S. Schubert, “An Aqueous Redox-Flow Battery with High Capacity and Power: The TEMPTMA/MV System,” *Angew. Chemie Int. Ed.*, vol. 55, pp. 14427–14430, 2016, doi: 10.1002/anie.201606472.
- [78] E. S. Beh, D. De Porcellinis, R. L. Gracia, K. T. Xia, R. G. Gordon, and M. J. Aziz, “A Neutral pH Aqueous Organic – Organometallic Redox Flow Battery with Extremely High Capacity Retention,” *ACS Energy Lett.*, vol. 2, no. 3, pp. 639–644, 2017, doi: 10.1021/acsenergylett.7b00019.
- [79] Y. Liu *et al.*, “A Long-Lifetime All-Organic Aqueous Flow Battery Utilizing TMAP-TEMPO Radical,” *Chem*, vol. 5, pp. 1861–1870, Jul. 2019, doi: 10.1016/j.chempr.2019.04.021.
- [80] S. Jin *et al.*, “A Water-Miscible Quinone Flow Battery with High Volumetric Capacity and Energy Density,” *ACS Energy Lett.*, vol. 4, pp. 1342–1348, Jun. 2019, doi: 10.1021/acsenergylett.9b00739.
- [81] W. Lee, K. S. Yoo, and Y. Kwon, “Alkaline aqueous redox flow batteries using 2,5-dihydroxy-1,4-benzoquinone and ferrocyanide adopting bismuth and carboxylic acid functionalized carbon nanotube catalyst,” *Int. J. Energy Res.*, pp. 1–13, Aug. 2022, doi: 10.1002/er.8652.

- [82] S. Guiheneuf, T. Godet-Bar, J.-M. Fontmorin, C. Jourdin, D. Floner, and F. Geneste, "A new hydroxyanthraquinone derivative with a low and reversible capacity fading process as negolyte in alkaline aqueous redox flow batteries," *J. Power Sources*, vol. 539, p. 231600, Aug. 2022, doi: 10.1016/j.jpowsour.2022.231600.
- [83] L. Xia *et al.*, "A Low-Potential and Stable Bis-Dimethylamino-Substituted Anthraquinone for pH-Neutral Aqueous Redox Flow Batteries," *ChemElectroChem*, vol. 9, p. e202200224, Jun. 2022, doi: 10.1002/celec.202200224.
- [84] K. Lin *et al.*, "Alkaline quinone flow battery," *Science (80-.)*, vol. 349, no. 6255, pp. 1529–1532, 2015, doi: 10.1126/science.aab3033.
- [85] M. Wu *et al.*, "Extremely Stable Anthraquinone Negolytes Synthesized from Common Precursors," *Chem*, vol. 6, pp. 1432–1442, Jun. 2020, doi: 10.1016/j.chempr.2020.03.021.
- [86] M. Wu, M. Bahari, E. M. Fell, R. G. Gordon, and M. J. Aziz, "High-performance anthraquinone with potentially low cost for aqueous redox flow batteries," *J. Mater. Chem. A*, vol. 9, no. 47, pp. 26709–26716, 2021, doi: 10.1039/D1TA08900E.
- [87] L. Hooper-Burkhardt *et al.*, "A New Michael-Reaction-Resistant Benzoquinone for Aqueous Organic Redox Flow Batteries," *J. Electrochem. Soc.*, vol. 164, no. 4, pp. A600–A607, 2017, doi: 10.1149/2.0351704jes.
- [88] H. Fan *et al.*, "Mitigating Ring-Opening to Develop Stable TEMPO Catholytes for pH-Neutral All-Organic Redox Flow Batteries," *Adv. Funct. Mater.*, vol. 32, no. 33, pp. 1–9, 2022, doi: 10.1002/adfm.202203032.
- [89] T. Liu, X. Wei, Z. Nie, V. Sprenkle, and W. Wang, "A Total Organic Aqueous Redox Flow Battery Employing a Low Cost and Sustainable Methyl Viologen Anolyte and 4-HO-TEMPO Catholyte," *Adv. Energy Mater.*, vol. 6, no. 3, 2016, doi: 10.1002/aenm.201501449.
- [90] X. Li *et al.*, "Symmetry-breaking design of an organic iron complex catholyte for a long cyclability aqueous organic redox flow battery," *Nat. Energy*, vol. 6, no. 9, pp. 873–881, 2021, doi: 10.1038/s41560-021-00879-6.
- [91] B. Zhang *et al.*, "Zwitterionic Ferrocenes: An Approach for Redox Flow Battery (RFB) Catholytes," *Inorg. Chem.*, vol. 61, no. 21, pp. 8117–8120, 2022, doi: 10.1021/acs.inorgchem.2c00722.

- [92] B. Hu, C. Debruler, Z. Rhodes, and T. L. Liu, “Long-Cycling aqueous organic Redox flow battery (AORFB) toward sustainable and safe energy storage,” *J. Am. Chem. Soc.*, vol. 139, no. 3, pp. 1207–1214, 2017, doi: 10.1021/jacs.6b10984.
- [93] J. Luo *et al.*, “Unprecedented Capacity and Stability of Ammonium Ferrocyanide Catholyte in pH Neutral Aqueous Redox Flow Batteries,” *Joule*, vol. 3, no. 1, pp. 149–163, 2019, doi: 10.1016/j.joule.2018.10.010.
- [94] J. Luo, B. Hu, M. Hu, W. Wu, and T. L. Liu, “An Energy-Dense, Powerful, Robust Bipolar Zinc–Ferrocene Redox-Flow Battery,” *Angew. Chemie - Int. Ed.*, vol. 61, no. 30, 2022, doi: 10.1002/anie.202204030.
- [95] G. Kear, A. A. Shah, and F. C. Walsh, “Development of the all-vanadium redox flow battery for energy storage: a review of technological, financial and policy aspects,” *Int. J. Energy Res.*, vol. 36, pp. 1105–1120, Sep. 2012, doi: 10.1002/er.1863.
- [96] M. Ulaganathan, V. Aravindan, Q. Yan, S. Madhavi, M. Skyllas-Kazacos, and T. M. Lim, “Recent Advancements in All-Vanadium Redox Flow Batteries,” *Adv. Mater. Interfaces*, vol. 3, no. 1, pp. 1–22, 2016, doi: 10.1002/admi.201500309.
- [97] Q. Chen *et al.*, “Organic Electrolytes for pH-Neutral Aqueous Organic Redox Flow Batteries,” *Adv. Funct. Mater.*, vol. 32, p. 2108777, Feb. 2022, doi: 10.1002/adfm.202108777.
- [98] A. Korshunov, A. Gibalova, M. Gruenebaum, B. J. Ravoo, M. Winter, and I. Cekic-Laskovic, “Supramolecular Viologen-Cyclodextrin Electrolytes for Aqueous Organic Redox Flow Batteries,” *ACS Appl. Energy Mater.*, vol. 4, no. 11, pp. 12353–12364, 2021, doi: 10.1021/acsaem.1c02156.
- [99] Y. Liu *et al.*, “Redox-Modulated Host–Guest Complex Realizing Stable Two-Electron Storage Viologen for Flow Battery,” *Ind. Eng. Chem. Res.*, 2022, doi: 10.1021/acs.iecr.2c02272.
- [100] O. Nolte, P. Rohland, N. Ueberschaar, M. D. Hager, and U. S. Schubert, “Stability of TMA-TEMPO-based aqueous electrolytes for redox-flow batteries,” *J. Power Sources*, vol. 525, no. February, p. 230996, 2022, doi: 10.1016/j.jpowsour.2022.230996.
- [101] P. Rohland, O. Nolte, K. Schreyer, H. Görls, M. D. Hager, and U. S. Schubert, “Structural alterations on the TEMPO scaffold and their impact on the performance as active materials for redox flow batteries,” *Mater. Adv.*, pp.

4278–4288, 2022, doi: 10.1039/d1ma00663k.

- [102] Z. Li, T. Jiang, M. Ali, C. Wu, and W. Chen, “Recent Progress in Organic Species for Redox Flow Batteries,” *Energy Storage Mater.*, vol. 50, no. April, pp. 105–138, 2022, doi: 10.1016/j.ensm.2022.04.038.
- [103] J. B. Gerken *et al.*, “Comparison of Quinone-Based Catholytes for Aqueous Redox Flow Batteries and Demonstration of Long-Term Stability with Tetrasubstituted Quinones,” *Adv. Energy Mater.*, vol. 10, no. 20, pp. 1–7, 2020, doi: 10.1002/aenm.202000340.
- [104] J. A. Ibacache, J. A. Valderrama, J. Faúndes, A. Danimann, F. J. Recio, and C. A. Zúñiga, “Green synthesis and electrochemical properties of mono- And dimers derived from Phenylaminoisoquinolinequinones,” *Molecules*, vol. 24, no. 23, pp. 1–13, 2019, doi: 10.3390/molecules24234378.
- [105] B. Huskinson, S. Nawar, M. R. Gerhardt, and M. J. Aziz, “Novel Quinone-Based Couples for Flow Batteries,” *ECS Meet. Abstr.*, vol. MA2013-01, no. 9, pp. 493–493, 2013, doi: 10.1149/ma2013-01/9/493.
- [106] S. Chen, M. Zhang, P. Zou, B. Sun, and S. Tao, “Historical development and novel concepts on electrolytes for aqueous rechargeable batteries,” *Energy Environ. Sci.*, pp. 1805–1839, 2022, doi: 10.1039/d2ee00004k.
- [107] D. M. Morales and M. Risch, “Seven steps to reliable cyclic voltammetry measurements for the determination of double layer capacitance,” *JPhys Energy*, vol. 3, no. 3, 2021, doi: 10.1088/2515-7655/abee33.
- [108] W. Lee, G. Park, and Y. Kwon, “Alkaline aqueous organic redox flow batteries of high energy and power densities using mixed naphthoquinone derivatives,” *Chem. Eng. J.*, vol. 386, no. November 2019, p. 123985, 2020, doi: 10.1016/j.cej.2019.123985.
- [109] P. Rohland, E. Schröter, O. Nolte, G. R. Newkome, M. D. Hager, and U. S. Schubert, “Redox-active polymers: The magic key towards energy storage – a polymer design guideline progress in polymer science,” *Prog. Polym. Sci.*, vol. 125, p. 101474, 2022, doi: 10.1016/j.progpolymsci.2021.101474.
- [110] P. S. Guin, S. Das, and P. C. Mandal, “Electrochemical Reduction of Quinones in Different Media: A Review,” *Int. J. Electrochem.*, vol. 2011, pp. 1–22, 2011, doi: 10.4061/2011/816202.
- [111] N. El-Najjar, H. Gali-Muhtasib, R. A. Ketola, P. Vuorela, A. Urtti, and H. Vuorela, “The chemical and biological activities of quinones: overview and

- implications in analytical detection,” *Phytochem. Rev.*, vol. 10, pp. 353–370, Sep. 2011, doi: 10.1007/s11101-011-9209-1.
- [112] Y. Ding, C. Zhang, L. Zhang, Y. Zhou, and G. Yu, “Molecular engineering of organic electroactive materials for redox flow batteries,” *Chem. Soc. Rev.*, vol. 47, pp. 69–103, 2018, doi: 10.1039/C7CS00569E.
- [113] N. Hayashi *et al.*, “Exchange of Quinone and Hydroquinone Moieties in Mixed Solutions of Biquinone and Bihydroquinone,” *Chem. Lett.*, vol. 40, pp. 947–949, Sep. 2011, doi: 10.1246/cl.2011.947.
- [114] G. Park, W. Lee, and Y. Kwon, “Aqueous organic redox flow batteries using naphthoquinone and iodide maintaining pH of electrolytes desirably by adoption of carboxylic acid functionalized carbon nanotube catalyst,” *Int. J. Energy Res.*, vol. 46, no. 3, pp. 3362–3375, 2022, doi: 10.1002/er.7386.
- [115] C. E. Pereyra, R. F. Dantas, S. B. Ferreira, L. P. Gomes, and F. P. Silva-Jr, “The diverse mechanisms and anticancer potential of naphthoquinones,” *Cancer Cell Int.*, vol. 19, p. 207, Dec. 2019, doi: 10.1186/s12935-019-0925-8.
- [116] L. Ramos-Peralta, L. I. Lopez-Lopez, S. Y. Silva-Belmares, A. Zugasti-Cruz, R. Rodriguez-Herrera, and C. N. Anguilar-Gonzalez, “Naphthoquinone: Bioactivity and Green Synthesis,” in *The Battle Against Microbial Pathogens: Basic Science, Technological Advances and Educational Programs*, 1st ed., Formatex Research Center, 2015, pp. 542–550.
- [117] R. M. Cory and D. M. McKnight, “Fluorescence Spectroscopy Reveals Ubiquitous Presence of Oxidized and Reduced Quinones in Dissolved Organic Matter,” *Environ. Sci. Technol.*, vol. 39, pp. 8142–8149, Nov. 2005, doi: 10.1021/es0506962.
- [118] L. Xia *et al.*, “Noncovalent interactions induced self-association in anthraquinone-iron aqueous redox flow batteries,” *Sustain. Energy Fuels*, vol. 6, pp. 2045–2052, 2022, doi: 10.1039/D1SE01895G.
- [119] Y. Zhu *et al.*, “Anthraquinone-based anode material for aqueous redox flow batteries operating in nondemanding atmosphere,” *J. Power Sources*, vol. 501, p. 229984, Jul. 2021, doi: 10.1016/j.jpowsour.2021.229984.
- [120] W. Lee, G. Park, Y. Kim, D. Chang, and Y. Kwon, “Nine watt – Level aqueous organic redox flow battery stack using anthraquinone and vanadium as redox couple,” *Chem. Eng. J.*, vol. 398, p. 125610, Oct. 2020, doi: 10.1016/j.cej.2020.125610.

- [121] W. Lee, A. Permatasari, and Y. Kwon, "Neutral pH aqueous redox flow batteries using an anthraquinone-ferrocyanide redox couple," *J. Mater. Chem. C*, vol. 8, pp. 5727–5731, 2020, doi: 10.1039/D0TC00640H.
- [122] P. Leung *et al.*, "Recent developments in organic redox flow batteries: A critical review," *J. Power Sources*, vol. 360, no. October, pp. 243–283, 2017, doi: 10.1016/j.jpowsour.2017.05.057.
- [123] Y. Demir, "Naphthoquinones, benzoquinones, and anthraquinones: Molecular docking, ADME and inhibition studies on human serum paraoxonase-1 associated with cardiovascular diseases," *Drug Dev. Res.*, vol. 81, pp. 628–636, Aug. 2020, doi: 10.1002/ddr.21667.
- [124] K. O. Eyong, V. Kuete, and T. Efferth, "Quinones and Benzophenones from the Medicinal Plants of Africa," in *Medicinal Plant Research in Africa*, Elsevier, 2013, pp. 351–391. doi: 10.1016/B978-0-12-405927-6.00010-2.
- [125] J. V. Christiansen *et al.*, "Fungal quinones: diversity, producers, and applications of quinones from *Aspergillus*, *Penicillium*, *Talaromyces*, *Fusarium*, and *Arthrinium*," *Appl. Microbiol. Biotechnol.*, vol. 105, pp. 8157–8193, Nov. 2021, doi: 10.1007/s00253-021-11597-0.
- [126] R. B. Jethwa, E. W. Zhao, R. N. Kerber, E. Jónsson, D. S. Wright, and C. P. Grey, "Designing for conjugate addition: an amine functionalised quinone anolyte for redox flow batteries," *J. Mater. Chem. A*, vol. 9, pp. 15188–15198, 2021, doi: 10.1039/D1TA02870G.
- [127] M. Quan, D. Sanchez, M. F. Wasylikiw, and D. K. Smith, "Voltammetry of Quinones in Unbuffered Aqueous Solution: Reassessing the Roles of Proton Transfer and Hydrogen Bonding in the Aqueous Electrochemistry of Quinones," *J. Am. Chem. Soc.*, vol. 129, pp. 12847–12856, Oct. 2007, doi: 10.1021/ja0743083.
- [128] Y.-O. Kim, Y. M. Jung, S. Bin Kim, B. H. Hong, K. S. Kim, and S.-M. Park, "Mechanistic Study on Electrochemical Reduction of Calix[4]quinone in Acetonitrile Containing Water," *J. Phys. Chem. B*, vol. 108, pp. 4927–4936, Apr. 2004, doi: 10.1021/jp049864n.
- [129] W. Lee, A. Konovalova, E. Tsoy, G. Park, D. Henkensmeier, and Y. Kwon, "Alkaline naphthoquinone-based redox flow batteries with a crosslinked sulfonated polyphenylsulfone membrane," *Int. J. Energy Res.*, vol. 46, pp. 12988–13002, Jul. 2022, doi: 10.1002/er.8079.
- [130] L. Tong *et al.*, "UV-Vis spectrophotometry of quinone flow battery

- electrolyte for in situ monitoring and improved electrochemical modeling of potential and quinhydrone formation,” *Phys. Chem. Chem. Phys.*, vol. 19, pp. 31684–31691, 2017, doi: 10.1039/C7CP05881K.
- [131] P. Sun *et al.*, “110th Anniversary: Unleashing the Full Potential of Quinones for High Performance Aqueous Organic Flow Battery,” *Ind. Eng. Chem. Res.*, vol. 58, pp. 3994–3999, Mar. 2019, doi: 10.1021/acs.iecr.8b06391.
- [132] Y. Jing *et al.*, “Anthraquinone Flow Battery Reactants with Nonhydrolyzable Water-Solubilizing Chains Introduced via a Generic Cross-Coupling Method,” *ACS Energy Lett.*, vol. 7, pp. 226–235, Jan. 2022, doi: 10.1021/acsenergylett.1c02504.
- [133] C. Wang *et al.*, “N-alkyl-carboxylate-functionalized anthraquinone for long-cycling aqueous redox flow batteries,” *Energy Storage Mater.*, vol. 36, pp. 417–426, Apr. 2021, doi: 10.1016/j.ensm.2021.01.019.
- [134] C. Wang *et al.*, “Alkaline soluble 1,3,5,7-tetrahydroxyanthraquinone with high reversibility as anolyte for aqueous redox flow battery,” *J. Power Sources*, vol. 524, p. 231001, Mar. 2022, doi: 10.1016/j.jpowsour.2022.231001.
- [135] S. B. Kristensen, T. van Mourik, T. B. Pedersen, J. L. Sørensen, and J. Muff, “Simulation of electrochemical properties of naturally occurring quinones,” *Sci. Rep.*, vol. 10, p. 13571, Dec. 2020, doi: 10.1038/s41598-020-70522-z.
- [136] W. Schlemmer *et al.*, “2-Methoxyhydroquinone from Vanillin for Aqueous Redox-Flow Batteries,” *Angew. Chemie - Int. Ed.*, vol. 59, no. 51, pp. 22943–22946, 2020, doi: 10.1002/anie.202008253.
- [137] A. Orita, M. G. Verde, M. Sakai, and Y. S. Meng, “A biomimetic redox flow battery based on flavin mononucleotide,” *Nat. Commun.*, vol. 7, p. 13230, Dec. 2016, doi: 10.1038/ncomms13230.
- [138] I. Abraham, R. Joshi, P. Pardasani, and R. . Pardasani, “Recent Advances in 1,4-Benzoquinone Chemistry,” *J. Braz. Chem. Soc.*, vol. 22, no. 3, pp. 385–421, Mar. 2011, doi: 10.1590/S0103-50532011000300002.
- [139] M. Ameri, A. Asghari, A. Amoozadeh, M. Bakherad, and D. Nematollahi, “Facile and one-pot, electro-organic synthesis of a new bis-quinone by the ECCE mechanism in green media,” *Chinese Chem. Lett.*, vol. 25, no. 12, pp. 1607–1610, 2014, doi: 10.1016/j.ccllet.2014.06.022.
- [140] P. Fischer, P. Mazúr, and J. Krakowiak, “Family Tree for Aqueous Organic

Redox Couples for Redox Flow Battery Electrolytes: A Conceptual Review,” *Molecules*, vol. 27, p. 560, Jan. 2022, doi: 10.3390/molecules27020560.

- [141] K. Wedege, E. Dražević, D. Konya, and A. Bentien, “Organic Redox Species in Aqueous Flow Batteries: Redox Potentials, Chemical Stability and Solubility,” *Sci. Rep.*, vol. 6, p. 39101, Dec. 2016, doi: 10.1038/srep39101.
- [142] P. Hu *et al.*, “Renewable-lawsone-based sustainable and high-voltage aqueous flow battery,” *Energy Storage Mater.*, vol. 19, pp. 62–68, May 2019, doi: 10.1016/j.ensm.2018.10.017.
- [143] J. V. Christiansen, T. Isbrandt, R. Asferg, S. A. Jarmusch, T. O. Larsen, and J. C. Frisvad, “Phoenicin Switch: Discovering the Trigger for Radical Phoenicin Production in Multiple Wild-Type *Penicillium* Species,” *Appl. Environ. Microbiol.*, vol. 88, no. 12, Jun. 2022, doi: 10.1128/aem.00302-22.
- [144] S. A. S. Mapari, K. F. Nielsen, T. O. Larsen, J. C. Frisvad, A. S. Meyer, and U. Thrane, “Exploring fungal biodiversity for the production of water-soluble pigments as potential natural food colorants,” *Curr. Opin. Biotechnol.*, vol. 16, pp. 231–238, Apr. 2005, doi: 10.1016/j.copbio.2005.03.004.
- [145] L. Dufossé, M. Fouillaud, Y. Caro, S. A. S. Mapari, and N. Sutthiwong, “Filamentous fungi are large-scale producers of pigments and colorants for the food industry,” *Curr. Opin. Biotechnol.*, vol. 26, pp. 56–61, Apr. 2014, doi: 10.1016/j.copbio.2013.09.007.
- [146] T. Sen, C. J. Barrow, and S. K. Deshmukh, “Microbial Pigments in the Food Industry—Challenges and the Way Forward,” *Front. Nutr.*, vol. 6, p. 7, Mar. 2019, doi: 10.3389/fnut.2019.00007.
- [147] Z. Yao, W. Tang, X. Wang, C. Wang, C. Yang, and C. Fan, “Synthesis of 1,4-benzoquinone dimer as a high-capacity (501 mA h g⁻¹) and high-energy-density (>1000 Wh kg⁻¹) organic cathode for organic Li-Ion full batteries,” *J. Power Sources*, vol. 448, p. 227456, Feb. 2020, doi: 10.1016/j.jpowsour.2019.227456.
- [148] N. Hayashi, T. Yoshikawa, T. Ohnuma, H. Higuchi, K. Sako, and H. Uekusa, “Synthesis, Structure, and Properties of Benzoquinone Dimer and Trimers Bearing t-Bu Substituents,” *Org. Lett.*, vol. 9, pp. 5417–5420, Dec. 2007, doi: 10.1021/ol702289u.
- [149] B. Genorio, “The Synthesis of Diquinone and Dihydroquinone Derivatives of Calix[4]arene and Electrochemical Characterization on Au(111) surface,” *Acta Chim. Slov.*, vol. 63, pp. 496–508, Sep. 2016, doi:

10.17344/acsi.2016.2289.

- [150] T. Yokoji, Y. Kameyama, N. Maruyama, and H. Matsubara, “High-capacity organic cathode active materials of 2,2'-bis-p-benzoquinone derivatives for rechargeable batteries,” *J. Mater. Chem. A*, vol. 4, pp. 5457–5466, 2016, doi: 10.1039/C5TA10713J.
- [151] M. Christensen, J. C. Frisvad, and D. Tuthill, “Taxonomy of the *Penicillium miczynskii* group based on morphology and secondary metabolites,” *Mycol. Res.*, vol. 103, pp. 527–541, May 1999, doi: 10.1017/S0953756298007515.
- [152] E. A. H. Friedheim, “Recherches sur la biochimie des champignons inférieurs. I. Isolement du pigment rouge de *Penicillium phoeniceum* (Phoenicine),” *Helv. Chim. Acta*, vol. 21, pp. 1464–1465, 1938, doi: 10.1002/hlca.193802101181.
- [153] J. V. Christiansen, T. O. Larsen, and J. C. Frisvad, “Production of Fungal Quinones: Problems and Prospects,” *Biomolecules*, vol. 12, p. 1041, Jul. 2022, doi: 10.3390/biom12081041.
- [154] C. O. Wilhelmsen *et al.*, “Demonstrating the Use of a Fungal Synthesized Quinone in a Redox Flow Battery,” *Batter. Supercaps*, p. e202200365, Nov. 2022, doi: 10.1002/batt.202200365.
- [155] M.-A. Goulet and M. J. Aziz, “Flow Battery Molecular Reactant Stability Determined by Symmetric Cell Cycling Methods,” *J. Electrochem. Soc.*, vol. 165, pp. A1466–A1477, May 2018, doi: 10.1149/2.0891807jes.
- [156] M. Uchimiya and A. T. Stone, “Reversible redox chemistry of quinones: Impact on biogeochemical cycles,” *Chemosphere*, vol. 77, pp. 451–458, Oct. 2009, doi: 10.1016/j.chemosphere.2009.07.025.
- [157] D. P. Tabor, R. Gómez-Bombarelli, L. Tong, R. G. Gordon, M. J. Aziz, and A. Aspuru-Guzik, “Mapping the frontiers of quinone stability in aqueous media: implications for organic aqueous redox flow batteries,” *J. Mater. Chem. A*, vol. 7, pp. 12833–12841, 2019, doi: 10.1039/C9TA03219C.
- [158] J. Sivanadanam, R. Murugan, H. Khan, I. S. Aidhen, and K. Ramanujam, “Investigation of Alkyl Amine Substituted Quinone Derivatives for the Redox Flow Battery Applications in Acidic Medium,” *J. Electrochem. Soc.*, vol. 169, p. 020533, Feb. 2022, doi: 10.1149/1945-7111/ac505f.
- [159] M. A. Goulet *et al.*, “Extending the Lifetime of Organic Flow Batteries via Redox State Management,” *J. Am. Chem. Soc.*, vol. 141, pp. 8014–8019,

2019, doi: 10.1021/jacs.8b13295.

- [160] L. Briot, M. Petit, Q. Cacciuttolo, and M.-C. Pera, “Aging phenomena and their modelling in aqueous organic redox flow batteries: A review,” *J. Power Sources*, vol. 536, p. 231427, Jul. 2022, doi: 10.1016/j.jpowsour.2022.231427.
- [161] C. Wiberg, T. J. Carney, F. Brushett, E. Ahlberg, and E. Wang, “Dimerization of 9,10-anthraquinone-2,7-Disulfonic acid (AQDS),” *Electrochim. Acta*, vol. 317, pp. 478–485, Sep. 2019, doi: 10.1016/j.electacta.2019.05.134.
- [162] B. Wermeckes and F. Beck, “Acid Catalyzed Disproportionation of Anthrahydroquinone to Anthraquinone and Anthrone,” *Denki Kagaku*, vol. 62, no. 12, pp. 1202–1205, 1994, doi: 10.5796/electrochemistry.62.1202.
- [163] O. Nolte, I. A. Volodin, C. Stolze, M. D. Hager, and U. S. Schubert, “Trust is good, control is better: a review on monitoring and characterization techniques for flow battery electrolytes,” *Mater. Horizons*, vol. 8, pp. 1866–1925, 2021, doi: 10.1039/D0MH01632B.
- [164] J. Rubio-Garcia, A. Kucernak, A. Parra-Puerto, R. Liu, and B. Chakrabarti, “Hydrogen/functionalized benzoquinone for a high-performance regenerative fuel cell as a potential large-scale energy storage platform,” *J. Mater. Chem. A*, vol. 8, pp. 3933–3941, 2020, doi: 10.1039/C9TA12396B.
- [165] T. J. Carney, S. J. Collins, J. S. Moore, and F. R. Brushett, “Concentration-Dependent Dimerization of Anthraquinone Disulfonic Acid and Its Impact on Charge Storage,” *Chem. Mater.*, vol. 29, pp. 4801–4810, 2017, doi: 10.1021/acs.chemmater.7b00616.
- [166] Q. Chen, L. Eisenach, and M. J. Aziz, “Cycling Analysis of a Quinone-Bromide Redox Flow Battery,” *J. Electrochem. Soc.*, vol. 163, no. 1, pp. A5057–A5063, 2016, doi: 10.1149/2.0081601jes.
- [167] D. Wu *et al.*, “2022 Roadmap on aqueous batteries,” *J. Phys. Energy*, vol. 4, no. 4, p. 041501, Oct. 2022, doi: 10.1088/2515-7655/ac774d.
- [168] Y. Yao, J. Lei, Y. Shi, F. Ai, and Y.-C. Lu, “Assessment methods and performance metrics for redox flow batteries,” *Nat. Energy*, vol. 6, pp. 582–588, Jun. 2021, doi: 10.1038/s41560-020-00772-8.
- [169] R. Seeber, C. Zanardi, and G. Inzelt, “The inherent coupling of charge transfer and mass transport processes: the curious electrochemical reversibility,” *ChemTexts*, vol. 2, p. 8, Jun. 2016, doi: 10.1007/s40828-016-0027-3.

- [170] F. Scholz, "Voltammetric techniques of analysis: the essentials," *ChemTexts*, vol. 1, p. 17, Dec. 2015, doi: 10.1007/s40828-015-0016-y.
- [171] J. Heinze, "Cyclic Voltammetry—'Electrochemical Spectroscopy,'" *Angew. Chemie Int. Ed. English*, vol. 23, pp. 831–847, Nov. 1984, doi: 10.1002/anie.198408313.
- [172] T. Shinagawa, A. T. Garcia-Esparza, and K. Takanabe, "Insight on Tafel slopes from a microkinetic analysis of aqueous electrocatalysis for energy conversion," *Sci. Rep.*, vol. 5, no. August, pp. 1–21, 2015, doi: 10.1038/srep13801.
- [173] F. Scholz, *Electroanalytical Methods*, 2nd ed. Springer, 2010. doi: 10.1007/978-3-642-02915-8.
- [174] M. Bogdan, D. Brugger, W. Rosenstiel, and B. Speiser, "Estimation of diffusion coefficients from voltammetric signals by support vector and gaussian process regression," *J. Cheminform.*, vol. 6, no. 1, p. 30, Dec. 2014, doi: 10.1186/1758-2946-6-30.
- [175] C. Sandford *et al.*, "A synthetic chemist's guide to electroanalytical tools for studying reaction mechanisms," *Chem. Sci.*, vol. 10, pp. 6404–6422, 2019, doi: 10.1039/C9SC01545K.
- [176] M. Aleksic, J. Pantic, and V. Kapetanovic, "Evaluation of kinetic parameters and redox mechanism of quinoxaline at glassy carbon electrode," *Facta Univ. - Ser. Physics, Chem. Technol.*, vol. 12, no. 1, pp. 55–63, 2014, doi: 10.2298/fupct1401055a.
- [177] A. J. Bard and L. R. Faulkner, *Electrochemical Methods - Fundamentals and Applications*, no. 2. 2001.
- [178] N. Aristov and A. Habekost, "Cyclic Voltammetry - A Versatile Electrochemical Method Investigating Electron Transfer Processes," *World J. Chem. Educ.*, vol. 3, no. 5, pp. 115–119, 2015, doi: 10.12691/wjce-3-5-2.
- [179] P. T. Kissinger and W. R. Heineman, "Cyclic voltammetry," *J. Chem. Educ.*, vol. 60, pp. 702–706, Sep. 1983, doi: 10.1021/ed060p702.
- [180] D. Thomas, Z. Rasheed, J. S. Jagan, and K. G. Kumar, "Study of kinetic parameters and development of a voltammetric sensor for the determination of butylated hydroxyanisole (BHA) in oil samples," *J. Food Sci. Technol.*, vol. 52, pp. 6719–6726, Oct. 2015, doi: 10.1007/s13197-015-1796-1.

- [181] E. M. Espinoza, J. A. Clark, J. Soliman, J. B. Derr, M. Morales, and V. I. Vullev, "Practical Aspects of Cyclic Voltammetry: How to Estimate Reduction Potentials When Irreversibility Prevails," *J. Electrochem. Soc.*, vol. 166, pp. H3175–H3187, Jan. 2019, doi: 10.1149/2.0241905jes.
- [182] J. G. He, Y. Li, X. X. Xue, H. Q. Ru, X. W. Huang, and H. Yang, "Cyclic voltammetry study of Ce(IV)/Ce(III) redox couple and Ce(IV)-F complex in sulfuric acid medium," *Metalurgija*, vol. 55, pp. 687–690, 2016.
- [183] A. A. Al Owais, I. S. El-Hallag, and E. H. El-Mossalamy, "The application of cyclic voltammetry and digital simulation for the examination of hydroquinone oxidation at a polycrystalline gold electrode in HClO₄," *Int. J. Electrochem. Sci.*, vol. 17, p. 220631, Jun. 2022, doi: 10.20964/2022.06.32.
- [184] C. Chauhan, "Contemporary voltammetric techniques and its application to pesticide analysis: A review," *Mater. Today Proc.*, vol. 37, pp. 3231–3240, 2021, doi: 10.1016/j.matpr.2020.09.092.
- [185] S. S. Beshahwored, "Cyclic Voltammetric (Cv) Evaluation of Electro Chemical Behaviors of K₃ [Fe (Cn) 6] and Uric Acid," *Int. Res. J. Nat. Sci.*, vol. 8, pp. 52–59, 2020.
- [186] G. S. Nambafu *et al.*, "An organic bifunctional redox active material for symmetric aqueous redox flow battery," *Nano Energy*, vol. 89, no. PB, p. 106422, 2021, doi: 10.1016/j.nanoen.2021.106422.
- [187] S. Treimer, A. Tang, and D. C. Johnson, "A Consideration of the Application of Koutecký-Levich Plots in the Diagnoses of Charge-Transfer Mechanisms at Rotated Disk Electrodes," *Electroanalysis*, vol. 14, p. 165, Feb. 2002, doi: 10.1002/1521-4109(200202)14:3<165::AID-ELAN165>3.0.CO;2-6.
- [188] G. K. H. Wiberg and A. Zana, "Levich Analysis and the Apparent Potential Dependency of the Levich B Factor," *Anal. Lett.*, vol. 49, pp. 2397–2404, Oct. 2016, doi: 10.1080/00032719.2016.1149188.
- [189] S. Black and F. Muller, "On the Effect of Temperature on Aqueous Solubility of Organic Solids," *Org. Process Res. Dev.*, vol. 14, pp. 661–665, May 2010, doi: 10.1021/op100006y.
- [190] R. M. Dell and D. A. J. Rand, "Charging regimes," in *Understanding batteries*, The Royal Society of Chemistry, 2001, pp. 36–38.
- [191] H. Wu, Y. Zhang, A. Kjøniksen, X. Zhou, and X. Zhou, "Wearable Biofuel Cells: Advances from Fabrication to Application," *Adv. Funct. Mater.*, vol.

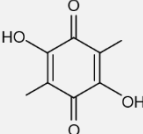
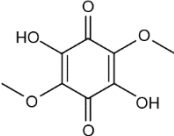
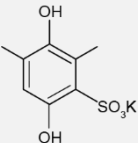
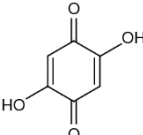
- 31, p. 2103976, Nov. 2021, doi: 10.1002/adfm.202103976.
- [192] T. Hagemann *et al.*, “A bipolar nitronyl nitroxide small molecule for an all-organic symmetric redox-flow battery,” *NPG Asia Mater.*, vol. 9, pp. e340–e340, Jan. 2017, doi: 10.1038/am.2016.195.
- [193] M. V. Holland-Cunz, F. Cording, J. Friedl, and U. Stimming, “Redox flow batteries—Concepts and chemistries for cost-effective energy storage,” *Front. Energy*, vol. 12, pp. 198–224, Jun. 2018, doi: 10.1007/s11708-018-0552-4.
- [194] N. Elgrishi, K. J. Rountree, B. D. McCarthy, E. S. Rountree, T. T. Eisenhart, and J. L. Dempsey, “A Practical Beginner’s Guide to Cyclic Voltammetry,” *J. Chem. Educ.*, vol. 95, pp. 197–206, Feb. 2018, doi: 10.1021/acs.jchemed.7b00361.
- [195] J. Wu, W. Wang, M. Wang, H. Liu, and H. Pan, “Electrochemical Behavior and Direct Quantitative Determination of Tanshinone IIA in Micro-emulsion,” *Int. J. Electrochem. Sci.*, vol. 11, pp. 5165–5179, Jun. 2016, doi: 10.20964/2016.06.55.
- [196] R. Gulaboski *et al.*, “Hydroxylated derivatives of dimethoxy-1,4-benzoquinone as redox switchable earth-alkaline metal ligands and radical scavengers,” *Sci. Rep.*, vol. 3, p. 1865, Dec. 2013, doi: 10.1038/srep01865.
- [197] J. A. Pedersen, “On the application of electron paramagnetic resonance in the study of naturally occurring quinones and quinols,” *Spectrochim. Acta Part A*, vol. 58, pp. 1257–1270, Apr. 2002, doi: 10.1016/S1386-1425(01)00715-6.
- [198] C. O. Wilhelmsen *et al.*, “Four-Electron Energy Storage in Biosynthesized Phoenicin Flow Battery Negolyte,” Submitted to: *ACS Sustain. Chem. Eng.*, 2022.
- [199] A. G. Medentsev and V. K. Akimenko, “Naphthoquinone metabolites of the fungi,” *Phytochemistry*, vol. 47, pp. 935–959, Mar. 1998, doi: 10.1016/S0031-9422(98)80053-8.
- [200] A. M. Bailey, R. J. Cox, K. Harley, C. M. Lazarus, T. J. Simpson, and E. Skellam, “Characterisation of 3-methylorcinaldehyde synthase (MOS) in *Acremonium strictum*: first observation of a reductive release mechanism during polyketide biosynthesis,” *Chem. Commun.*, no. 39, p. 4053, 2007, doi: 10.1039/b708614h.
- [201] R. J. Cox *et al.*, “Rapid cloning and expression of a fungal polyketide synthase

gene involved in squalestatin biosynthesis,” *Chem. Commun.*, no. 20, p. 2260, 2004, doi: 10.1039/b411973h.

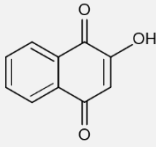
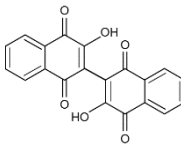
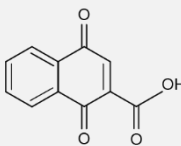
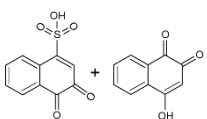
- [202] M. R. Nielsen *et al.*, “A new vector system for targeted integration and overexpression of genes in the crop pathogen *Fusarium solani*,” *Fungal Biol. Biotechnol.*, vol. 6, no. 1, p. 25, Dec. 2019, doi: 10.1186/s40694-019-0089-2.
- [203] K. Westphal, R. Wollenberg, F.-A. Herbst, J. Sørensen, T. Sondergaard, and R. Wimmer, “Enhancing the Production of the Fungal Pigment Aurofusarin in *Fusarium graminearum*,” *Toxins (Basel)*, vol. 10, p. 485, Nov. 2018, doi: 10.3390/toxins10110485.
- [204] B. Huskinson *et al.*, “A metal-free organic–inorganic aqueous flow battery,” *Nature*, vol. 505, pp. 195–198, Jan. 2014, doi: 10.1038/nature12909.

Appendix A. Quinone table

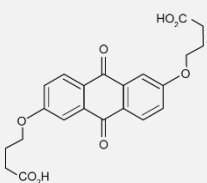
Table A1. Some quinone-based RFBs from the literature. The quinones are divided into benzoquinones, naphthoquinones, and anthraquinones. The structure and the solubility belong to the quinone highlighted in bold. The cell potential, electrolyte pH, capacity fade rate (both cycle and temporal), coulombic efficiency as well as the year of publication are given as results from full-cell testing using the electrolyte combinations shown.

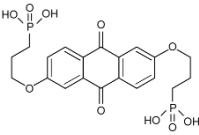
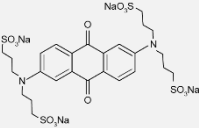
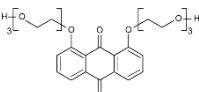
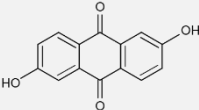
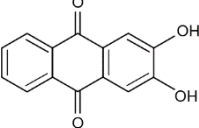
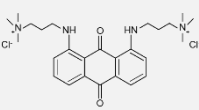
Electrolytes (Negolyte/posolyte)	Solu- bility	Theo. Cap.	Cell Pot.	pH	Capacity fade rate	CE	Year
Benzoquinones							
⁽¹⁾ 0.1 M DMBQ/ 0.1 M K ₄ Fe(CN) ₆	-	5.3 Ah L ⁻¹	1.3 V	14	0.12% cycle ⁻¹ / 22% day ⁻¹	>98%	2019 [131]
							
⁽²⁾ 0.1 M DMOBQ/ 0.1 M K ₄ Fe(CN) ₆	-	5.3 Ah L ⁻¹	1.2 V	14	0.19% cycle ⁻¹ / 35% day ⁻¹	>98%	2019 [131]
							
1 M 2,7-AQDS/ ⁽³⁾ 1 M DHDMS	2.0 M	53.6 Ah L ⁻¹	0.6 V	0	1.0% cycle ⁻¹ / 3.5% day ⁻¹	~100%	2017 [87]
							
⁽⁴⁾ 0.5 M DHBQ/ 0.4 M K ₄ Fe(CN) ₆	4.3 M	26.8 Ah L ⁻¹	1.2 V	14	0.24% cycle ⁻¹ / 9% day ⁻¹	99%	2017 [73]
							

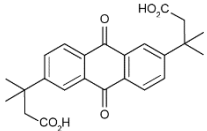
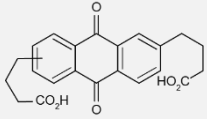
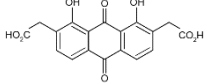
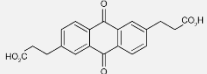
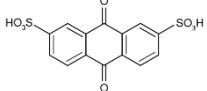
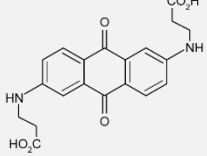
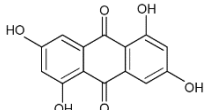
Naphthoquinones

⁽⁵⁾ 0.1 M Lawsone/ 0.2 M 4-HO-TEMPO 	0.7 M	5.3 Ah L ⁻¹	1.3 V	7	0.0079% cycle ⁻¹ / -	97%	2019 [142]
⁽⁶⁾ 0.5 M Bislawsone/ 0.4 M K ₄ Fe(CN) ₆ 	0.6 M	26.8 Ah L ⁻¹	1.1 V	14	0.038% cycle ⁻¹ / 0.74% day ⁻¹	99.7%	2019 [68]
⁽⁷⁾ 0.5 M 2,3-HCNQ/ 0.4 M K ₄ Fe(CN) ₆ 	1.2 M	26.8 Ah L ⁻¹	1.0 V	14	0.053% cycle ⁻¹ / 3.4% day ⁻¹	~100%	2018 [49]
⁽⁸⁾ 0.6 M NQSO/ 0.4 M K ₄ Fe(CN) ₆ 	1.6 M	32.2 Ah L ⁻¹	1.0 V	14	0.01% cycle ⁻¹ / 0.70% day ⁻¹	99.7%	2022 [129]

Anthraquinones

⁽⁹⁾ 0.5 M 2,6-DBEAQ/ 0.3 M K ₄ Fe(CN) ₆ 	0.6 M	26.8 Ah L ⁻¹	1.0 V	12	0.001% cycle ⁻¹ / 0.04% day ⁻¹	99.9%	2018 [29]
---	-------	-------------------------	-------	----	---	-------	--------------

(10) 0.5 M 2,6-DPPEAQ/								
0.4 M $K_4Fe(CN)_6$								
	0.8 M	26.8 Ah L ⁻¹	1.0 V	~9	0.0004% cycle ⁻¹ / 0.014% day ⁻¹	99.9%	2019	[32]
(11) 0.1 M 2,6-N-TSAQ/								
0.1 M $K_4Fe(CN)_6$								
	0.5 M	5.3 Ah L ⁻¹	1.1 V	14	0.00024% cycle ⁻¹ / 0.025% day ⁻¹	99.9%	2022	[50]
(12) 1.5 M PEGAQ/								
1.5 M $K_4Fe(CN)_6$								
	2.2 M	80.4 Ah L ⁻¹	1.0 V	7	0.043% cycle ⁻¹ / 0.5% day ⁻¹	~100%	2019	[80]
(13) 0.5 M 2,6-DHAQ/								
0.5 M $K_4Fe(CN)_6$								
	0.6 M	26.8 Ah L ⁻¹	1.2 V	14	0.1% cycle ⁻¹ / 8% day ⁻¹	99%	2015	[84]
(14) 0.3 M 2,3-DHAQ/								
0.5 M $K_4Fe(CN)_6$								
	0.7 M	16.1 Ah L ⁻¹	1.1 V	14	0.022% cycle ⁻¹ / 0.45% day ⁻¹	99.7%	2022	[82]
(15) 0.4 M 1,8-BDPAQC1₂/								
0.9 M Fe(gly) ₂ Cl ₂								
	0.5 M	21.4 Ah L ⁻¹	1.3 V	7	0.048% cycle ⁻¹ / 0.88% day ⁻¹	96.6%	2022	[83]

<p>(16) 0.5 M DPivOHAQ/ 0.4 M $K_4Fe(CN)_6$</p> 	0.7 M	26.8 Ah L ⁻¹	1.0 V	14	0.00004% cycle ⁻¹ / 0.0018% day ⁻¹	99.9%	2020 [85], [102]
<p>(17) 0.5 M DBAQ/ 0.4 M $K_4Fe(CN)_6$</p> 	1.0 M	26.8 Ah L ⁻¹	1.0 V	12	0.0002% cycle ⁻¹ / 0.0084% day ⁻¹	99.9%	2020 [85], [102]
<p>(18) 0.75 M DCDHAQ/ 0.3 M $K_4Fe(CN)_6$</p> 	1.3 M	40.2 Ah L ⁻¹	1.1 V	14	0.0029% cycle ⁻¹ / 0.03% day ⁻¹	99.8%	2021 [86]
<p>(19) 0.1 M AQDP/ 0.1 M $K_4Fe(CN)_6$</p> 	1.0 M	5.3 Ah L ⁻¹	1.0 V	12	0.0003% cycle ⁻¹ / 0.0128% day ⁻¹	99.3%	2022 [132]
<p>(20) 1.0 M AQDS/ 3.0 M HBR</p> 	1.0 M	53.6 Ah L ⁻¹	0.9 V	0	0.78% cycle ⁻¹	99.2%	2014 [204]
<p>(21) 0.1 M DAEAQ/ 0.15 M $K_4Fe(CN)_6$</p> 	1.0 M	5.3 Ah L ⁻¹	1.1 V	14	0.0008% cycle ⁻¹ / 0.19% day ⁻¹	99.9%	2021 [133]
<p>(22) 0.5 M 1,3,5,7-THAQ/ 0.4 M $K_4Fe(CN)_6$</p> 	1.9 M	26.8 Ah L ⁻¹	1.2 V	14	0.0044% cycle ⁻¹ / 0.36% day ⁻¹	~100%	2022 [134]

Papers

List of Papers

1. **Wilhelmsen, C.O.**; Kristensen, S.B.; Nolte, O.; Volodin, I.; Christiansen, J.V.; Isbrandt, T.; Sørensen, T.; Petersen, C.; Sondergaard, T.E.; Nielsen, K.L.; Larsen, T.O.; Frisvad, J.C.; Hager, M.; Schubert, U.S.; Muff, J.; Sørensen, J.L. (2022) *Demonstrating the use of a Fungal Synthesized Quinone in a Redox Flow Battery*.
Batteries & Supercaps, doi:10.1002/batt.202200365
2. **Wilhelmsen, C.O.**; Kavounis-Pasadakis, A.; Christiansen, J.V.; Isbrandt, T.; Almind, M.R.; Larsen, T.O.; Hjelm, J.; Sørensen, J.L.; Muff, J. (2022) *Four-Electron Energy Storage in Biosynthesized Phenolic Flow Battery Negolyte*.
Manuscript submitted to ACS Sustainable Chemistry and Engineering
3. **Wilhelmsen, C.O.**; Muff, J.; Sørensen, J.L. (2022) *Are biologically synthesized electrolytes the future in green energy storage?*
Manuscript submitted to Energy Storage

Side project:

1. Tang, Z.; Sangwongwanich, A.; Yang, Y., **Wilhelmsen, C.O.**; Kristensen, S.B.; Sørensen, J.L.; Muff, J.; Blaabjerg, F. (2021) *Lifetime Modelling and Analysis of Aqueous Organic Redox-flow Batteries for Renewable Energy Application*.
IEEE Energy Conversion Congress and Exposition (ECCE), doi: 10.1109/ECCE47101.2021.9595507

Paper 1

Wilhelmsen, C.O.; Kristensen, S.B.; Nolte, O.; Volodin, I.; Christiansen, J.V.; Isbrandt, T.; Sørensen, T.; Petersen, C.; Sondergaard, T.E.; Nielsen, K.L.; Larsen, T.O.; Frisvad, J.C.; Hager, M.; Schubert, U.S.; Muff, J.; Sørensen, J.L. (2022) *Demonstrating the use of a Fungal Synthesized Quinone in a Redox Flow Battery.*

Due to rights and permissions is this paper not present for publishing.

Paper 2

Wilhelmsen, C.O.; Kavounis-Pasadakis, A.; Christiansen, J.V.; Isbrandt, T.; Almind, M.R.; Larsen, T.O.; Hjelm, J.; Sørensen, J.L.; Muff, J. (2022) *Four-Electron Energy Storage in Biosynthesized Phoenicin Flow Battery Negolyte*.

Due to rights and permissions is this paper not present for publishing.

Paper 3

Wilhelmsen, C.O.; Muff, J.; Sørensen, J.L. (2022) *Are biologically synthesized electrolytes the future in green energy storage?*

Due to rights and permissions is this paper not present for publishing.

Paper 4

Tang, Z.; Sangwongwanich, A.; Yang, Y., Wilhelmsen, C.O.; Kristensen, S.B.; Sørensen, J.L.; Muff, J.; Blaabjerg, F. (2021) *Lifetime Modelling and Analysis of Aqueous Organic Redox-flow Batteries for Renewable Energy Application*

Due to rights and permissions is this paper not present for publishing.

